MONTHLY NOTICES

OF THE

ROYAL ASTRONOMICAL SOCIETY

Vol. 108 No. 5

MEETING OF 1948 OCTOBER 8

Professor W. M. H. Greaves, President, in the Chair

The election by the Council of the following Fellows was duly confirmed:—

Robert Lloyd Baglow, Emmanuel College, Cambridge (proposed by R. O. Redman);

William P. Bidelman, Ph.D., Yerkes Observatory, Williams Bay, Wisconsin, U.S.A. (proposed by S. Chandrasekhar);

Joseph Steel Hughes, M.A., Kew Observatory, Richmond, Surrey (proposed by H. Jeffreys);

E. Ralph Lapwood, M.A., Cheriton, Histon Road, Cambridge (proposed by H. Jeffreys);

Cyril Walter Thomas Layton, 21 Regent Terrace, Gateshead-on-Tyne (proposed by C. L. Twentyman);

George Read, 106 Millon Road, West Hartlepool (proposed by T. Silcock); and

The Rt. Hon. Viscount Trafalgar, Trafalgar House, Salisbury (proposed by F. G. G. Carr).

The election by Council of the following Junior Members was duly confirmed:—

Franz Daniel Kahn, Balliol College, Oxford (proposed by S. Chapman); and

Alexander Ross McKenzie, 254 Milton Road East, Edinburgh (proposed by N. G. Matthew).

Two hundred presents were announced as having been received since the last meeting, including:—

H. Jeffreys, *The Theory of Probability* (presented by the author);

J. Houtgast, *The variation in the Profiles of strong Fraunhofer Lines along a radius of the Solar Disk* (presented by the author);

G. N. Harvey, *New Developments in the Correction of Magnetic Compasses* (Admiralty Bulletin, No. 9);

M. G. J. Minnaert, *On the Temperature of Cometary Nuclei* (presented by the author);

A. Schwassman and P. J. van Rhijn, *Bergedorfer Spektral-Durchmüsterung*, Band 3 (presented by the Hamburger Sternwarte); and

Five-Figure Tables of Natural Trigonometrical Functions (presented by H.M. Nautical Almanac Office).

SOME CHARACTERISTICS OF SOLAR RADIO EMISSIONS

J. S. Hey, S. J. Parsons and J. W. Phillips

(Received 1948 September 9)

Summary

An analysis is given of solar radio emissions, observed mainly at a wave-length of 4·1 metres between 1946 March and 1947 September, and their relation to visual solar phenomena and their geophysical accompaniments.

The associations of solar radio bursts with flares are considered in detail and it is shown that the most intense flares are the most likely to produce radio bursts. It is also shown that in general the radio emission lags by several minutes behind the visual or ultra-violet flare radiations.

The apparent tendency for coincidences between flares and bursts to be greater on the eastern than on the western half of the Sun's disk is discussed. The distribution of coincidences with respect to solar longitude from central meridian is contrasted with the sharply-beamed pattern of continuous radiation associated with sunspots.

1. *Introduction*

The observations of the intense solar radio emissions at metre wave-lengths here described form a continuation of the experimental investigations made at the Army Operational Research Group in 1942 February and 1946 February, which have been described by Appleton and Hey.* These investigations showed that intense electromagnetic radiations could emanate from the Sun during the transit of a large sunspot across the Sun's disk. It was demonstrated that the received radio intensity was particularly high in the region of 5 metres wave-length and that the average level of radiation reached its maximum value when the spot was within a few days of central meridian passage. It was also found that there were sudden increases in radio power flux of 10–100 times the mean level which occurred at approximately the same time as solar flares and radio communication fade-outs.

Observation of solar radio emissions was subsequently made at various times until 1946 July, since when recordings at a wave-length of 4·1 metres have been made almost continuously every day from sunrise to sunset. Occasionally, additional measurements have been made of the solar radiation at several wave-lengths between 1·5 metres and 12·5 metres. It became evident that the relationship between visual and radio solar emissions was very complex. It was possible to find examples of striking correlations between solar and radio phenomena, but there were also many occasions in which such association was absent. A comprehensive account can, therefore, only be given after consideration of a large number of cases. These may be analysed so as to determine the numbers of coincidences and an assessment of their significance can be made on a statistical basis. It will then be of particular value to distinguish any trends in the correlations with variations in the measurable properties of the different phenomena. The present investigation is an attempt to achieve this object. The principal phenomena with which we deal are the intensities of the solar radio

* J. S. Hey, *Nature*, **157**, 47, 1946; AORG Memo J4, 1942, and Report **275**, **1945** [Restricted Circulation]. E. V. Appleton and J. S. Hey, *Phil. Mag.*, **37**, 73, 1946.

emissions, the magnitudes and positions of sunspots and solar flares, and the geomagnetic disturbances which give indirect evidence of solar activity.

2. *The Measurement of Solar Radio Intensities*

2.1. *The Apparatus.*—A sensitive radio receiver was operated on a mean wave-length of 4·1 metres with a band-width of 3 Mc./s. The rectified output of the receiver was marked on a recording ammeter, the overall time constant of response being of the order of 1 second. The recording chart moved at the rate of 6 inches per hour. Hourly timing-marks were made on the recording chart by means of a chronometer relay. The chronometer was checked daily against G.M.T. by G.P.O. telephone. By these means any solar noise recorded on the chart could be timed to an accuracy better than $\frac{1}{2}$ minute.

The recorded output was calibrated in terms of the radio noise input in absolute units by means of a noise-signal generator which presented an impedance approximately equal to that of the aerial.

The aerial system consisted of a twin yagi array using horizontal polarization. The array was normally tilted at 20° elevation which gave adequate sensitivity up to 40° elevation. For those times of day during the summer months when the Sun's elevation exceeded 40°, the tilt of the yagi array was altered to 60°. The aerial sensitivity in the vertical plane was known approximately from previous measurements on similar arrays using a small oscillator suspended on a balloon as the source of signal. A rough check of aerial sensitivity was made by comparing the solar noise received by the yagi array with that received simultaneously by a single dipole. The aerial gain in the direction of maximum sensitivity was estimated to be about $5\frac{1}{2}$ times that of a half-wave dipole in free space.

The aerial array was mounted on the receiver cabin which was rotated about a vertical axis by a motor drive adjusted to keep the aerials to within a few degrees of the bearing of the Sun. A knowledge of the aerial sensitivity in the vertical plane and of the calibration characteristics of the receiver thus made it possible to calculate the power flux of radiation in the incident wave to an accuracy of about 25 per cent.

2.2. *Intensity Measurements.*—Radio emissions may be classed into two types, continuous emission of fluctuating intensity and sudden bursts of intensity which are often of the order of a few minutes in duration. Previous work * has indicated that the former type is more particularly associated with spots and reaches a maximum near central meridian passage, whilst the latter type is more particularly associated with flares.

The recordings of solar radio emissions have been converted into absolute power flux received at the Earth's surface in watts/sq.m.cyc./sec. band-width. These values can, if desired, be converted into equivalent solar black-body temperatures for the wave-length under consideration.† It must be noted,

* E. V. Appleton and J. S. Hey, *loc. cit.* L. L. McCready, J. L. Pawsey and R. Payne Scott, *Proc. Roy. Soc. A.*, **190**, 357, 1947. M. Ryle and D. D. Vonberg, *Proc. Roy. Soc. A.*, **193**, 98, 1948.

† The power flux at the Earth's surface, assuming the Sun to be a black-body radiator, is

$$F = \frac{2KT\, d\nu \,.\, d\Omega}{\lambda^2},$$

where K = Boltzmann's const.
T = absolute temperature.
$d\nu$ = frequency band-width.
$d\Omega$ = solid angle subtended by the Sun.
λ = wave-length.

however, that such temperatures have no significance except as alternative indications of magnitude. Not only is the source of radiation not the whole Sun, but both the spectrum and the great intensity of the radio emission suggest that it is of non-thermal origin.

For convenience of analysis the radio bursts have been classified in intensity according to an arbitrary scale of 3. This plan was adopted for simplicity in order to divide the occurrences into a few intensity groups in a similar manner to the accepted classification of solar flares. During the analysis it was found desirable to introduce a further group for minor radio bursts and this has been numbered $\frac{1}{2}$. The radio scale of intensity for radio bursts was chosen as follows:—

Scale Number	Radio Intensity in units of 10^{-22} watts/sq.m.c.p.s. (horizontal polarization)
0	<20
$\frac{1}{2}$	20–100
1	100–500
2	500–1500
3	>1500

The unit of intensity, 10^{-22} watts/sq.m.c.p.s. band-width, is of the order of the smallest detectable signal with the present apparatus. Since the smallest measurable intensity varies with the altitude of the Sun, and because of uncertainties in distinguishing minute bursts from interference, it was considered desirable to count as category 0 all intensities below a certain small level, namely <20 units. It should be noted also that receiver noise would be equivalent to a power flux of about 10 units at the aerial when the Sun is in the direction of maximum aerial sensitivity, whilst galactic noise represents a further 20 units on the average. Hence our unit of intensity corresponds to only 3·3 per cent of receiver plus average galactic noise. In terms of equivalent temperature this unit of power flux at 4·1 metres wave-length is equivalent to approximately $1{\cdot}8 \times 10^6$ degrees Kelvin. Martyn* has shown that we should expect the effective black-body temperature of the quiescent Sun at this wave-length to be the electron temperature of the corona and hence about a million degrees. Thus our unit of intensity is of the same order as the expected black-body radiation for the Sun at this wave-length.

3. *Correlations of Radio Bursts with Solar Flares*

3.1. *Solar Flares Observed Visually.*—An analysis of the solar flare and radio burst data will now be made in order to determine the extent to which these phenomena are correlated. The visual solar flare data have been obtained from the I.A.U. Bulletin on Solar Activity, which at the time of writing is available up to 1947 March. The available solar data after that time have been supplied by the Observatories at Greenwich, Muswell Hill (Mr Sellers) and Sherborne (Dr Ellison).

Visual solar data are necessarily intermittent, being obtainable only in clear weather conditions. The solar flare observations have, therefore, been chosen as the primary entity and the radio burst data have been examined to find on which occasions bursts coincide with flares. To do this, some choice of time

* D. F. Martyn, *Proc. Roy. Soc.*, **193**, 44, 1948.

interval has to be made in counting a burst as coincident with a flare. Only in a proportion of the flare observations was the actual beginning and end of the flare seen. In this connection it is of interest to note the summary of flare characteristics given by Newton and Barton.* They found that the average duration of flares varied from about 20 minutes for low-intensity flares to about 40 minutes for those of high intensity. The periods of visual observations of the Sun vary considerably between a few minutes and several hours. A further complication arises if there exists a variable time difference between the occurrence of a flare and an associated radio burst. There is evidence that such time differences do exist and these are discussed more fully later (in Section 3.5). It is, therefore, possible that a radio burst associated with a flare may occur outside the period of visual watch. With these considerations taken into account it was felt that a reasonable time allowance would be made by counting bursts as coincident with flares if they occurred within the flare period ± 5 minutes when the beginning or end of the flare was observed, or within the flare observation period ± 20 minutes, if the beginning or end of the flare was not seen (if, for example, a flare was already in progress on initial viewing of the solar disk and the termination of the flare was seen, then a burst was counted if it occurred within the flare observation period extended from 20 minutes before the beginning to 5 minutes after the end of the flare). The coincidence rates graded according to flare and burst intensities are given in Table I. It must be emphasized that if several radio bursts occur in a single observation period the occurrence is reckoned as a single flare-burst coincidence. If several flares occur simultaneously the one of highest intensity is considered. Whatever arbitrary definition of a coincidence between a flare and a burst is chosen it is of course necessary to examine the probability of significance. This is revealed in one way by trends in the coincidence rate with variations in the flare characteristics. A detailed discussion of significance is given later in Section 3.4.

TABLE I

Chances of coincidences between solar flares and radio bursts

Flare Intensity	Number of Cases	Percentage of Cases with Radio Bursts of Intensity :—			
		>0	$>\frac{1}{2}$	>1	>2
1	170	32	23	12	3
2	46	48	39	30	13
3	14	57	57	43	21

The average duration of all the cases is 42 minutes.

The results in Table I indicate that there is a progressive increase in the chance of a coincident measured burst with an increase in flare intensity. The number of observations of high-intensity flares made when the solar set was in operation was small. Fortunately radio communications fade-outs provide a more complete record of high-intensity flares, and the coincidence of fade-outs and radio bursts will be discussed in the next section.

* H. W. Newton and H. J. Barton, *M.N.*, **97**, 594, 1937.

3.2. *Indirect Evidence of Solar Flares by Radio Communication Fade-outs.*— Radio communication fade-outs are caused by absorption of radio waves in the D-layer when the ionization is enhanced by ultra-violet solar radiation. The analysis of the relation between solar flares and fade-outs by Newton and Barton * shows that when a radio fade-out occurs there is a high probability of there being a solar flare. The converse is not true, since there are many solar flares which do not produce fade-outs. The highest incidence of associated fade-outs occurs for the most intense flares. We may thus consider a radio communication fade-out as a geophysical accompaniment of a solar flare very probably of high intensity. When the fade-out is complete it is almost certain that the flare is of the type class 3 or 3+. Details of fade-outs on wave-lengths of 16–25 metres have been supplied to us by Cable and Wireless Ltd., and these provide, therefore, an important indirect record of high-intensity flares free from the visibility limitations which so severely restrict the numbers observed directly. As in the case of solar flares, an arbitrary time interval must be chosen in which to count a radio burst as coincident with a fade-out. For comparative analysis of coincidences it is further required that the average time interval should be approximately the same in both cases. The onset of the fade-out is usually fairly abrupt, but the subsequent recovery of signal strength is gradual and the end of the fade-out often very indefinite. After consideration of the time differences between the occurrences of bursts and fade-outs, as discussed in Section 3.5, the rule chosen was to count as coincidences those cases in which a burst occurred not more than 10 minutes before the first reported onset time and 20 minutes after the mean onset time.† The fade-outs may be graded in intensity according to the number of communication links affected and the degree of attenuation produced. The analysis of surges coincident with fade-outs is given in Table II.

TABLE II

Coincidences between Radio Communication Fade-outs and Solar Radio Bursts

Type of Fade-out	Number of Cases	Percentage of Cases with Radio Bursts of Intensity :—			
		>0	$>\frac{1}{2}$	>1	>2
Weakening	69	33	27	22	10
Some Links C.F.O.	39	51	38	36	23
All Links C.F.O.	42	69	62	50	36

The average time interval of all the cases is approximately 42 minutes.
C.F.O.=Complete Fade-out.

Table II thus provides a confirmation of Table I and clearly points to a progressive increase with flare intensity in the number of coincidences with radio bursts and in the proportion of bursts of high intensity.

* H. W. Newton and H. J. Barton, *loc. cit.*

† As stated in Section 3.5, in the great majority of cases the fade-out onset precedes the burst.

3.3. *Indirect Evidence of Solar Flares from Magnetic Crochets.*—A grade of solar flares of even higher intensity is probably indicated by those accompanied by magnetic crochets. These deviations of the magnetic elements have been described in detail by Newton.* Table III lists distinct magnetic crochets observed at Abinger between 1946 March and 1947 September while the solar noise recording apparatus was in operation. This suggests a very high probability that a flare of intensity sufficient to produce a magnetic crochet will be accompanied by a radio burst of high intensity.

TABLE III

Coincidences between Magnetic Crochets and Solar Radio Bursts

Date	Magnetic Crochet		Solar Radio Burst			Time Differences Radio Burst minus Crochet	
	Onset	Maximum	Onset	Maximum	Intensity	Onset	Maxima
	h m	h m	h m	h m		m	m
1946 Mar. 5	11 28	11 29	11 31	11 31	3	3	2
1947 Apr. 6	11 52	11 55	11 59	11 59	3	7	4
1947 May 6	10 14	10 15	10 17	10 17	2	3	2
1947 June 14	10 36	10 40	10 40	10 40	3	4	0
1947 Aug. 1	15 17	15 19	...	...	0	...	...
1947 Aug. 31	14 54	14 58	14 43*, 53	14 54	3	−11*, −1	−4
1947 Sept. 2	08 57	08 59	...	...	0 †	...	...

* In this instance, the rise of intensity of the major burst commenced at $14^h\ 53^m$; the preceding minor burst commenced 10 minutes earlier.

† A burst occurred at wave-lengths of 1·5 and 2 metres, onset at $09^h\ 00^m$ and maximum at $09^h\ 02^m$.

3.4. *Significance of Solar Flare and Radio Burst Coincidences.*—In order to appreciate the significance of the percentage coincidences between radio bursts and flares (or fade-outs) it is necessary to know what are the chances of a burst occurring in a similar period of time when there is no flare present on the Sun's disk. This has been estimated in the following way. The average time period of flare observation, extended as described in Sections 3.1 and 3.2, is approximately 42 minutes. Now the average chance of a radio burst occurring in any 42-minute period, irrespective of the occurrence of flares, can readily be obtained from the radio-noise recordings. With a knowledge of the chances of occurrence of flares of various intensities it is then possible to derive, from the observed coincidence rates of bursts with flares, the average rate of occurrence of bursts in a 42-minute interval when no flare is present.

Let p_1, p_2, p_3 be the chances of a burst occurring in the given interval when flares of intensity 1, 2 and 3 respectively are observed, and let q_1, q_2, q_3 be the chances of occurrence of flares 1, 2 and 3 in this time interval; if more than one flare occurs in the time interval, the intensity taken is that of the greatest. Let p_0 be the average chance of occurrence of a burst when there is no flare, and p_a the average chance irrespective of the occurrence of a flare, the time interval being the same, namely 42 minutes in each case. Then we have:—

$$p_a = p_1q_1 + p_2q_2 + p_3q_3 + p_0[1 - (q_1 + q_2 + q_3)]. \qquad (1)$$

* H. W. Newton, *M.N., Geophys. Suppl.*, **5**, 200, 1948.

From this expression p_0 may be determined as follows. The values p_1, p_2 and p_3 for the observed chances of flare-burst coincidences are given in Table I. (Although 42 minutes is the average time interval, and the distribution of individual time intervals with respect to the average may bias the results, it is considered that any such bias would probably be small and would not affect the general conclusions.) p_a, the average rate of occurrence of bursts, determined from the 1947 radio-noise records, is given in Table IV, line a. The average chance of the occurrence of flares was derived from the I.A.U. Bulletin for the first quarter of 1947 from the data of flare occurrences when the Sun was under continuous visual observation for periods of 42 minutes or more. It was found that the chance of a flare occurring during a 42-minute interval was 11 per cent. The total number of cases is too small for a reliable determination of the intensity distribution. The proportions derived by Newton and Barton * have therefore been used; they found that of all flares observed in 1935 and 1936 the relative proportions with intensities 1, 2 and 3 were 77 : 19 : 4. Our criterion, that if more than one flare occurs only the largest is counted, affects the distribution only very slightly. The chances of occurrence, q_1, q_2, q_3 of flares of intensity 1, 2 and 3 are thus estimated to be 8·5 per cent, 2·1 per cent and 0·4 per cent respectively. Equation (1) may now be used to derive p_0, the chance of occurrence of bursts in a 42-minute period when there is no flare, and the results obtained are given in Table IV, line b.

A quantitative assessment of the significant correlations can now be made. For if P_1, P_2, and P_3 are the chances of a significantly correlated radio burst occurring when there are flares of intensity 1, 2 and 3 respectively, then we have:—

$$P_1 = \frac{p_1 - p_0}{1 - p_0} \text{ and similar expressions for } P_2 \text{ and } P_3.$$

TABLE IV

Summarized table of coincidences between solar flares and radio bursts

	Flare Phenomena during 42 minute interval		Percentage of Cases with Radio Bursts of Intensity :—			
			>0	$>\frac{1}{2}$	>1	>2
a	Irrespective of Flares		26	17	$6\frac{1}{2}$	3
b	No Flare		25	$15\frac{1}{2}$	5	$2\frac{1}{2}$
c	Flares of Intensity	1	32 (10)	23	12	3
		2	48 (31)	39	30	13
		3	57 (43)	57	43	21
d	Type of Fade-out	Weakening	33 (11)	27	22	10
		Some links C.F.O.	51 (34)	38	36	23
		All links C.F.O.	69 (59)	62	50	36

The figures in brackets are corresponding numbers for radio bursts which are assessed as significantly correlated with the flare phenomena.

* H. W. Newton and H. J. Barton, *loc. cit.*

The results of this assessment are given in Table IV, line c, for visually observed flares, and in Table IV, line d, for the flares which produce the radio communication fade-outs.

Table IV shows that the chance of a significant burst occurring increases with increasing flare intensity. The significance of the coincidences also tends to increase with radio burst intensity. Some examples of large radio bursts and the associated flare data are shown in Figs. 1, 2 and 3.

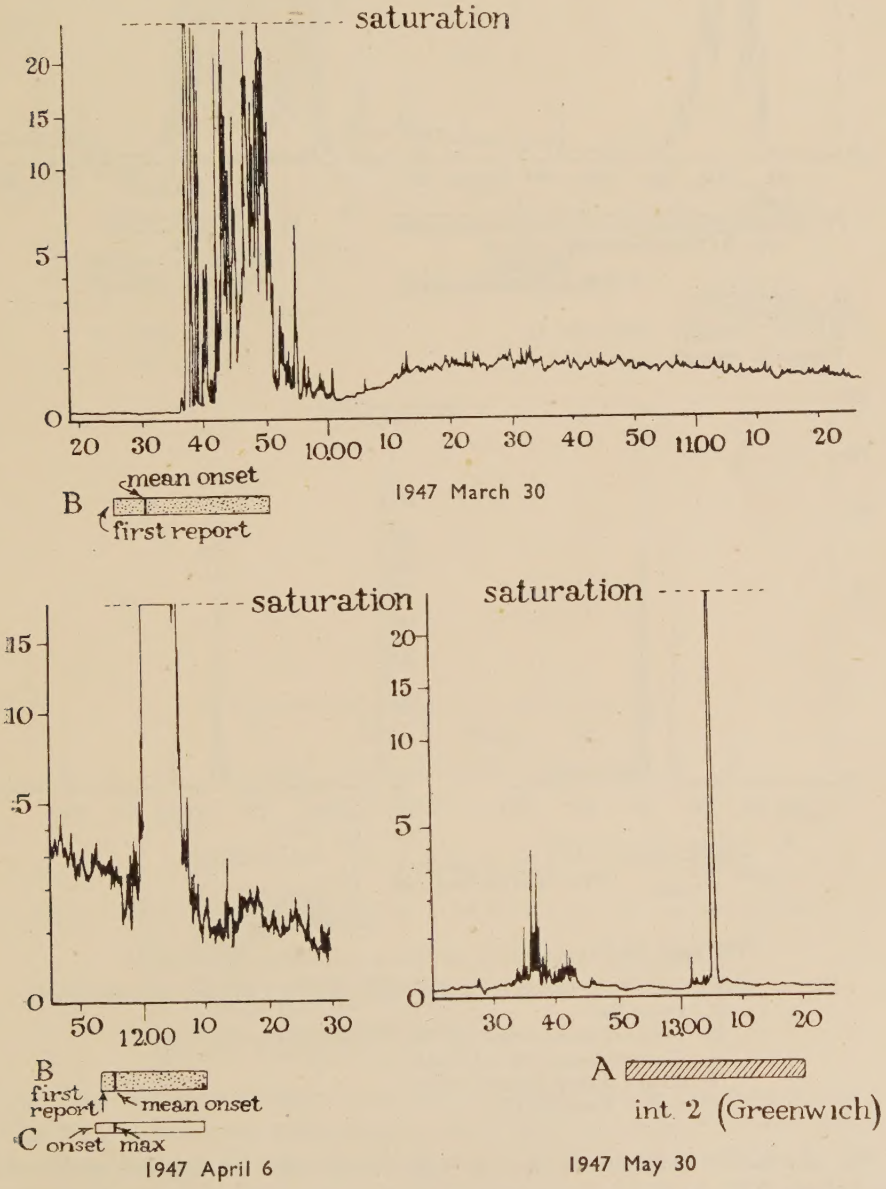

FIG. 1.—*Large radio bursts (observed at A.O.R.G. on λ=4·1 m.) and associated data.*
A: *Solar flare.*
B: *Radio communication fade-out (Cable and Wireless Ltd.).*
C: *Magnetic crochet (Abinger).*
Ordinates: Power (relative units).
Abscissae: Time (U.T.).

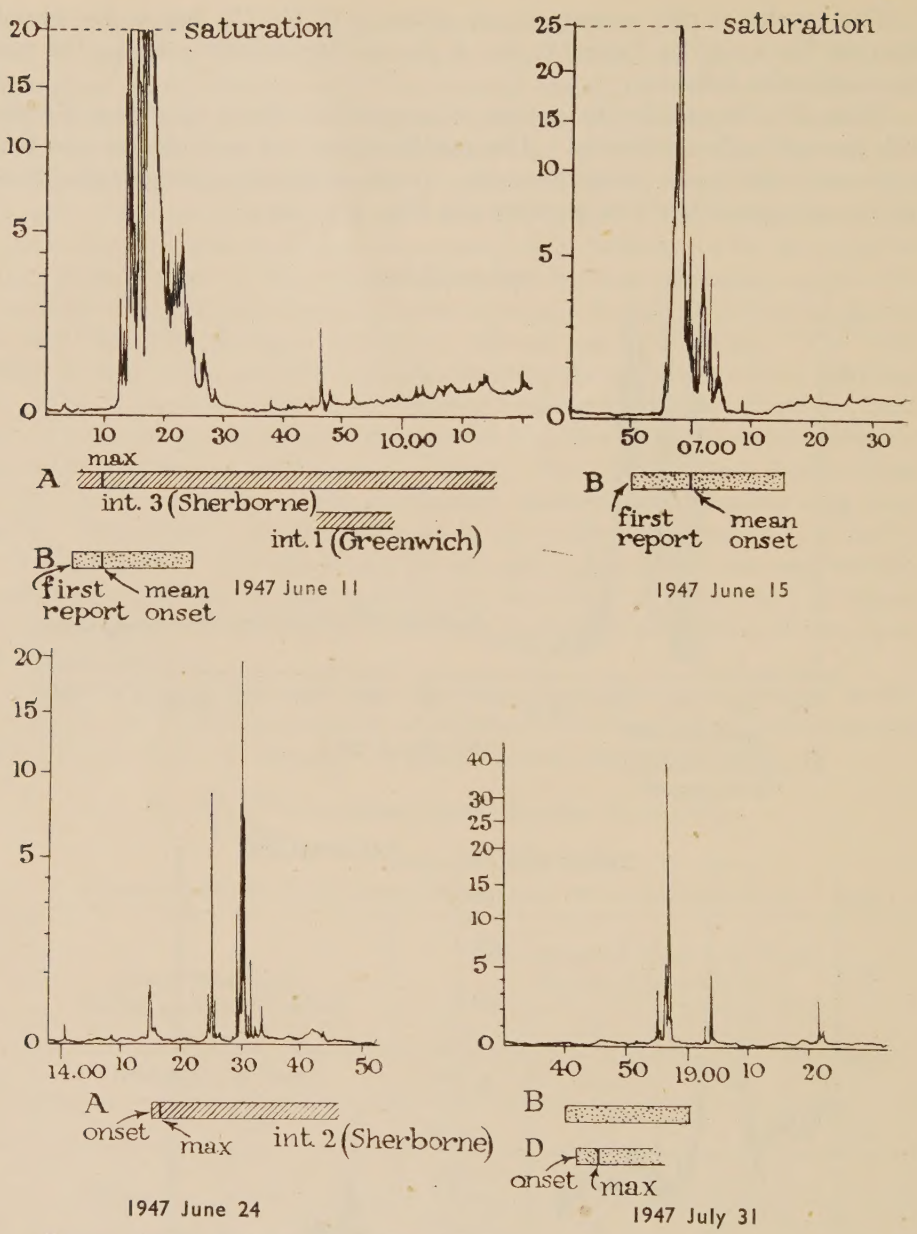

FIG. 2.—*Large radio bursts (observed at A.O.R.G. on λ=4·1 m.) and associated data.*
A : *Solar flare.*
B : *Radio communication fade-out (Cable and Wireless Ltd.).*
D : *Galactic noise fade (A.O.R.G.).*
Ordinates : Power (relative units).
Abscissae : Time (U.T.).

An alternative method of testing significance can be applied to the radio fade-out data by comparing the rate of occurrence of bursts a few hours before and after with that within the fade-out period. Such a test has been carried out for a period of $\pm 1\frac{1}{2}$ hours beyond the counted fade-out period. If the rate of occurrence of bursts within the fade-out period was greater than that in the

adjacent periods, then we may regard the coincidence of bursts and fade-out as probably significant. It was found that 92 per cent of the cases satisfied this test. This suggests that the significant proportion as given in Table IV is not overestimated.

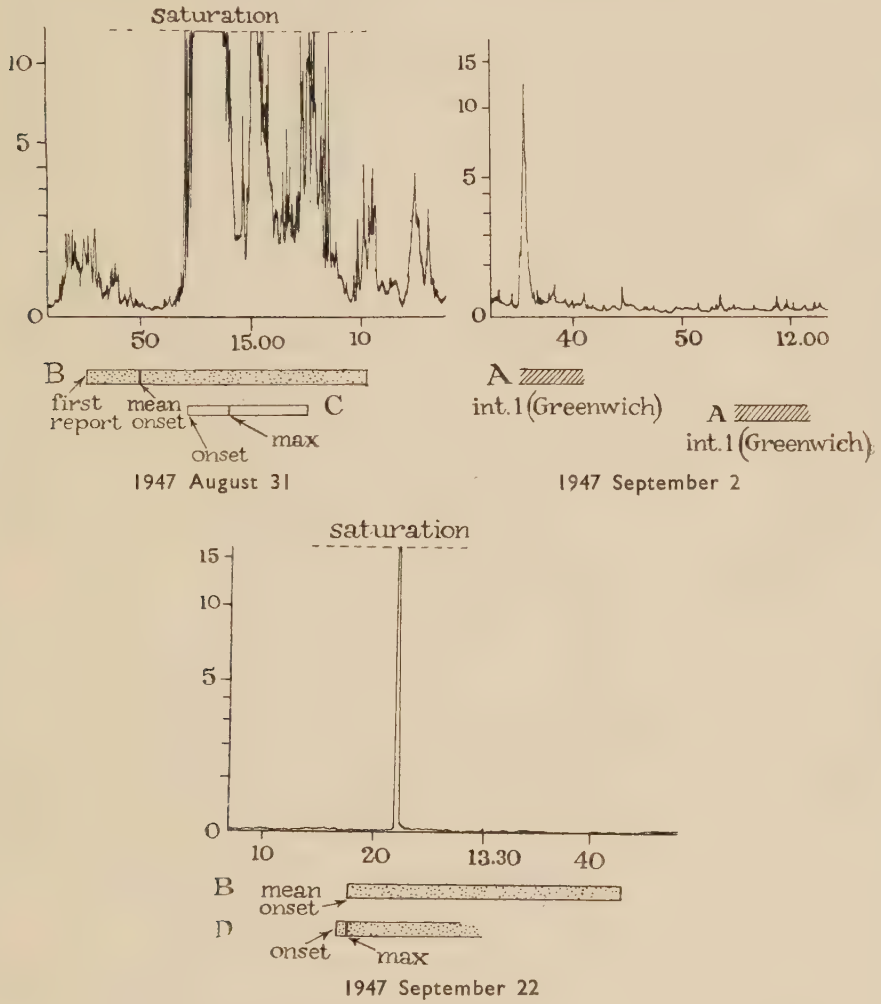

FIG. 3.—*Large radio bursts (observed at A.O.R.G. on λ=4·1 m.) and associated data.*
A : *Solar flare.*
B : *Radio communication fade-out (Cable and Wireless Ltd.).*
C : *Magnetic crochet (Abinger).*
D : *Galactic noise fade (A.O.R.G.).*
Ordinates : Power (relative units).
Abscissae : Time (U.T.).

3.5. *Time Difference between Radio Bursts and Solar Flares.*—Isolated examples of a time lag of radio bursts with respect to flares have been reported by the authors * and by Payne Scott, Yabsley and Bolton.† We know from Table IV that a coincidence between an intense flare and an intense burst has a high probability of being a significant association. Unfortunately the number of cases in which

* J. S. Hey, S. J. Parsons and J. W. Phillips, *Nature*, **160**, 371, 1947.
† J. L. Payne Scott, D. E. Yabsley and J. G. Bolton, *Nature*, **160**, 256, 1947.

such bursts have occurred when a visual flare has been seen for which the times of commencement and maximum intensity are known are too few for any general appreciation of time differences.

We must, therefore, again rely on radio communication fade-outs to provide a more comprehensive list of cases. If we take only those cases which satisfy the significance test referred to at the end of Section 3.4 and for which not less than two communication links reported complete fade-outs, we find that in 88 per cent of the cases the burst onset came later than the first reported fade-out commencement and the average time lag of the bursts was $13\frac{1}{2}$ minutes. Now Newton and Barton * found that on the average the reported fade-out commencement was 4 minutes after the beginning of the solar flare. If we take this into consideration, then the average time lag of the onset of the radio burst after the onset of the flare is more than 17 minutes. Although, then, from the available information one cannot rule out the possibility of a significantly connected burst occurring before the flare onset, there is plainly a marked tendency for the bursts to occur after the beginning of the flares. This accords with the explanation offered by the authors (1947) and by Payne Scott, Yabsley and Bolton (1947), that the visible and ultra-violet emissions from a flare occur at a chromospheric level where the electron density is too great for a radio disturbance to escape; if the disturbance travels outwards from the Sun with a velocity less than that of light (for example, as a corpuscular stream) associated radio emissions will be able to escape when the disturbance reaches higher levels in the corona where the electron density is sufficiently small.

A discussion of time differences between phenomena would be incomplete without a comparison of the curves of intensity plotted as a function of time. Newton and Barton † state that, in general, flares rise rapidly to maximum intensity in 5 to 10 minutes and decline slowly. Ellison ‡ has demonstrated the type of intensity curve in detail by a series of measurements of $H\alpha$ line-width made at short intervals during the progress of a number of flares. Comparison with the intensity curves for radio bursts, as illustrated in Figs. 1, 2 and 3, indicates that the latter are far more spasmodic and irregular in form. The radio emission fluctuates tremendously in amplitude, but there is often discernible a major peak which may, in the largest radio bursts, represent an increase of intensity of the order of 1000 times occurring in a time of the order of a minute.

As the variation of intensity generally shows different forms for the radio and visual radiations associated with solar flares, it is of interest to compare not only the differences between the times of onset but also the differences between the times of maximum intensity. Unfortunately, details of the times of the maxima for high-intensity flares with associated radio bursts are available in only a few instances during the present period of analysis.

Ellison § made detailed measurements of $H\alpha$ line-width during the great flare (intensity 3+) of 1946 July 25. He describes the radiation burst in $H\alpha$ emission lasting 2–3 minutes and he estimates the peak to have occurred at $16^h\ 27^m \pm 1^m$. Radio observations by the authors showed a peak reaching saturation between $16^h\ 24^m$ and $16^h\ 32^m$. An examination of the curves of $H\alpha$

* H. W. Newton and H. J. Barton, *loc. cit.*
† H. W. Newton and H. J. Barton, *loc. cit.*
‡ M. A. Ellison, *M.N.*, **103**, 3, 1943; *M.N.*, **106**, 500, 1946.
§ M. A. Ellison, *loc. cit.*

line-width and radio intensity indicates that in this instance the peaks were approximately simultaneous. On the other hand, the radio intensity curve shown in Fig. 2, obtained on 1947 June 24 while a flare (intensity 2) was being observed at Sherborne, may be taken as an example of a time difference between the maxima of the two phenomena. The maximum flare intensity occurred at $14^h\ 17^m$, but Fig. 2 shows the maximum intensity of radio emission at about $14^h\ 30^m$; it may be noted that the first radio burst probably associated with this flare occurred at the same time as the flare onset $14^h\ 15^m$. The radio burst associated with a flare (intensity 3+) on 1947 June 11, shown in Fig. 2, is an example of a time lag in the onsets and maxima of the radio burst with respect to $H\alpha$ emission. The flare was already in progress at $09^h\,06^m$, the commencement of the visual observations at Sherborne, and the maximum $H\alpha$ intensity occurred at $09^h\ 10^m$. The radio burst commenced at $09^h\ 12^m$, and although the time of maximum intensity is somewhat uncertain owing to saturation of the receiver, it was not before $09^h\ 13^m$.

The examination of the time differences may be supplemented by the analysis of the intensity-time relations between solar radio bursts and the D-layer ionization arising from the enhanced ultra-violet radiation from solar flares. The D-layer ionization is perhaps best indicated by the attenuation of galactic radio noise at wave-lengths of about 12–15 metres, as described by Jansky * and the authors †, but, unfortunately, owing to the difficulty of making highly-directional aerials at long wave-lengths, the attenuation may be masked by solar radio emissions. Alternatively, D-layer ionization is roughly indicated by the data of radio communication fade-outs. A comparison of 15 cases where time of maximum galactic radio attenuation (at $\lambda = 12$ metres) could be compared with the mean time at which the various communication links reported the fade-outs, showed that the time difference, maximum galactic noise attenuation minus mean fade-out onset was in every case not more than a few minutes, the average value being $2^m{\cdot}3$. An analysis of 31 cases of intense radio fade-outs and associated radio bursts shows that the mean time difference, maximum of solar radio burst minus mean fade-out onset is $6^m{\cdot}9$. Thus, if we assume that the maximum D-layer ionization is on the average $2^m{\cdot}3$ later than the mean fade-out onset, we find that the radio burst maximum occurs on the average about $4\frac{1}{2}^m$ after the maximum D-layer ionization. We thus conclude that, in general, the maximum radio burst intensity lags behind the maximum ultra-violet flare emission, but the time difference is smaller than that between the onsets of the two phenomena. It may be noted here that the absorption of radio waves by the D-layer is proportional to λ^2, and at a wave-length of 4·1 metres used for the observation of solar radio bursts it is generally negligible. We may thus disregard this as an effect making any real contribution to the time differences estimated above.

The curves shown in Figs. 1, 2 and 3 serve to illustrate the time-differences discussed above. The curve of radio intensity for 1947 September 22 in Fig. 3, for example, shows a striking single burst at $13^h\ 22^m$ of duration approximately $\frac{1}{2}^m$. The fade-out was very sharp for all links at $13^h\ 18^m$ and the maximum galactic radio-noise attenuation occurred at $13^h\ 18^m$ also. The radio burst phenomenon thus lags by approx. 4^m. Similarly, examples of radio burst time

* K. G. Jansky, *Proc. I.R.E.*, **25**, 1517, 1937.
† J. S. Hey, S. J. Parsons and J. W. Phillips, *loc. cit.*

lags will be seen in Figs. 1, 2 and 3; but in one case, that of 1947 June 15 in Fig. 2, although the radio burst onset at $06^h\ 55^m$ came after the first fade-out report at $06^h\ 50^m$, the maximum of the burst at $06^h\ 57^m$ occurred before both the mean fade-out onset report at $07^h\ 00^m$ and the maximum galactic noise attenuation estimated at about $07^h\ 03^m$. Cases of the radio burst phenomenon preceding the enhanced $H\alpha$ or ultra-violet radiation are exceptional.

Several cases of the time relations between magnetic crochets and radio bursts are given in Table III. With one exception, the radio burst phenomena come a few minutes later.

3.6. *Effect of Solar Longitude from Central Meridian on the Correlation of Solar Flares and Radio Bursts.*—Any influence of position on the relation between solar flares and radio bursts can, of course, only be studied for flares seen directly on the Sun's disk. This means that the number of cases for any given region of the Sun is fairly small for a period of analysis as short as eighteen months. It was noticed, however, when the coincidences between solar flares and radio bursts were plotted in coordinates of solar latitude and longitude, that both in 1946 and in 1947 there was a tendency for the proportion of coincidences to be higher for eastern than for western flares. The eastern half of the Sun's disk is the visible surface which, as the Sun rotates, is approaching central meridian passage, while the western half is the receding visible surface. This asymmetrical effect of solar longitude on flare-burst coincidences is shown in Fig. 4. The results are plotted (a) as the proportions of coincidences for groups within longitude intervals chosen so as to keep the numbers in each group approximately constant, in this case around 20, and (b) as the average radio burst intensity per flare. As we have shown, however, that the significant proportion of coincidences between flares and bursts is little more than 30 per cent for flares of intensity 1, and these form the greater part of the observations, too much reliance cannot be placed on the form of the distribution shown in Fig. 4. More data are needed before firm conclusions can be drawn.

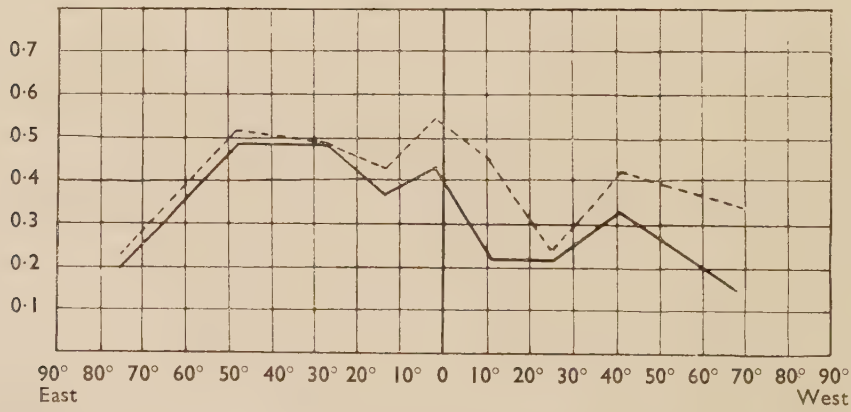

Fig. 4.—*Effect of solar longitude from central meridian on coincidences between solar flares and radio bursts.*
Continuous line: No. of bursts/No. of flares. Broken line: Burst intensities/No. of flares.

A radio burst asymmetry with respect to solar longitude from central meridian might be caused in the following manner. Solar flares occur in the vicinity of sunspots, that is in disturbed regions of the Sun. Now Milne * has shown

* E. A. Milne, *M.N.*, **86**, 457, 1926.

that from disturbed regions one might expect atoms and ions to be expelled with velocities of the order of 1600 km. per sec. As pointed out by Chapman and Ferraro *, the streams would be likely to consist of neutral and ionized atoms and electrons, the latter being carried forward with the positive ions by electrostatic attraction. If the electron density and collision rate are sufficient, radio waves which traverse a solar corpuscular stream may undergo appreciable absorption. The geometry of solar streams has been discussed by Chapman †, who considered the possibility of detecting such streams by their absorption of solar light. He showed that although we may expect the particles to move essentially in straight lines from the Sun, the effect of the Sun's rotation is such that the envelope of the stream becomes curved, as shown in Fig. 5. This diagram also illustrates how the envelope of the stream overtakes the Earth in its orbital motion. It is also seen that owing to the curvature of the stream the straight path from the disturbed region to the Earth traverses a considerable distance within the stream when the region is West of central meridian, but not when the region is East. If appreciable absorption of radio bursts occurs a lower correlation of radio bursts and solar flares West of central meridian might be expected.

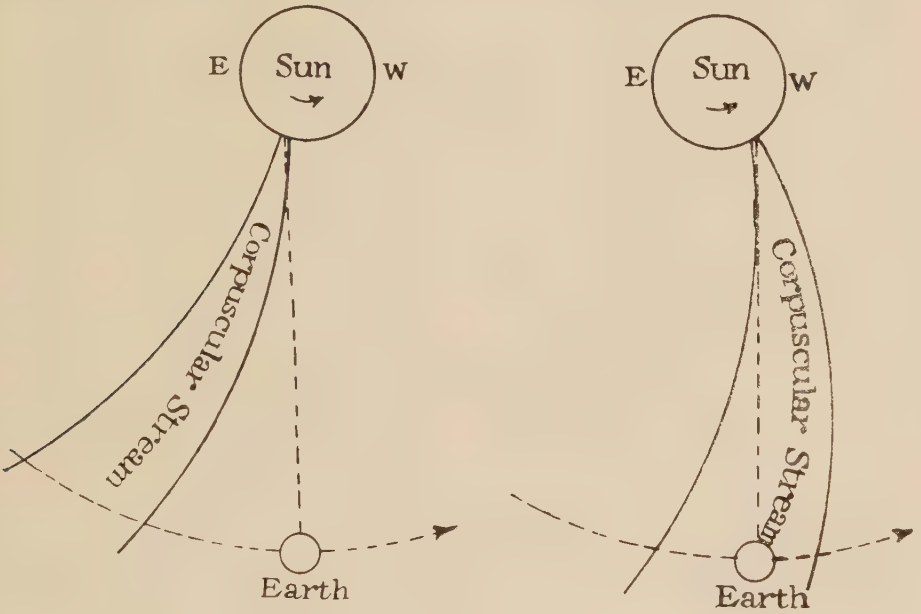

Fig. 5.—*Illustration of asymmetrical effect of solar corpuscular streams.*

Fig. 4 suggests that such absorption effects may occur over a considerable range of solar longitudes and are particularly marked from about 0° to 50° W. We would expect the extent to depend on the initial angular width of the emitted stream and on the velocity which determines the curvature of the envelope. Chapman ‡ derived an angular width of the order of 25° from a consideration of the average duration of the mature-stream type of magnetic storm. Newton § showed that for the great magnetic storms associated with intense solar flares

* S. Chapman and V. C. A. Ferraro, *M.N.*, **89**, 470, 1929.
† S. Chapman, *M.N.*, **89**, 456, 1929.
‡ S. Chapman, *M.N.*, *loc. cit.*
§ H. W. Newton, *M.N.*, **103**, 4, 1944; *M.N.*, **104**, 244, 1944.

the average stream velocities agree well with the values predicted on Milne's theory. Newton found that the equivalent cone of emission may be sometimes as great as 90°. The suggested explanation of the flare-burst asymmetry in terms of solar stream absorption seems feasible from considerations of stream-width. It would appear that a test of the correctness of the absorption theory might be made by comparing the flare-burst coincidence rates for flares which occur just prior to and during magnetic storms with those at other times. At present the total numbers of occurrences are insufficient for any conclusions to be reached. The asymmetry should also be more marked at longer radio wave-lengths, since radio absorption increases with wave-length.

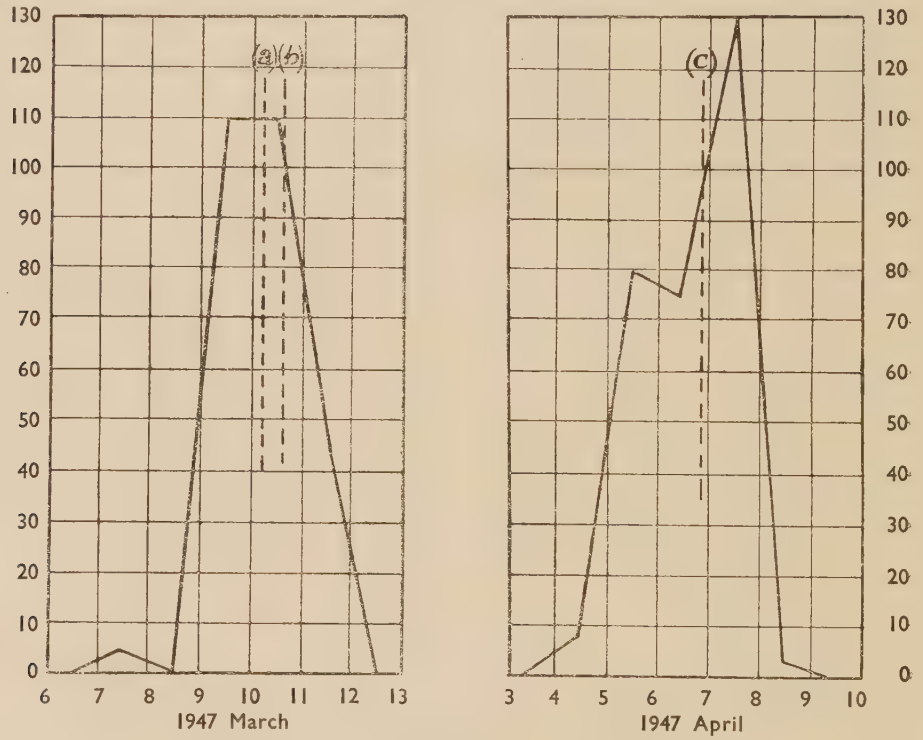

FIG. 6.—*Mean level of solar radio emission from sunspots.*

(*a*) *Central meridian passage*: *March* 10·2
Area: 4300. *Latitude*: −23°.
Earth's latitude: −7°.

(*b*) *Central meridian passage*: *March* 10·6
Area: 1400. *Latitude*: +13°.

(*c*) *Central meridian passage*: *April* 6·8
Area: 5400. *Latitude*: −24°.
Earth's latitude: −7°.

Ordinates: *Power flux in units of* 10^{-21} *watts/sq. m.c.p.s.*

4. *Radio Emission from Sunspots.*—The more continuous emission of radio noise which can be associated with sunspots will now be considered. The intensity of the sunspot radiation often fluctuates very considerably and rapidly, but it is usually possible to make rough estimates of mean level. The average levels around noon for several spots are shown in Figs. 6 and 7. An inspection of the radio and spot data * has shown that of the spots with areas greater than

* The spot data have been obtained from the Solar Notes in *The Observatory*, and from *Publications of the Astronomical Society of the Pacific*.

1000 millionths of the Sun's visible hemisphere, fewer than half produced any measurable continuous radio emission; and although there tends to be a greater chance of emission with increasing size of spots there is no simple proportionality.

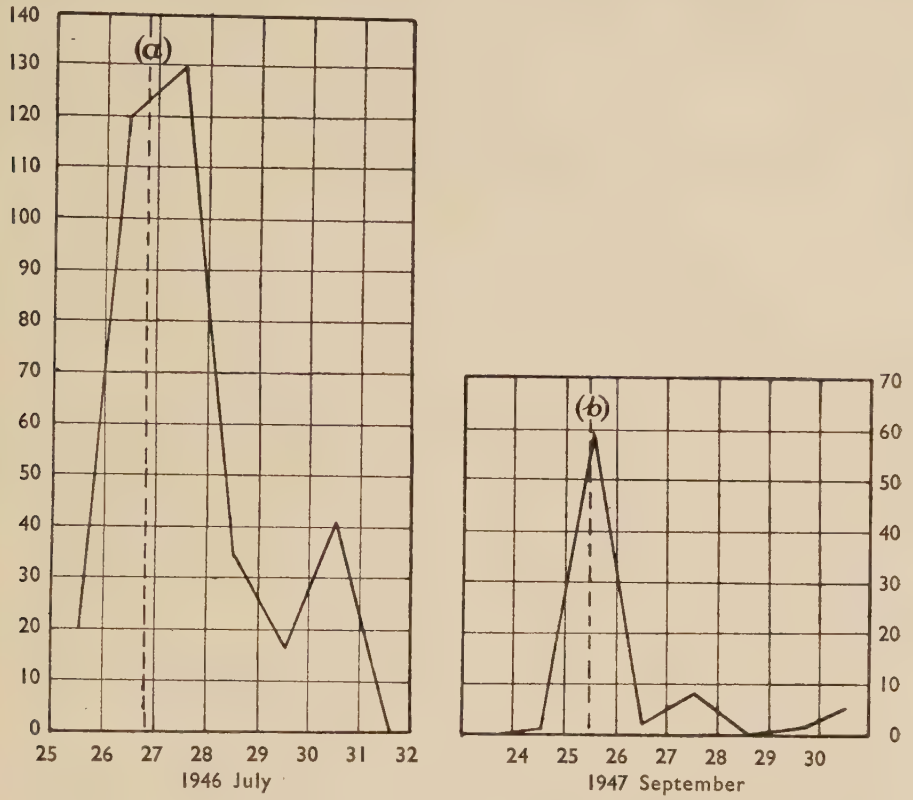

FIG. 7.—*Mean level of radio emission from sunspots.*
(*a*) *Central meridian passage*: *July* 26·9. *Area*: 3685. *Latitude*: +23°. *Earth's latitude*: +6°.
(*b*) *Central meridian passage*: *September* 25·5. *Area*: 750. *Latitude*: +17°. *Earth's latitude*: +6°.
Ordinates: *Power flux in units of* 10^{-21} *watts/sq. m.c.p.s.*

It is readily seen from Figs. 6 and 7 that the intensity of the radiation attains a sharp peak near central meridian passage of the spots. Particulars of the five most strongly radiating spots which occurred between 1946 March and 1947 September are listed below.

TABLE V

Date of Central Meridian Passage	Area of Spot (in millionths of solar hemisphere)	Max. Radio Int. Level (in units of 10^{-22} watts/sq. m.c.p.s.)	Solar Rotation between Radio Int. Levels $\frac{1}{10}$ of Max.	Heliographic Latitude of	
				Spot	Earth
1946 July 26·9	3685	1300	56°	+23°	+6°
1946 Dec. 17·0	2600	500	25	− 6	−1
1947 Mar. 10·2	4300	1100	49	−23	−7
1947 Apr. 6·8	5400	1300	48	−24	−7
1947 Sept. 25·5	750	600	24	+17	+6

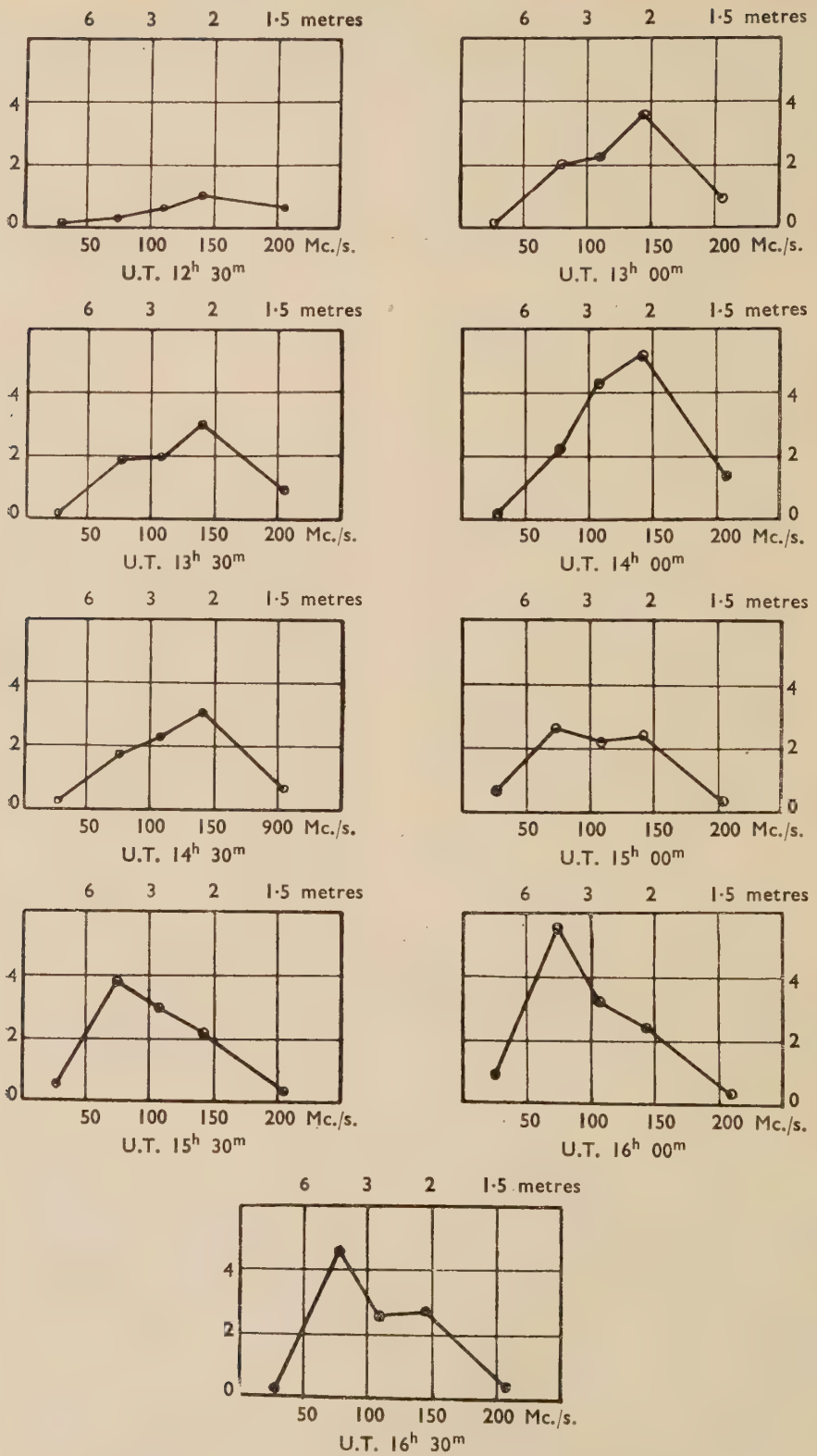

FIG. 8.—*Solar radio spectrum obtained on 1947 September 25.*
Wave characteristics shown in wave-length (metres) and frequency (Mc./s).
Ordinates: Power flux in units 10^{-20} *watts/sq.metre/c/s band-width.*

The mean angle of solar rotation between mean intensity levels of $\frac{1}{10}$ maximum for these spots is 40°. From the heliographic latitudes given in Table V (the difference between that of the spot and that of the Earth is in all cases less than half the solar rotation) it can be seen that the average beam-width across the centre of the spot will not be much greater than 40°. We thus have a fairly directional beam with its axis approximately normal to the spot. There are too few examples and the mean level is too uncertain to establish whether any bias exists with respect to central meridian passage. The narrowness of the beam would in any case make it difficult to detect the asymmetry observed in flares. It may be of interest to note here the possibility of a bias due to another cause. A. S. D. Maunder * found that on the average more spots occur on the eastern half of the Sun than on the western, and an interpretation has been suggested by Minnaert † by assuming that the spot axes are tilted westwards from the vertical by amounts of the order of 5° for long-lived spots.

In conclusion it must be emphasized that the wave-length of 4·1 metres for observation of the solar radio emissions was to some extent an arbitrary choice, and simultaneous observation over a very wide radio wave-length band is desirable. In Table III, for example, we referred to a radio burst which appeared at wave-lengths of 1·5 metres and 2 metres but not at 4·1 metres. Measurements of sunspot radio emission made at five wave-lengths between 1·5 metres and 12 metres on 1947 September 25, are illustrated in Fig. 8; these show the maximum intensity of power flux first at about 2 metres and 2 hours later at about 4 metres. Nevertheless, experience so far has indicated that both the continuous type of emission from sunspots and the bursts associated with flares can generally be detected over a wide band of wave-lengths, and that although the spectral distribution is variable the maximum intensity often appears to be in the region of 5 metres.

5. *Acknowledgments.*—We are particularly indebted to Mr H. W. Newton, of the Royal Observatory, Greenwich, with whom we have had many valuable discussions. We also wish to thank Sir Edward Appleton, Professor S. Chapman, Dr R. d'E. Atkinson and Dr A. Hunter for helpful remarks included in the revision of the text.

We are indebted to the Astronomer Royal, Dr M. A. Ellison and Mr F. Sellers for the supply of data in advance of publication from the Observatories at Greenwich, Abinger, Sherborne and Muswell Hill, and to Cable and Wireless Ltd. for data of radio communication fade-outs.

We wish to thank all our assistants at the Operational Research Group for their valuable help in the preparation and maintenance of the radio-noise apparatus, and in the subsequent analysis of the results.

Finally, we wish to thank the Scientific Adviser and Deputy Scientific Adviser, War Office, and Superintendent, Army Operational Research Group, for their interest in the work and permission to publish this paper.

Army Operational Research Group,
Broadoaks, West Byfleet:
1948 *September 7.*

* A. S. D. Maunder, *M.N.*, **67**, 451, 1907.
† M. G. J. Minnaert, *M.N.*, **106**, 98, 1946.

A NEW MODEL FOR THE EXPANDING UNIVERSE

F. Hoyle

(Received 1948 August 5)

Summary

By introducing continuous creation of matter into the field equations of general relativity a stationary universe showing expansion properties is obtained without recourse to a cosmical constant.

---

1. *Introduction.*—Creation of matter was mentioned about twenty years ago by Jeans (1) who remarked:

"The type of conjecture which presents itself, somewhat insistently, is that the centres of the nebulae (galaxies) are of the nature of singular points, at which matter is poured into our universe from some other and entirely extraneous spatial dimension, so that, to a denizen of our universe, they appear as points at which matter is being continually created". Subsequent astrophysical developments have, however, shown little support for this particular form of creation.

More recently Dirac (2) has pointed out that continuous creation of matter can be related to the wider questions of cosmology. The following work is concerned with this aspect of the matter and arose from a discussion with Mr T. Gold who remarked that through continuous creation of matter it might be possible to obtain an expanding universe in which the proper density of matter remained constant. This possibility seemed attractive, especially when taken in conjunction with aesthetic objections to the creation of the universe in the remote past. For it is against the spirit of scientific enquiry to regard observable effects as arising from "causes unknown to science", and this in principle is what creation-in-the-past implies.

The writer's thanks are due to Mr H. Bondi for valuable comments on the present paper and also for many discussions on the general problems of cosmology.

2. *Newtonian Universes.*—We begin by mentioning the difficulties occurring in current theories of the expanding universe. A comprehensive review of cosmology, based on Einstein's general theory of relativity, has been given by Robertson (3). Milne and McCrea (4) have obtained the remarkable result that Newtonian analogues exist for all the more important models considered by Robertson. Although later we shall go over to the formalism of the relativity theory, it is convenient in these preliminary remarks to use the Newtonian equivalent models.

The work of Milne and McCrea starts from the cosmological principle applied in the narrow sense. According to the narrow cosmological principle, the distribution of material and momentum relative to an observer attached to a particular particle is identical with the distribution relative to an observer attached to any other particle, provided the comparison *refers to the same value of the time.* The latter proviso weakens the equivalence of observers. When the cosmological principle is used in its wide sense this proviso is removed and equivalence would have to be applied even if the two observers carried out their measurements at different times. It is important to notice that the cosmological principle ignores proper motions arising from local condensations of matter. That is,

we refer to an approximation in which the matter within the extragalactic nebulae is regarded as being smeared into a continuous background. This approximation will be used throughout the present paper, except in the general discussion in Section 5.

Take an observer attached to a given particle and let $\boldsymbol{r}$ be a position vector measured by this observer. The relative motion of a particle situated at $\boldsymbol{r}$ at time t will be denoted by $\boldsymbol{v}(\boldsymbol{r}, t)$. Then it is easy to show (**4**) that the narrow cosmological principle requires the material density ρ to be a function of t only, and that $\boldsymbol{v}(\boldsymbol{r}, t)$ must be of the form $F(t)\boldsymbol{r}$, where $F(t)$ also depends only on the time. Defining $R(t)$ by

$$R(t) = \exp\left\{\int_{t_0}^{t} F(t)\,dt\right\}, \tag{1}$$

where t_0 is arbitrary, we obtain

$$\boldsymbol{v}(\boldsymbol{r}, t) = R'\boldsymbol{r}/R, \tag{2}$$

where $R' = dR/dt$. In the strictly Newtonian problem a particle at $\boldsymbol{r}$ experiences an acceleration $\boldsymbol{G}$, relative to our observer, given by

$$\boldsymbol{G} = -4\pi\gamma\rho\boldsymbol{r}/3, \tag{3}$$

where γ is the Newtonian constant of gravitation. The equations of motion are

$$\partial\rho/\partial t + \operatorname{div}(\rho\boldsymbol{v}) = 0, \tag{4}$$

$$\partial\boldsymbol{v}/\partial t + \tfrac{1}{2}\operatorname{grad}\boldsymbol{v}^2 = \boldsymbol{G}. \tag{5}$$

In deriving (5) from the standard Eulerian equation we neglect the hydrostatic pressure, which is small in the cosmological problem, and we take account of the fact that $\operatorname{curl}\boldsymbol{v} = 0$.

It can be verified that

$$\rho R^3 = B, \tag{6}$$

$$\boldsymbol{v}^2 = (8\pi\gamma\rho/3 - k/R^2)\boldsymbol{r}^2, \tag{7}$$

where B, k are constants of integration, give the general solution of (4), (5). When $k = 0$ the material possesses the minimum kinetic energy necessary for unlimited expansion. Unlimited expansion also occurs in the case $k < 0$, since the material then has excess kinetic energy. But when $k > 0$ expansion is of limited duration. These cases are conveniently described as parabolic, hyperbolic and elliptic. As a description of the expanding universe, the elliptic case is evidently inferior to the parabolic and hyperbolic cases. Moreover, the parabolic case is superior to the hyperbolic case, *since localized condensations, necessary for the formation of extragalactic nebulae, can readily occur in a parabolic but not in a hyperbolic universe.* For in the parabolic case condensations will form even if the density only exceeds the mean value by a small margin, whereas an appreciable increase of density would be required in the hyperbolic case. Accordingly it is sufficient to confine the discussion of (7) to the case $k = 0$. We then have the Newtonian analogue, derived by Milne (**4**), of the Einstein-de Sitter relativistic model in flat expanding space (**5**).

With the simplification $k = 0$, (7) may be integrated by using (2) and (6). This gives, for the solution representing outward motion,

$$\boldsymbol{v} = 2\boldsymbol{r}/3t, \tag{8}$$

$$\rho = 1/6\pi\gamma t^2, \tag{9}$$

the zero of time being arranged so that $R=0$ at $t=0$. Now the velocity-distance relation, found by Hubble and Humason from the observation of extragalactic nebulae, can be written as

$$\boldsymbol{v} \doteq (5/3) \cdot 10^{-17} \boldsymbol{r} \tag{10}$$

when time is measured in seconds. We see that for (8) to agree with (10), t must be about 4×10^{16} sec., which is about $1{\cdot}3 \times 10^{9}$ years. The corresponding value of ρ is about 5×10^{-28} g. per cm.^{3}.

It is important to notice that, in common with all current cosmological models, no attempt is made to show how the required distribution of material and momentum comes to be set up. The implication of (8), (9) is that if these equations are satisfied for one value of t, then they will be satisfied at all subsequent times. Thus, according to these equations, ρ, $\boldsymbol{v}^2$ were infinite at $t=0$; that is, about $1{\cdot}3 \times 10^{9}$ years ago. Although effects not considered in our equations would intervene to prevent strict divergence, the conclusion seems inescapable that near $t=0$ the density would be very large compared with the present value. Quite apart from its unsatisfactory nature, this conclusion is in discordance with astrophysical data which strongly suggest that physical conditions have not changed appreciably over a period of about 5×10^{9} years. In this connection it may be noted that geophysical studies give about 2×10^{9} years for the age of the Earth.

These difficulties suggest that alternative possibilities, based on the introduction of a cosmical constant into (3), be considered. When (3) is altered to

$$\boldsymbol{G} = \tfrac{1}{3}(-4\pi\gamma\rho + \lambda c^2)\boldsymbol{r}, \tag{3'}$$

where λ is a constant, the solution of (4), (5) is given by (2), (6) and by

$$\boldsymbol{v}^2 = (8\pi\gamma\rho/3 - k/R^2 + \lambda c^2/3)\boldsymbol{r}^2. \tag{7'}$$

This solution admits of two cases that satisfy the wide cosmological principle. First, we have the analogue of Einstein's static universe when

$$4\pi\gamma\rho = \lambda c^2 = k/R^2. \tag{11}$$

These conditions give $\boldsymbol{v}=0$, $\partial\boldsymbol{v}/\partial t=0$, $\boldsymbol{G}=0$, and R is independent of time. Since $\boldsymbol{G}=0$, localized condensations may occur in this model. Second, the analogue of the de Sitter empty universe is obtained by putting $k=0$, $\rho=0$. Then physically observable quantities, such as $\boldsymbol{v}$, are independent of time, but R, which is not directly observable, varies like $\exp\{(\lambda/3)^{\frac{1}{2}} ct\}$. Unfortunately neither of these cases satisfies observational requirements; the Einstein model has no expansion and the de Sitter model contains no material.

The Friedmann non-stationary models can be obtained by taking other values of λ, k. A specially interesting case, considered by Lemaître and Eddington, arises from a perturbed Einstein static universe. For, as Eddington (**6**) has pointed out, the Einstein model is unstable against a small change of R. A decrease in R leads to contraction, whereas a slight increase of R leads to unlimited expansion. In the Lemaître-Eddington model the latter case is assumed. The rate of expansion is at first very slow, but as the $8\pi\gamma\rho/3$, k/R^2 terms in (7') become small compared with the $\lambda c^2/3$ term, the Lemaître-Eddington model tends asymptotically to the de Sitter empty universe.

Objections to the Lemaître-Eddington universe are subtler than the difficulties occurring in other models. The force $\boldsymbol{G}$ is repulsive except during the pre-expansion stage. Thus, localized condensations can only be formed during

this stage (**7**, **8**). This conclusion is in contradiction with astrophysical data which indicate that, quite apart from their general expansion, the extragalactic nebulae are in a vigorous state of dynamical evolution. Furthermore, there are aesthetic objections. For the Lemaître-Eddington universe depends on the introduction of a cosmical constant which, as Einstein has remarked, is an unsatisfactory device. Moreover, the wide cosmological principle is not satisfied.

In this connection it may be noted that Lemaître now prefers a model with point-source creation. The constants λ, k and the initial velocity of expansion are adjusted so that there is a stage in the expansion approximating to the Einstein static universe. Later stages in the expansion are then the same as in the Lemaître-Eddington model.

The aim of the present paper is to overcome the difficulties outlined above. Using continuous creation of matter, we shall attempt to obtain, within the framework of the general theory of relativity, but without introducing a cosmical constant, a universe satisfying the wide cosmological principle that shows the required expansion properties and in which localized condensations are continually being formed.

3. *The Mathematical Formalism.*—Following a procedure similar to that based on Weyl's postulate (Robertson **3**), we first obtain a simple form for the Riemannian quadratic metric

$$ds^2 = g_{\mu\nu}\, dx^\mu\, dx^\nu.$$

Take the pencil of geodesics passing through a definite point O in the space-time continuum. Three independent coordinates are required to specify a particular geodesic belonging to this pencil. The first restriction placed on the metric is that there shall be a unique geodesic (remembering that we are considering the smoothed out problem) joining O to a general point P of space-time. Then P can be described by four coordinates in the following way. The three coordinates defining the unique geodesic give the "space" coordinates x_1, x_2, x_3 of P, while the absolute length (interval) measured along this geodesic from a fixed reference point to P gives the product ct, where c is a constant and t is the "time" coordinate. Next we use the geometrical property that the reference points on the various geodesics can be chosen so that the time sections, defined by equations of the form $t = \text{constant}$, are orthogonal to the geodesics themselves. Accordingly, the metric can be written as

$$ds^2 = c^2\, dt^2 + g_{ij}(t, x_1, x_2, x_3)\, dx_i dx_j; \qquad i, j = 1, 2, 3. \tag{12}$$

The discussion of the previous paragraph is of a geometrical character. Connection with the physical world is introduced by the requirement that the narrow cosmological principle shall be satisfied in every time section. This condition can be converted into geometrical terms by using results due to Lie, Killing, and Fubini (see Robertson **3**), which show that (12) can then be reduced to the more specialized form

$$ds^2 = c^2\, dt^2 - R^2(t) h_{ij}(x_1, x_2, x_3)\, dx_i dx_j; \qquad i, j = 1, 2, 3, \tag{13}$$

where the subspace

$$du^2 = h_{ij}\, dx_i dx_j \tag{14}$$

has constant Riemannian curvature. We now introduce the final simplification of taking this curvature to be zero. Then it can be shown (**3**) that the coordinates

describing the geodesics through O can be chosen to give

$$ds^2 = c^2\,dt^2 - R^2(t)(dx_1^2 + dx_2^2 + dx_3^2). \tag{15}$$

In this connection it may be noted that if a stationary universe showing expansion is to be obtained, then formal similarities with the de Sitter empty model must be expected. In Section 2 it was seen that $k=0$ in the Newtonian form of this model. Since the condition $k=0$ is the Newtonian equivalent of zero Riemannian curvature, the reason underlying the final reduction of (13) will be readily understood.

For convenience in later work we note that the only non-vanishing Christoffel symbols are

$$\{ij, 0\} = RR'\delta_{ij}/c^2, \qquad \{i0, j\} = R'\delta_{ij}/R, \qquad i, j = 1, 2, 3, \tag{16}$$

where δ_{ij} is the Kronecker symbol. The only non-vanishing components of the Ricci tensor $G_{\mu\nu}$ are

$$\begin{aligned} G_{ij} &= -(RR'' + 2R'^2)\delta_{ij}/c^2, \qquad i, j = 1, 2, 3, \\ G_{00} &= 3R''/R, \end{aligned} \tag{17}$$

and the spur of this tensor is given by

$$G = 6(RR'' + R'^2)/R^2c^2. \tag{18}$$

We now diverge from the usual procedure by introducing at each point P of space-time a vector C_μ of fixed length directed along the geodesic from O to P. The sense of this vector is always taken as being away from O. Thus, in terms of our coordinate system we have, at each point, a vector with components proportional to (1, 0, 0, 0). The constant of proportionality which will be written as $3c/a$, determines the length of the vector. Accordingly, the vector field is given by

$$C_\mu = 3c/a(1, 0, 0, 0). \tag{19}$$

By differentiation a symmetrical tensor field $C_{\mu\nu}$ is obtained. That is

$$C_{\mu\nu} = \partial C_\mu/\partial x^\nu - \{\mu\nu, \alpha\}C_\alpha. \tag{20}$$

Since $\partial C_\mu/\partial x^\nu$ is everywhere zero, we obtain, by using (16), the following non-vanishing components of $C_{\mu\nu}$,

$$C_{ij} = -3RR'\delta_{ij}/ac; \qquad i, j = 1, 2, 3. \tag{21}$$

The essential step in the present work is the introduction of the tensor $C_{\mu\nu}$ into the Einstein field equations. Thus we write

$$G_{\mu\nu} - \tfrac{1}{2}g_{\mu\nu}G + C_{\mu\nu} = -\kappa T_{\mu\nu}, \tag{22}$$

where $\kappa = 8\pi\gamma/c^4$ and $T_{\mu\nu}$ is the material energy tensor. Neglecting both kinetic energy terms and the hydrostatic pressure, the only non-vanishing component of $T_{\mu\nu}$ is

$$T_{00} = \rho c^4, \tag{23}$$

where ρ is the proper density of matter. The $C_{\mu\nu}$ term in (22) plays a rôle similar to that of the cosmical constant in the de Sitter model, with the important difference, however, that there is no contribution from the C_{00} component. As we shall see, this difference enables a universe, formally similar to the de Sitter model, to be obtained, but in which ρ is non-zero.

The field equations (22) now give

$$2RR'' + R'^2 - 3cRR'/a = 0, \tag{24}$$

$$3R'^2 = \kappa\rho c^4 R^2. \tag{25}$$

Choosing the zero of time so that $R = 1$ at $t = 0$ it is easy to see that

$$R = e^{ct/a}, \qquad \kappa\rho c^2 = 3/a^2 \tag{26}$$

is a solution of (24), (25). Thus we obtain a metric identical in form with the de Sitter model, but in the present universe the proper density of matter is a constant non-zero quantity.

The solution (26) is stable against fluctuations in the value of R'/R. Thus, suppose $R'/R = \alpha c/a$ at $t = 0$, where $\alpha \neq 1$. Then (24) can be integrated to give

$$\left.\begin{aligned} 3ct/4a &= \tanh^{-1}(2aR'/cR - 1) - \tanh^{-1}(2\alpha - 1) \text{ if } \alpha < 1, \\ 3ct/4a &= \coth^{-1}(2aR'/cR - 1) - \coth^{-1}(2\alpha - 1) \text{ if } \alpha > 1. \end{aligned}\right\} \tag{27}$$

It can be seen from (27) that R'/R approaches c/a in a time of order a/c even if α is appreciably different from unity. Thus we see that a/c is a natural unit of time.

Taking the divergence of (22) we obtain

$$(C^{\mu\nu})_\nu = -\kappa(T^{\mu\nu})_\nu, \tag{28}$$

since the divergence of $G_{\mu\nu} - \frac{1}{2}g_{\mu\nu}G$ vanishes on account of the four identities. Using (16), together with the relation

$$(C^{\mu\nu})_\nu = \partial C^{\mu\nu}/\partial x^\nu + \{\alpha\nu, \mu\}C^{\alpha\nu} + \{\alpha\nu, \nu\}C^{\mu\alpha}, \tag{29}$$

it can be shown that

$$\left.\begin{aligned} (C^{i\nu})_\nu &= 0, \qquad i = 1, 2, 3, \\ (C^{0\nu})_\nu &= -9R'^2/ac^3R^2. \end{aligned}\right\} \tag{30}$$

Thus

$$\left.\begin{aligned} (T^{i\nu})_\nu &= 0, \qquad i = 1, 2, 3, \\ \kappa(T^{0\nu})_\nu &= 9R'^2/ac^3R^2. \end{aligned}\right\} \tag{31}$$

By working out $(T^{0\nu})_\nu$ the second of equations (31) gives

$$\kappa\left\{\frac{\partial\rho}{\partial t} + 3\rho\frac{R'}{R}\right\} = \frac{9R'^2}{ac^3R^2}, \tag{32}$$

which reduces to $\partial\rho/\partial t = 0$ when (26) is satisfied. Equation (32) could have been obtained directly from (24) ,(25).

4. *The Physical Interpretation of the Formalism.*—We now consider the relation of physical measurement to the coordinate system used above. Since $(C^{0\nu})_\nu \neq 0$, matter is being created. But because $(C^{i\nu})_\nu = 0$ for $i = 1, 2, 3$, the matter possesses zero momentum in our system of coordinates. Thus a particle created at a point P moves away from O along a geodesic joining O and P. In principle, changes in the coordinate t are given by the proper time measured by an observer attached to such a particle. In practice, however, an observer on the Earth has not exactly a geodesic through O as world-line. Deviations arise when local condensations are formed, since electromagnetic forces are introduced in the condensation process (through atomic collisions). Remembering, however, that local condensations only have a small effect on the large-scale problem, the proper time measured by an observer on the Earth gives a good approximation for changes in the coordinate t.

Similarly we neglect the effect of local condensation on the measurement of the space coordinates. The coordinates x_1, x_2, x_3 can be chosen so that

$$x_1 = r\sin\theta\cos\phi, \quad x_2 = r\sin\theta\sin\phi, \quad x_3 = r\cos\theta, \tag{33}$$

where r, θ, ϕ are spherical polar coordinates measured relative to a terrestrial observer. The angular coordinates θ, ϕ are easily determined by the usual sextant type of observation, but the determination of r raises an important question. At a particular time t the absolute distance (interval) from the Earth of an event occurring at a point with space coordinates r, θ, ϕ is $R(t)r$ and not the "parametric" distance r. Now, according to the postulates of the relativity theory, a measuring rod has the same absolute length for all values of t. It follows therefore that distances obtained by surveying methods give $R(t)r$ and not r.

Large distances are in practice obtained from the apparent intensity of a standard light source. In the Galaxy and the nearer extragalactic nebulae Cepheid variables are used as the standard, while at the greatest distances the whole emission from a galaxy is employed. This method has been discussed by Tolman (**9**) and by Whittaker (**10**), who find that, when the time sections have zero Riemannian curvature, such measurements also give $R(t)r$.

It is seen therefore that, neglecting the effect of local condensations, normal methods of measurement determine proper volumes and not "coordinate" volumes. Thus on the basis of (26) we expect that measurements of the mean intergalactic density would give a value independent of t.

It will be noticed that practical measurement of r, θ, ϕ is entirely based on light tracks. In particular, it is a necessary consequence of the sextant method of determining θ, ϕ that these coordinates are constant along a light track. Thus the path of a light pulse emitted by the observer satisfies the equation

$$\frac{dr}{dt} = \frac{c}{R(t)}. \tag{34}$$

Accordingly, a light pulse emitted by the observer at time t_1 reaches at time $t(>t_1)$ a point whose r coordinate is given by

$$r = c\int_{t_1}^{t} \frac{dt'}{R(t')}. \tag{35}$$

Using (26) this becomes

$$r = a(e^{-ct_1/a} - e^{-ct/a}), \tag{36}$$

which tends to $ae^{-ct_1/a}$ as $t\to\infty$. This means that a light signal emitted by the observer at time t_1 can never reach points with r coordinates greater than $ae^{-ct_1/a}$. Similarly a light signal emitted at time t_1 from a point with r coordinate greater than $ae^{-ct_1/a}$ cannot reach the observer. This result may be stated in a more significant form in terms of absolute distances. In any time section a light signal emitted at an absolute distance greater than a from a point on a geodesic through O can never reach an observer with this geodesic as world-line. Thus a may be described as the radius of the "observable" universe.

According to (26) the total mass of material within the observable universe is independent of t and is given by

$$4\pi a/\kappa c^2. \tag{37}$$

This result deserves comment. Ignoring local condensations, each particle has a geodesic through O as world-line. Now the r coordinate is constant along

such a geodesic. Thus a particle with space coordinates r, θ, ϕ passes out of the observable universe at a time t given by

$$r = ae^{-ct/a}. \tag{38}$$

Particles passing out of the observable universe are compensated by the creation of new particles in accordance with (31). It is only through the creation of matter that an expanding universe can be consistent with conservation of mass within the observable universe.

Next we turn to a comparison of (26) with the observed velocity-distance law. Consider light emitted from an oscillatory source with a geodesic through O as world-line, and let this geodesic be characterized by the space coordinates r, θ, ϕ. Write t_1, t_1+dt_1 for the times of two successive maxima of the source, where t_1+dt_1 is taken such that

$$r < ae^{-c(t_1+dt_1)/a}. \tag{39}$$

Then light rays emitted at times t_1, t_1+dt_1 reach the observer at times t, $t+dt$ given by

$$r = c\int_{t_1}^{t}\frac{dt'}{R(t')} = c\int_{t_1+dt_1}^{t+dt}\frac{dt'}{R(t')}. \tag{40}$$

For small dt_1 (26) gives

$$dt/dt_1 = e^{c(t-t_1)/a}. \tag{41}$$

But dt/dt_1 is the ratio of the frequency, ν say, of the source itself to the apparent frequency, $\nu+d\nu$ say, of the light reaching the observer. Thus we have

$$-\frac{d\nu}{\nu} = \frac{r}{a}e^{ct/a}. \tag{42}$$

This apparent shift of frequency is towards the red, and corresponds to an apparent Doppler velocity

$$(cr/a)e^{ct/a}. \tag{43}$$

Accordingly a light source moving along a geodesic through O has an apparent recessional velocity at time t given by multiplying the absolute distance, at time t, between the source and the observer by the constant c/a. Remembering that physical measurements determine absolute distance, it follows by comparison with (10) that, when absolute distance is measured in centimetres and t is measured in seconds, the constant c/a is given by

$$c/a \doteqdot (5/3)\times 10^{-17}\ \text{sec.}^{-1}. \tag{44}$$

This equation, together with $c = 3\times 10^{10}$ cm. per sec., leads to the following results:—

(i) the radius a of the observable universe is about $1{\cdot}8\times 10^{27}$ cm.,
(ii) the unit of time a/c is about 6×10^{16} sec., or about 2×10^{9} years,
(iii) the proper density ρ is about 5×10^{-28} g. per cm.^{3},
(iv) the mass within the observable universe is about $1{\cdot}2\times 10^{55}$ g.

At a given time the present model is analogous to a Newtonian universe in which the instantaneous values of v^2, ρ are given by

$$v^2 = c^2r^2/a^2, \qquad \rho = 3c^2/8\pi\gamma a^2. \tag{45}$$

Eliminating a^2 we can write

$$v^2 = 8\pi\gamma\rho r^2/3, \tag{46}$$

which is similar to the equation for v^2 occurring in the case discussed in Section 2, in which $k=0$, $\lambda=0$. The important feature of this case was that condensations were formed wherever the local density increased slightly above the mean value. It is therefore to be expected that localized condensations will continually arise in the universe discussed above.

The following general picture of the condensation process suggests itself. Extragalactic nebulae are continually passing out of the observable universe, but the total number of nebulae within the observable universe remains approximately constant on account of the formation of new condensations. Thus a nebula, or a cluster of nebulae, condensing at an absolute distance d from the observer passes out of the observable universe after a time of about

$$2 \times 10^9 \log_e(a/d) \text{ years.} \tag{47}$$

The smallest value that can be taken for d corresponds approximately to the observed mean intergalactic distance of about $1{\cdot}5 \times 10^{24}$ cm. Accordingly, the oldest condensations within the observable universe (other than the condensation in which the observer happens to be situated, which may be of any age) has an age of about $1{\cdot}5 \times 10^{10}$ years. It is attractive to associate these condensations with the great nebular clusters. The youngest condensations, which have ages of about 2×10^9 years, are conveniently associated with the single field nebulae. Astrophysical evidence indicates that the "local group" of nebulae containing our Galaxy has an age of about 5×10^9 years. It is therefore satisfactory that this group shows a moderate degree of aggregation.

Hubble's estimation of about 5×10^{-31} g. per cm.^{3} for the mean density of luminous material, taken together with our estimate of 5×10^{-28} g. per cm.^{3} for the average density of *all* material, suggests that only about one part in a thousand of the intergalactic medium is at present in a condensed state.

5. *General Remarks.*—The work of Sections 3, 4 completes the main argument concerning the smoothed-out problem. The discussion becomes much more complicated when the effects of localized condensations are taken into account. Although such a discussion is outside the scope of the present paper, it seems desirable to make brief mention of the questions that arise.

The metric can always, in the present model, be reduced to (12), but the simplification leading to (13) neglects local condensation and, therefore, cannot be used in a strict theory. A symmetrical tensor field $C_{\mu\nu}$ can still be introduced, however, and field equations of the form (22) can be constructed. This question will be considered in a further paper.

In the usual formulation of cosmology (**3**) Weyl's postulate plays an important rôle. Neglecting the effect of localized condensations, this postulate requires material particles to move along geodesics that form a pencil. Although the work of Section 3 is formally similar to that based on Weyl's postulate, there is a difference of principle. For the status of Weyl's postulate in its original form is not clear. It cannot represent a "Law of Nature", since particles in local condensations do not in fact conform with the postulate. In the present model, on the other hand, there is a modified form for Weyl's postulate that can be applied even when local condensations are taken into account. This modified form defines the creation properties of matter. That is, at the time of its creation a particle follows a geodesic passing through O. But there is no requirement that it shall continue to do so and in fact the particle will subsequently move along a path not passing through O if it should be perturbed by an electromagnetic

field. Weyl's postulate is evidently of deeper significance when expressed in this modified form. It must be admitted, however, that the nature of the point O remains mysterious. In this connection we note that an event occurring at O cannot be observed at a point with finite t. For in order to reach O, time must be followed back to $t = -\infty$.

The present model has both an infinite future and an infinite past, and in the approximation in which the effects of local condensations are neglected, the wide cosmological principle is satisfied.

The origin of the fluctuations of density, necessary for the formation of local condensations, raises a question of interest. Such fluctuations evidently arise if condensations with proper motions are already present. But the presence of condensations is not a necessary condition, for density fluctuations will occur, even in the absence of condensations, provided matter is created in a quantum type of process. Quantum processes are not, of course, mentioned in the macroscopic treatment of Section 3. Nevertheless, quantum effects must be considered in the physical interpretation of the theory, since it is only through discontinuous processes that statistical fluctuations can be imposed on the universe in the first place. Thus, fluctuations, leading ultimately to approximate thermodynamic conditions being realized in extremely localized regions (in stars, for example), probably arise on account of the discrete particle nature of matter. These considerations are important in relation to the measurement of the coordinates. For in a universe containing no statistical fluctuations and satisfying the wide cosmological principle, there is no possibility of introducing the rod and clock equipment postulated in the relativity theory.

A further interesting feature is that the total "entropy" within the observable universe does not increase with time. Although entropy increases in a localized region, the total entropy remains approximately constant because local condensations carry entropy out of the observable universe. Thus thermodynamics has only localized application. There is no general thermodynamic degeneration of the observable universe as a whole.

It is not possible in the present state of nuclear physics to make a definite statement on the identity of the created particles. Neutron creation appears to be the most likely possibility. Subsequent disintegrations might be expected to supply the hydrogen required by astrophysics. Moreover, the electrical neutrality of the universe would then be guaranteed.

Finally, we notice that a dimensionless number is obtained by dividing the length $a/3$ appearing in (19) by the "range" k of nuclear forces. Using laboratory data for k, together with the determination given above for $a/3$ (on the basis of a comparison with the Hubble-Humason velocity-distance relation), we obtain about 4×10^{39} for this number. This value is close to the dimensionless number $2{\cdot}3 \times 10^{39}$ given by the ratio of the electrical to the gravitational force between a proton and an electron. Allowing for uncertainty in the determination of $a/3$, and in the interpretation of k, this coincidence suggests that the relation

$$a = 3ke^2/\gamma mM, \tag{48}$$

where m, M are the masses of the electron and proton, is of deep significance. Since the creation process is likely to be of an essentially quantum character, the relation (48) may be regarded as being entirely concerned with microscopic properties. Weyl has interpreted a relation similar to (48) as giving a connection between the radius a of the observable universe and the physical constants, and Eddington, in particular, has attached much importance to this interpretation.

But this view, which Eddington has adopted as the basis of his work on physical theory, may well prove to be a misconception, for according to the above discussion the radius of the observable universe is subsidiary to, and is determined by, the creation constant. Indeed, the possibility of interpreting (48) as an equation of microscopic physics gives perhaps the best indication that the work of Section 3 is not simply a formal device.

Cambridge :
1948 *August* 3.

References

(1) J. H. Jeans, *Astronomy and Cosmogony* (Cambridge 1928), page 352.
(2) P. A. M. Dirac, *Nature*, **139**, 323, 1937.
(3) H. P. Robertson, *Rev. Mod. Phys.*, **5**, 62, 1933.
(4) E. A. Milne, *Quart. Journ. Math.* (Oxford), **5**, 64, 1934.
W. H. McCrea and E. A. Milne, *Quart. Journ. Math.* (Oxford), **5**, 73, 1934.
(5) A. Einstein and W. de Sitter, *Proc. Nat. Acad. Sci.*, **18**, 213, 1932.
(6) A. S. Eddington, *M.N.*, **90**, 668, 1930.
(7) G. Gamow and E. Teller, *Phys. Rev.*, **55**, 654, 1939.
(8) A. S. Eddington, *M.N.*, **104**, 200, 1944.
(9) R. C. Tolman, *Proc. Nat. Acad. Sci.*, **16**, 511, 1930.
(10) E. T. Whittaker, *Proc. Roy. Soc.*, **133** A, 93, 1931.

A GENERAL STUDY OF A PROMINENCE FIELD

Helen W. Dodson

(Communicated by Robert R. McMath)

(Received 1948 August 16)

Summary

This study is an attempt to find some order or pattern in the motions of knots in a prominence field and to view the prominence against the background of the general solar neighbourhood. It is based on the nine moving knots of the prominence observed on 1947 September 16 which traversed similar, though not identical, trajectories, from a region high above a sunspot area to a point of attraction on the disk. Velocities of the knots increased from zero to more than 100 km./sec. under accelerations which became as large as one-third of solar gravity. Time-distance diagrams for the fast-moving knots are brought into coincidence for a large portion of the trajectory through arbitrary changes in the zero points from which the distances are measured. The similarity of these curves suggests that the velocity of the knots is a function of the distance, or time, from their starting-points, and that they form a system subject to the same force or forces.

Introduction.—Between 1947 September 14 and 18, a region associated with a complex pattern of spots, faculae and filaments crossed the western limb of the Sun. It lay between the solar equator and 30° north latitude, and ranged from 165° to 210° heliographic longitude. Throughout the sunlit hours of September 14, 16 and 17, the prominence activity associated with this region was photographed with the spectroheliograph of the 50-foot tower telescope and the Stone radial-velocity spectroheliograph of the McMath-Hulbert Observatory. A few spectroheliograms were secured on September 15 and 18. The limb photographs included three quite distinct features: (1) a rather low, quiescent prominence (height about 20,000 km.) which can be associated with the stable, dark filament clearly defined in the $H\alpha$ spectroheliogram of 1947 September 10; (2) a number of small surges (latitudes 19° N. to 25° N.) which emanate from the sunspot groups within these latitudes and between longitudes 184° to 205°; (3) a large, open, spider-like prominence with height of the order of 100,000 km. which continually sent material along streamers from a source-like region in latitude 23° N. to a point of attraction in latitude 12° N.–13° N. These features are shown as a, b and c, respectively in Plate 8. During part of September 16, knots or nodules could be seen moving in these streamers. A study of the motions of these knots forms the main material for this paper.

Measurement of the Knots.—The measurements of the spectroheliograms from the 50-foot tower were made on a table especially designed for this purpose. The image of the prominence was thrown upon an opaque, white surface and the position of a knot determined by bisection with two movable wires. The wire readings gave values of x and y for the knot in a rectangular system of coordinates with origin at an arbitrarily selected point. For this work the scale of projection

was such that one millimetre represented 1·38 seconds of arc in the sky, or 1000 kilometres at the distance of the Sun. The positions of the knots were recorded to the nearest millimetre in each coordinate. Repeated measures of the same knot gave an average difference of 1·5 mm. in the x-coordinate and 0·9 mm. in the y-coordinate, but with no measurable difference in the slopes of the repeated x-versus-time and y-versus-time curves. Difficulty in finding and maintaining a suitable origin throughout the measures accounts for some of the differences in measurement. This is especially true for the x-coordinate which was more sensitive than y to accidental shifts in the origin.

The following coordinate system was used in the measurement of the prominence here studied:

x-axis = direction tangent to the apparent solar disk, positive in the sense of decreasing position angle.

y-axis = direction of the radius of the apparent solar disk perpendicular to the x-axis, positive in the sense away from the Sun's centre.

z-axis = direction of the line of sight to the point of intersection of the x- and y-axes, positive in the sense away from the observer.

The origin was on the limb of the Sun and was fixed with reference to the quiescent prominence and small identifiable features of the chromosphere.

Spectroheliograms obtained with the Stone instrument were measured for radial velocity, V_z, by essentially the same method as that described in an earlier publication.*

Observations of 1947 *September* 16.—The scene of 1947 September 16 was selected for measurement and study because the prominence was open, relatively simple in structure, and the knots followed similar, though not identical, trajectories. The similarity of the paths suggested that the knots might form a system or family and that their motions might in some ways be related. The study covers the period September $16^d\ 14^h\ 14^m{\cdot}4$ U.T. to September $16^d\ 16^h\ 25^m{\cdot}3$ U.T. During this interval, nine knots moved over the system of streamers. Of these, two divided, so that there are eleven moving nodules to be investigated.

Data from spectroheliograms obtained with the 50-foot tower telescope are recorded in Table I. The photographs were taken at the rate of two per minute; all frames were measured and used in the investigation. Table I gives the data at intervals of 2·5 minutes. Quantities x and y refer to the coordinates of the centre of the knot read from a smoothed curve drawn through a graph of the original measures of x and y plotted versus time (see Fig. 1). V_x and V_y are the respective velocity components in km./sec., determined by measurement of the slopes of the above curves. V_{xy} and V_s both refer to the velocity along the trajectory in the xy-plane and should be the same except for differences of judgment in drawing curves and tangents. The former is the square root of the sum of V_x^2 and V_y^2; the latter is the slope of the time-distance curves. A_x and A_y are the acceleration components found from the slopes of the graphs of V_x and V_y plotted versus time, and A_{xy} is the magnitude of the total acceleration in the xy-plane. Accelerations are recorded in km./sec.^{2}. In these units, solar gravity has the value 0·2736. S is the distance along the trajectory, in thousands of kilometres, from a starting-point, S_0, defined in the latter portion of this paper.

* R. R. McMath, *Publications of the Observatory of the University of Michigan*, **8**, 57, 1940.

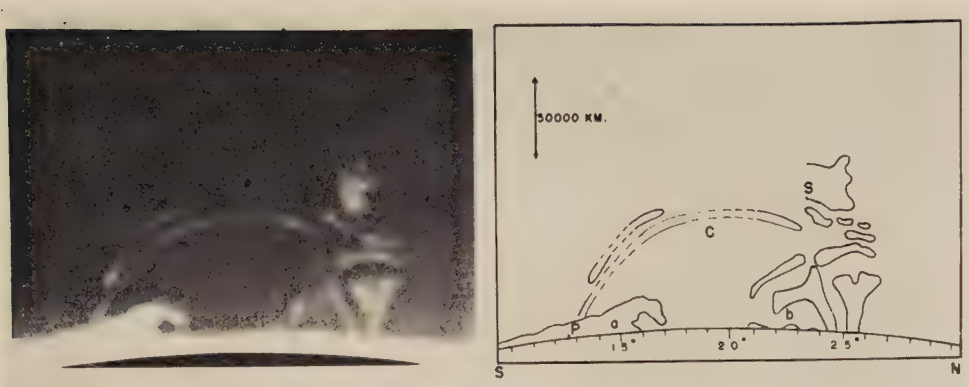

SEPT. 16^{d}.6, 1947

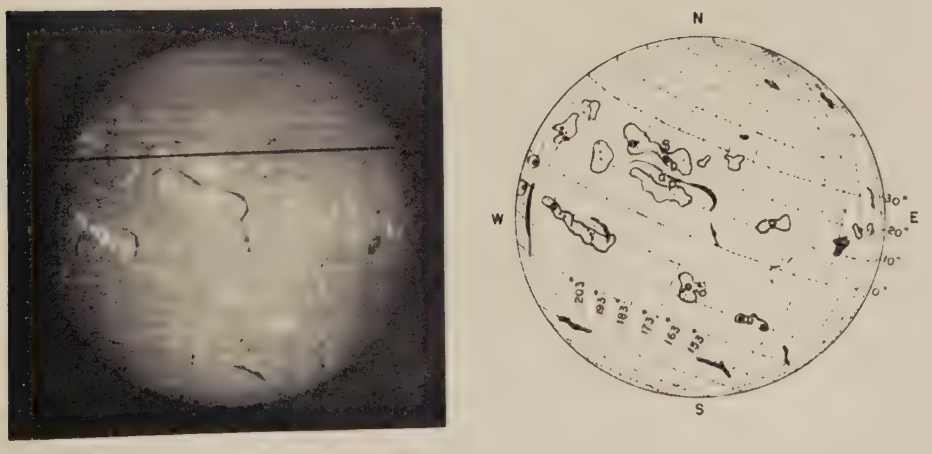

SEPT. 10^{d}.7, 1947

Above : Prominence of 1947 September 16, photographed in light of ionized calcium.

Below : $H\alpha$ spectroheliogram of 1947 September 10, showing disk features associated with the prominence.

H. W. Dodson, A General Study of a Prominence Field.

The above data refer to two-dimensional motion in the plane of the sky. In order for the velocities to represent true space motions it is necessary to include the radial velocity, V_z. It is often difficult to secure a complete record of radial velocities for faint nodules or for those moving rapidly in the xy-plane. If it can be shown that V_z is small in comparison to V_x and V_y, and that the motion is essentially in the xy-plane, then motion based on V_x and V_y alone, V_{xy}, will represent the essential features of the true space motion, V_{xyz}. Examination of the Stone spectroheliograms for 1947 September 16 indicates that there were no large radial velocities for any of the knots in this study. Furthermore, a comparison of V_{xy} and V_{xyz} for knot No. 1 shows that inclusion of the relatively small z-velocities in the measures does not significantly alter their relationships or values. The first spectroheliograms giving radial velocity were taken at $14^h\,45^m$, and nodule No. 1 could not be measured after $15^h\,20^m$. Velocities based on these measures are shown in Figs. 2 and 3. The striking similarity

TABLE I

Positions, Velocities and Accelerations for the Nine Knots of the Prominence of 1947 September 16

Time 1947 Sept. 16	x	y	V_x	V_y	V_{xy}	V_s	A_x	A_y	A_{xy}	S
				km./sec.				km./sec^2.		
h m						No. 1				
14 15·0	−24	69	0	0	0	0	...	...	...	0
17·5	−23	69	0	0	0	0	...	...	...	0
20·0	−23	69	0	0	0	0	...	...	...	0
22·5	−23	69	0	0	0	0	...	...	...	0
25·0	−23	68	0	0	0	0	...	...	...	0
27·5	−24	68	0	3	3	4	·009	·006	·011	1·0
30·0	−24	69	3	2	4	5	·009	·000	·009	1·5
32·5	−23	69	5	2	5	6	·009	·000	·009	2·0
35·0	−23	70	6	2	6	7	·009	·000	·009	4·0
37·5	−22	70	7	2	7	8	·011	·000	·011	4·0
40·0	−20	70	9	2	9	11	·017	·006	·018	6·0
42·5	−18	70	12	2	12	13	·030	·009	·031	7·0
45·0	−16	71	18	4	18	16	·034	·009	·035	9·0
47·5	[−14	71	22	5	23	20	·014	·005	·015	12·0]*
50·0	[−11	72	23	6	24	25	·006	·003	·007	15·5]
52·5	− 7	73	24	6	25	25	·004	·001	·004	19·0
55·0	− 3	73	25	4	25	25	·003	−·007	·008	23·5
14 57·5	1	74	25	3	25	25	·003	−·012	·012	27·0
15 00·0	5	74	25	1	25	25	·005	−·015	·016	31·0
02·5	8	74	28	− 1	28	25	·043	−·021	·048	35·0
05·0	14	74	44	− 3	44	41	·113	−·031	·117	40·0
07·5	22	73	59	− 9	60	60	·137	−·036	·142	49·0
10·0	32	71	73	−16	75	75	·033	−·050	·060	58·0
12·5	42	68	75	−26	79	78	·007	−·078	·078	70·0
15·0	54	64	74	−34	81	82	−·002	−·113	·113	81·5
17·5	65	56	75	−59	95	97	−·017	−·107	·108	96·0
20·0	76	46	68	−72	99	99	−·060	−·058	·083	110·0
22·5	84	35	54	−76	93	82	−·099	−·019	·101	125·0
15 25·0	93	23	39	−77	86	...	−·111	−·005	·111	137·0

* Parentheses indicate interpolated or uncertain values.

Time 1947 Sept. 16	x	y	V_x	V_y	V_{xy}	V_s	A_x	A_y	A_{xy}	S
				km./sec.				km./sec.^{2}		
h m						No. 2				
15 05·0	42	68	63	−23	67	80	·077	−·073	·106	62
07·5	54	64	70	−38	80	82	·020	−·073	·076	75
10·0	64	57	70	−46	84	87	−·026	−·073	·077	87
15 12·5	74	49	62	−60	86	92	−·054	−·073	·090	99
						No. 3				
15 00·0	55	61	71	−45	84	87	−·035	−·059	·069	79·5
02·5	66	54	65	−52	83	87	−·023	−·059	·063	91·0
05·0	75	45	62	−62	88	89	−·017	−·059	·061	105·0
07·5	84	34	61	−71	94	91	−·013	−·059	·060	118·5
15 10·0	93	23	61	−80	101	94	...	...	...	133·0
						No. 4				
14 25·0	38	71	21	− 3	21	...	...	...	...	30·0
27·5	41	70	21	− 6	22	17	·000	−·015	·015	32·5
30·0	44	69	21	− 9	23	19	·000	−·017	·017	35·5
32·5	47	67	21	−10	23	25	·000	−·022	·022	39·0
35·0	50	65	21	−14	25	27	·018	−·033	·038	43·0
37·5	54	62	30	−22	37	42	·107	−·047	·117	47·0
40·0	61	58	47	−28	55	58	·071	−·077	·105	56·0
42·5	68	52	54	−46	71	73	·031	−·107	·111	65·0
45·0	76	44	56	−62	84	87	·019	−·111	·113	78·0
47·5	[85	33]	58	−81	100	103	·012	−·089	·090	91·0
14 50·0	94	20	60	−92	110	109	·006	−·069	·069	107·0
						No. 5a				
14 27·5	59	72	61	−44	75	...	−·020	−·060	·063	51·0
30·0	67	65	61	−52	80	77	−·020	−·070	·073	63·0
32·5	76	56	56	−68	88	87	−·020	−·080	·082	75·0
35·0	84	45	56	−81	98	106	−·020	−·120	·122	89·0
37·5	92	31	51	−104	116	116	−·020	−·060	·063	105·0
14 40·0	100	15	50	−87	100	120	...	...	...	122·0
						No. 5b				
14 15·0	26	90	6	− 3	7	...	·070	−·010	·071	16·0
17·5	27	89	15	− 7	17	18	·070	−·010	·071	17·0
20·0	30	87	26	− 8	27	26	·048	−·010	·049	20·0
22·5	34	86	38	− 9	39	36	·028	−·010	·030	25·0
25·0	40	84	34	−12	36	43	·000	−·010	·010	30·0
27·5	45	81	28	−12	30	38	−·028	−·010	·030	37·0
30·0	50	80	30	−14	33	22	−·064	−·010	·065	41·0
32·5	51	79	6	−16	17	11	−·038	−·020	·043	44·0
35·0	53	76	18	−19	26	31	·079	−·020	·082	46·0
37·5	58	73	36	−21	42	44	·047	−·030	·056	53·0
40·0	64	69	36	−28	46	46	·000	−·030	·030	60·0
42·5	70	65	37	−34	50	48	·000	−·030	·030	67·0
45·0	76	59	38	−40	55	51	·000	−·030	·030	75·0
47·5	81	54	35	−42	55	54	−·010	−·030	·032	82·0
50·0	86	47	35	−45	57	58	−·010	−·030	·032	92·0
52·5	92	40	31	−53	61	60	−·020	−·030	·036	102·0
55·0	96	31	28	−56	63	63	−·030	−·020	·036	111·0
14 57·5	100	23	22	−58	62	63	−·030	−·010	·032	119·0
15 00·0	103	15	18	−60	63	65	−·030	−·010	·032	129·0

Time 1947 Sept. 16	x	y	V_x	V_y	V_{xy}	V_s	A_x	A_y	A_{xy}	S
h m				km./sec.				km./sec.^{2}		
					No. 6					
14 57·5	32	88	14	− 6	15	...	·000	·000	·000	8·0
15 00·0	34	86	15	− 7	17	18	·000	·000	·000	10·5
02·5	36	85	16	− 9	18	18	·000	·000	·000	13·0
05·0	39	84	18	− 9	20	19	·010	−·010	·014	16·0
07·5	41	82	18	− 9	20	20	·010	−·010	·014	19·0
10·0	44	81	19	−14	24	26	[·070	−·040	·081]	22·5
12·5	47	79	55	−21	59	36	[·160	−·050	·170]	27·0
15·0	51	77	38	−29	48	33	[−·190	·000	·190]	36·0
17·5	55	74	2	− 4	4	27	[−·210	·000	·210]	40·5
20·0	59	71	3	−14	14	20	[−·210	−·080	·220]	42·0
22·5	64	68	37	−25	45	42	[·090	−·080	·120]	46·0
25·0	70	63	47	−37	60	63	·050	−·080	·094	54·0
27·5	77	57	52	−50	72	71	·020	−·090	·092	63·0
30·0	85	48	53	−65	84	87	·000	−·070	·070	75·0
32·5	93	38	54	−84	100	92	−·010	−·060	·061	88·0
15 35·0	100	26	47	−58	75	79	−·070	−·040	·081	103·0
					No. 7					
15 00·0	−2	88	5	− 1	5	...	·000	·000	·000	−15·0
02·5	−1	88	4	− 1	4	7	·000	·000	·000	−14·5
05·0	0	88	4	− 1	4	0	·000	·000	·000	−14·0
07·5	0	88	5	− 1	5	5	·000	·000	·000	−13·5
10·0	1	88	4	− 1	4	5	·000	·000	·000	−12·0
12·5	2	88	3	− 1	3	5	·018	·000	·018	−11·5
15·0	3	88	14	− 1	14	15	·067	·000	·067	−10·0
17·5	5	88	23	− 1	23	27	·007	·000	·007	− 8·0
20·0	9	87	20	− 1	20	16	−·060	·000	·060	− 5·0
22·5	12	87	11	− 1	11	12	−·040	·000	·040	− 2·0
25·0	12	87	6	− 1	6	7	−·040	·000	·040	0·0
27·5	13	86	0	− 1	1	4	−·020	·000	·020	0·0
30·0	13	86	0	− 1	1	0	·000	·000	·000	1·0
32·5	13	86	0	− 1	1	0	·000	·000	·000	1·0
35·0	13	86	0	− 2	2	0	·000	·000	·000	1·5
37·5	13	85	0	− 2	2	1	·000	·000	·000	1·5
40·0	13	85	0	− 2	2	2	·000	·000	·000	1·5
42·5	13	84	4	− 1	4	5	·010	·000	·010	2·0
45·0	14	84	4	− 1	4	13	·020	·000	·020	3·0
47·5	16	84	20	− 1	20	18	·050	·000	·050	5·0
50·0	19	83	22	− 3	22	20	·040	·000	·040	8·0
52·5	22	83	20	− 4	20	18	−·003	−·005	·006	11·0
55·0	24	82	16	− 4	16	17	−·003	−·006	·007	13·5
15 57·5	27	82	16	− 4	16	17	−·003	−·006	·007	16·5
16 00·0	30	81	15	− 5	16	17	−·003	−·006	·007	19·0
02·5	32	80	15	− 6	16	17	·000	−·007	·007	21·0
05·0	34	79	17	− 7	18	18	·010	−·008	·013	23·0
07·5	36	78	19	− 7	20	20	·010	−·012	·016	26·5
10·0	39	76	20	− 9	22	22	·020	−·020	·028	29·5
12·5	42	75	24	−15	28	25	·060	−·040	·072	33·0
15·0	46	72	40	−20	45	53	·130	−·050	·139	37·0
17·5	54	68	65	−31	72	70	·000	−·050	·050	45·0
20·0	64	63	61	−38	72	75	−·020	−·050	·054	57·0
16 22·5	73	56	58	−44	73	82	−·020	−·050	·054	68·0

Time 1947 Sept. 16	x	y	V_x	V_y	V_{xy}	V_s	A_x	A_y	A_{xy}	S
h m				km./sec.				km./sec.^{2}		
					No. 8a*					
15 22·5	[28	85	27	− 6	28	...	·000	·000	·000	−10·0]
25·0	[33	84	26	− 6	27	28	·000	·000	·000	− 7·0]
27·5	[36	83	27	− 6	28	28	·000	·000	·000	− 3·0]
30·0	[40	82	26	− 6	27	24	·000	·000	·000	1·0]
32·5	[44	81	23	− 6	24	24	−·020	−·002	·020	5·0]
35·0	[47	80	23	− 7	24	22	−·030	−·002	·030	7·5]
37·5	[50	79	13	− 7	15	15	−·030	−·002	·030	10·0]
40·0	[52	78	10	− 7	12	13	−·020	−·002	·020	12·5]
42·5	[53	77	9	− 7	11	11	−·010	−·002	·010	14·5]
45·0	[55	76	9	− 8	12	10	·000	−·002	·002	16·0]
47·5	[56	75	8	− 8	11	10	·000	−·002	·002	18·0]
50·0	[57	74	9	− 8	12	10	·000	−·002	·002	19·5]
52·5	[58	73	10	− 7	12	10	·010	−·002	·010	21·0]
55·0	[59	72	10	− 8	13	11	·020	−·002	·020	23·0]
15 57·5	[61	70	12	− 9	15	12	·020	−·002	·020	24·0]
16 00·0	[63	68	16	− 9	18	13	·020	−·002	·020	27·0]
02·5	[66	67	20	−10	22	18	·020	−·028	·034	29·0]
05·0	67	66	33	−14	36	25	·020	−·060	·063	33·0
07·5	71	62	35	−28	45	33	·020	−·060	·063	37·0
10·0	77	57	37	−38	53	48	·020	−·060	·063	45·0
12·5	83	51	38	−43	57	55	·020	−·060	·063	52·0
15·0	88	44	41	−52	66	65	·020	−·060	·063	61·0
17·5	94	35	43	−63	76	75	·020	−·060	·063	72·5
16 20·0	100	26	48	−68	83	78	·020	−·060	·063	85·0

* Velocities in parentheses for knot No. 8a have been omitted from Figs. 7 and 8.

					No. 8b					
16 05·0	73	57	34	−28	44	38	·020	−·030	·036	43·0
07·5	78	53	35	−31	47	42	·020	−·030	·036	49·5
10·0	84	47	37	−36	52	44	·020	−·040	·045	56·0
16 12·5	89	41	39	−43	58	48	·020	−·050	·054	64·0
					No. 9					
15 22·5	41	81	47	−20	51	...	...	...	...	18
25·0	48	78	47	−26	54	54	−·011	·012	·016	25
27·5	55	74	45	−20	49	55	[−·013	·026	·029]	36
30·0	62	69	42	−17	45	36	[−·107	·056	·120]	44
32·5	64	68	0	0	0	0	[−·018	·047	·050]	45
35·0	64	68	0	0	0	6	[·018	−·062	·064]	45·5
37·5	65	65	9	−20	22	53	[·085	−·143	·166]	50
40·0	68	59	33	−47	57	68	·137	−·095	·167	59
42·5	76	51	47	−58	75	77	·047	−·067	·081	69
45·0	84	42	48	−67	82	85	−·009	−·064	·065	84
47·5	90	31	45	−77	89	92	−·009	−·042	·043	97
15 50·0	97	19	45	−80	92	98	−·009	−·024	·026	111

between V_{xy} and V_{xyz} in Fig. 2 and the nearly coincident graphs of time-versus-distance in Fig. 3 give evidence that the motion is essentially across the observer's line of sight. In the latter diagram, S_{xy} is computed from x- and y-displacements

only, while S_{xyz} includes the z-displacement derived from graphical integration of the curve showing V_z-versus-time. In view of these similarities for knot No. 1 and the consistent absence of large radial velocities for all other knots, it has been concluded that, for this prominence field, the velocities in the xy-plane represent the essential features of the space motions.

Although repeated measurements of the film and redeterminations of the velocities result in gratifyingly accordant values, the inherent uncertainty of the measures suggests the wisdom of focusing attention upon the general features of the motion rather than upon aspects that require extreme accuracy. This is especially true when a prominence has been selected for measurement because

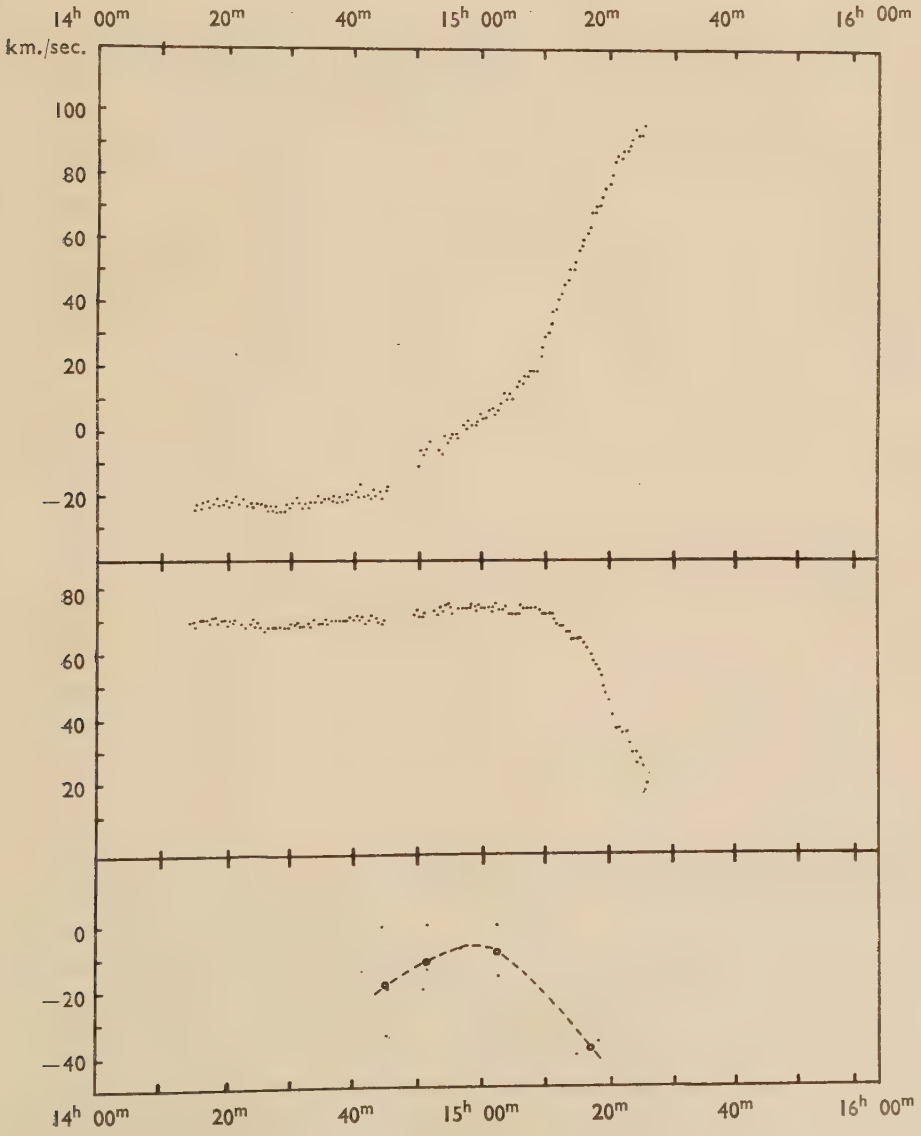

FIG. 1.—x, y *and* V_z *for knot No.* 1.

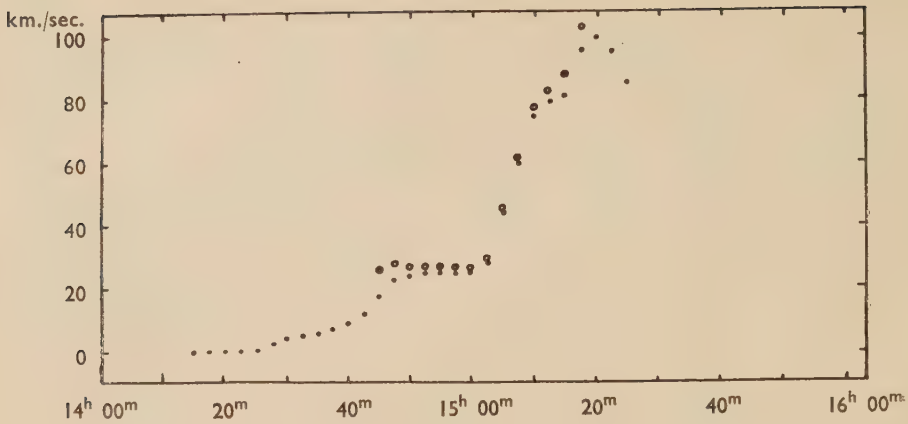

FIG. 2.—*Comparison of two- and three-dimensional velocities for knot No. 1. Dots represent V_{xy} and open circles V_{xyz}.*

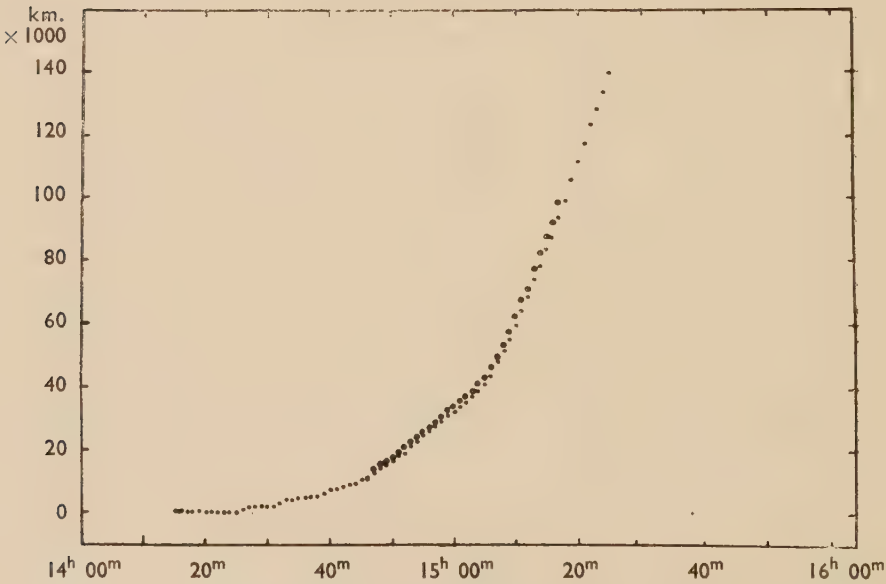

FIG. 3.—*Comparison of two- and three-dimensional time-distance curves for knot No. 1. The smaller dots represent S_{xy} and the larger dots S_{xyz}.*

of its relationship to the Sun as a whole or to a general solar problem, rather than because of the quality of the photography.

Distance along the trajectory, plotted as a function of time, is shown in Fig. 4, for all of the measured knots. In Section A of Fig. 4, S_{xy} is zero at the time when the knots first became measurable or, as in the case of Nos. 4 and 5, on the first available pictures. The measurements of No. 8 were highly uncertain. The object faded and almost disappeared between $15^h\ 35^m$ and $16^h\ 00^m$, and the connection between the early and late sections of curve 8a is questionable. Knots 5 and 8 each divided into fast and slow components; the former are designated by subscript a, the latter by subscript b. Although the curves show many individual differences, the portions with nearly identical slopes suggest possible order or

pattern in the motions. These regularities can be made more obvious by introducing the following arbitrary changes in the value of S:

Knot	ΔS in thousands of km.
1	0
2	+60
3	+80
4	+30
5	+50
6	+ 8
7	−15
8	−10
9	+20

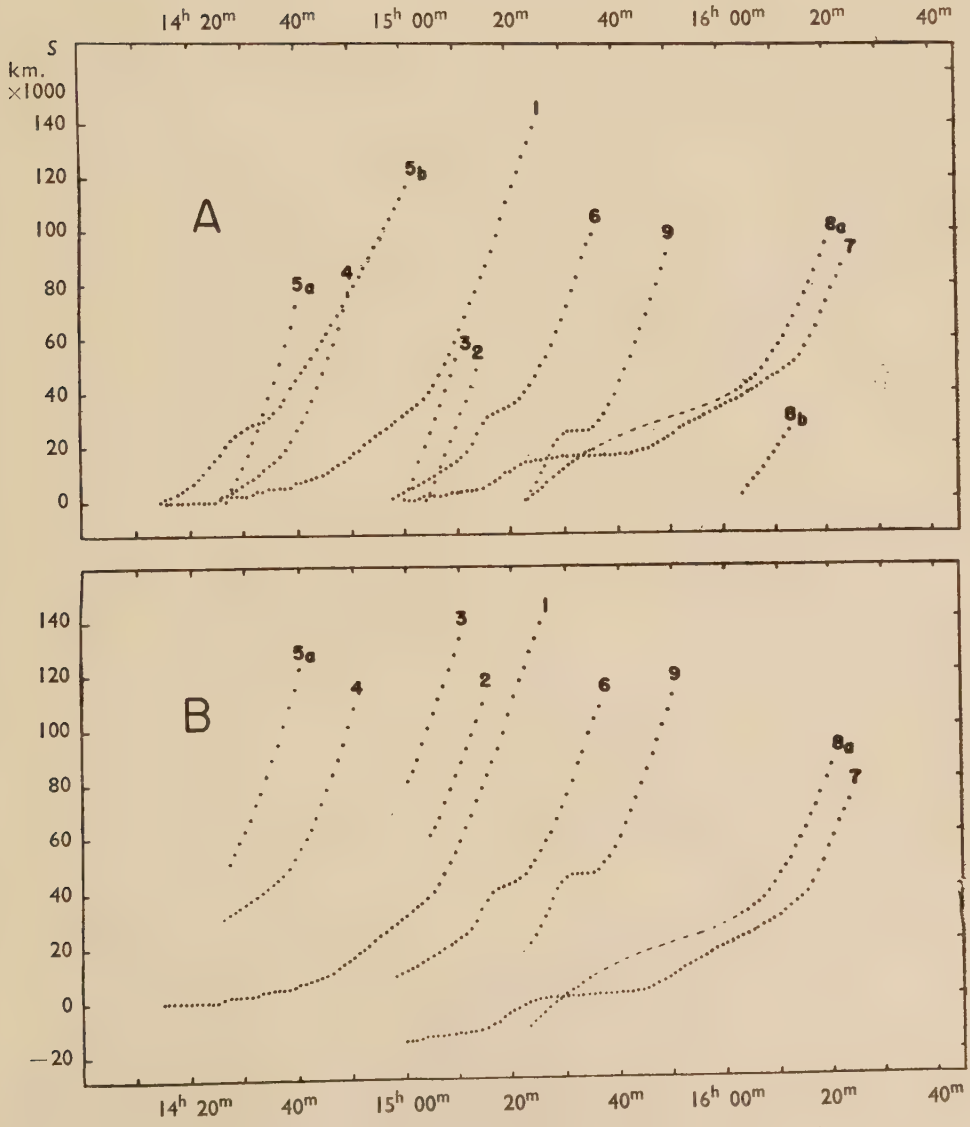

FIG. 4.—*Time-distance diagram for all knots in prominence field. From lower diagram 5b and 8b are omitted.*

The resulting curves, for all knots except the slow components of Nos. 5 and 8, are shown in Section B of Fig. 4. Superposition of the curves brings out even more clearly the relationships between them. This has been done in Fig. 5.

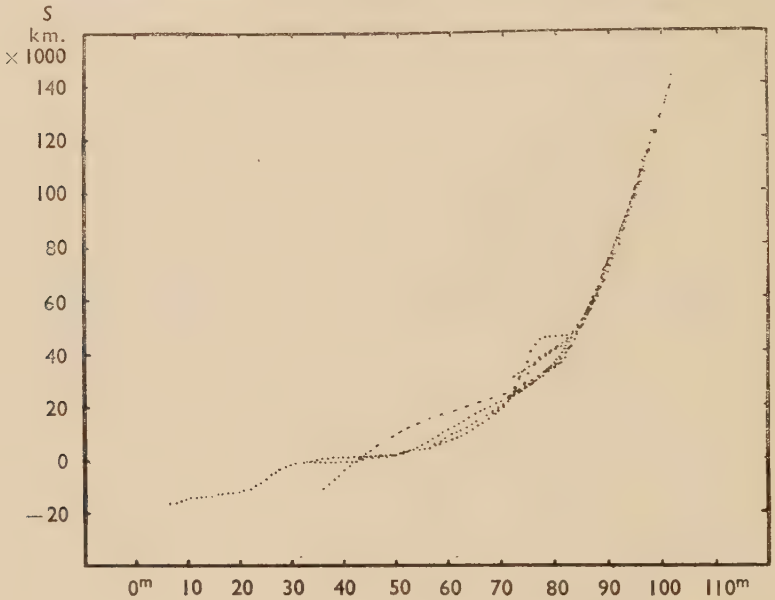

FIG. 5.—*Combined time-distance diagrams for the nine knots of prominence field.*

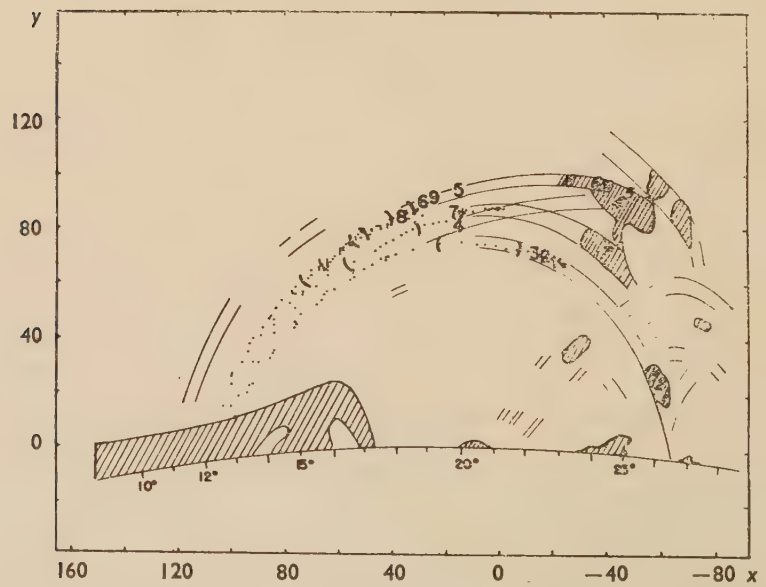

FIG. 6.—*Apparent trajectories, "starting-points" and source-points for all knots in prominence field.*

For S greater than 50,000 km. the curves coincide. When S is between 20,000 km. and 50,000 km., each knot undergoes major accelerations, decelerations, or both. These parts of the trajectories might well be called "regions of confusion". They are enclosed in parentheses in Fig. 6. The apparent confusion

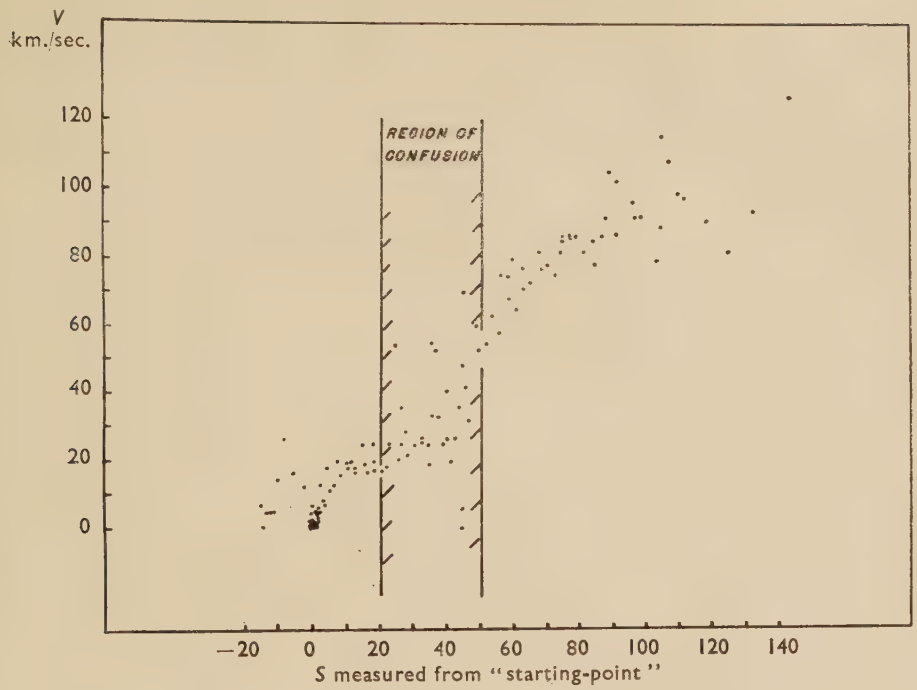

FIG. 7.—*Velocity versus distance for the nine fast-moving knots.*

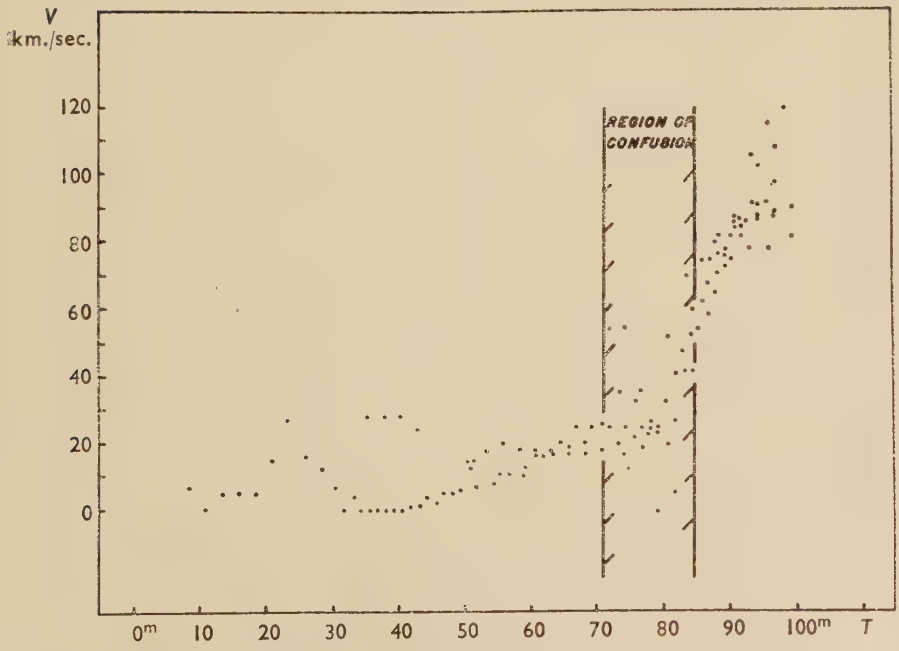

FIG. 8.—*Velocity versus time for the nine fast-moving knots.*

might be of photographic origin, due perhaps to the crossing of faint streamers, or it could be the result of some physical cause on the Sun. In general, for S less than 20,000 km., the observed knots moved very slowly except for an occasional brief impulse followed by a period of zero velocity.

Interpretation of the Observations of 1947 *September* 16.—If one looks upon the similarities of the nine time-distance curves of the fast-moving knots as other than fortuitous, they suggest that the velocity of a knot is a function of: (1) *its distance from some rather critical "starting-point", S_0;* (2) *the time elapsed since passage through this "starting-point"*. These relationships are shown in Figs. 7 and 8 where values of V_s, taken from Table I, are plotted versus distance and time. The zero point of the time-scale of Fig. 8 is arbitrary.

From the photographs of the prominence field, it is possible to locate the "starting-points" by measuring $\triangle S$ along the undifferentiated streamers associated with the nodules. The streamers were not all visible at the same time, hence the drawing in Fig. 6 represents a composite picture. The numbers of the knots, in vertical figures, are placed in the positions of the computed "starting-points". These points coincide for Nos. 1, 2 and 3, and lie very close together for Nos. 6 and 9. Further examination of the photographs shows that each of the "starting-points" is about the same distance (65,000 km.) along its own path from a bright region apparently at the root or source of each of the streamers. Therefore, the velocity of the knots can be considered as a function of the distance along the trajectory, either from the arbitrarily determined "starting-points" or from these apparent source-points. In Fig. 6 the positions of the source-points are marked with the numbers of the knots, in slanted figures. *It is to be noted that the knots, as such, are not visible until quite far from the bright source-points and that the faint streamers connecting them with the source-points are observable only part of the time.*

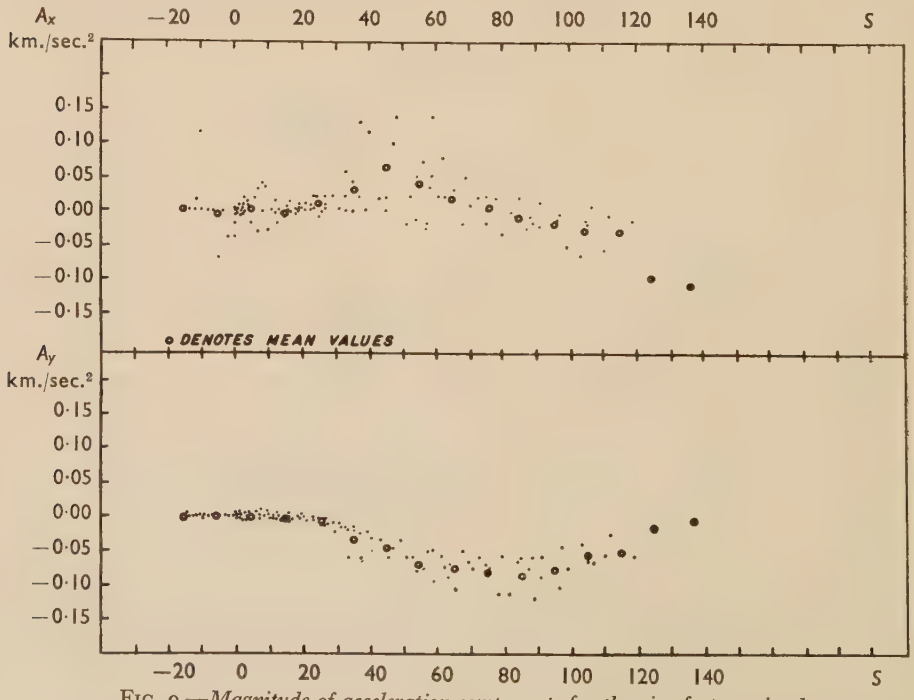

FIG. 9.—*Magnitude of acceleration components for the nine fast-moving knots.*

Accelerations of the knots must be determined from second differences of measures that are unquestionably difficult and often uncertain, and should be interpreted with caution. The slope of the graph of velocity-versus-time

gives the acceleration along the trajectory, which is equal to or less than the space acceleration. The latter, determined from the three space components, A_x, A_y and A_z, is the desired quantity, since it is proportional to the forces acting. If the motion is exactly in the plane of the sky, A_z is zero. The prominence field under consideration has been shown to be approximately of this type; hence, the discussion will be concerned primarily with A_x and A_y. The acceleration components, found by measuring the slopes of the graphs of V_x and V_y plotted versus time, are recorded in Table I. Although they show large variations, certain general statements can be made. When S is small, the accelerations are of the order of one-tenth of solar gravity; when S lies between 20,000 and 50,000 km., the accelerations become large, and in some cases tend to obscure the more general behaviour; when S is greater than 50,000 km., the accelerations are about one-third of solar gravity. If it be assumed, for the nine fast-moving knots, that the acceleration vectors are parallel at corresponding positions on the trajectory, then both the magnitude and direction of the acceleration should be functions of S. The graphs in Figs. 9 and 10 show this dependence. The acceleration vectors for Nos. 6 and 9, for values of S between 20 and 50, have been omitted from these graphs.

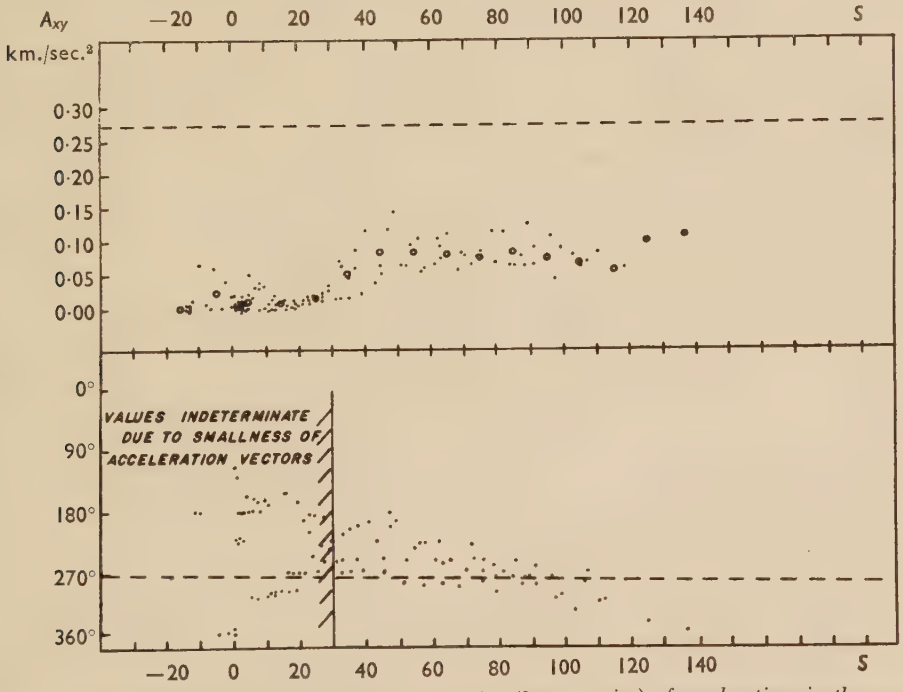

FIG. 10.—*Magnitude (upper section) and direction (lower section) of accelerations in the xy-plane for the nine fast-moving knots.*
Broken line indicates magnitude (upper section) and direction (lower section) of solar gravity.

The two slow components, 5*b* and 8*b*, must now be considered. A superposition of their time-distance curves upon those of the fast components shows that they emerge as "slow" only after passage through the "region of confusion". The velocity is one-half to three-fourths that of the fast components, and the accelerations are smaller, but point in approximately the same direction (see Fig. 11).

Prominence Motion in Relation to Disk Phenomena: 1947 *September* 16.—Examination of the films taken on 1947 September 14 to 17, reveals the continued visibility of that portion of the prominence field identified with the source-points. (Region S in Plate 8.) Analysis of the variations in apparent height * shows that this region crossed the solar limb at approximately September 16^{d} 00^{h}, at a height of 70,000 km., in heliographic longitude 193° and latitude 23° N. These coordinates place it 3° north and 4° west of Mount Wilson sunspot No. 8820, and 5° north and 11° east of No. 8819.† These sunspot groups are shown in Plate 8 in longitudes 190° and 205° respectively. The source-region might indeed have been between these two spots, but it is also within the uncertainty of the measures for it to have been directly over spot No. 8820.

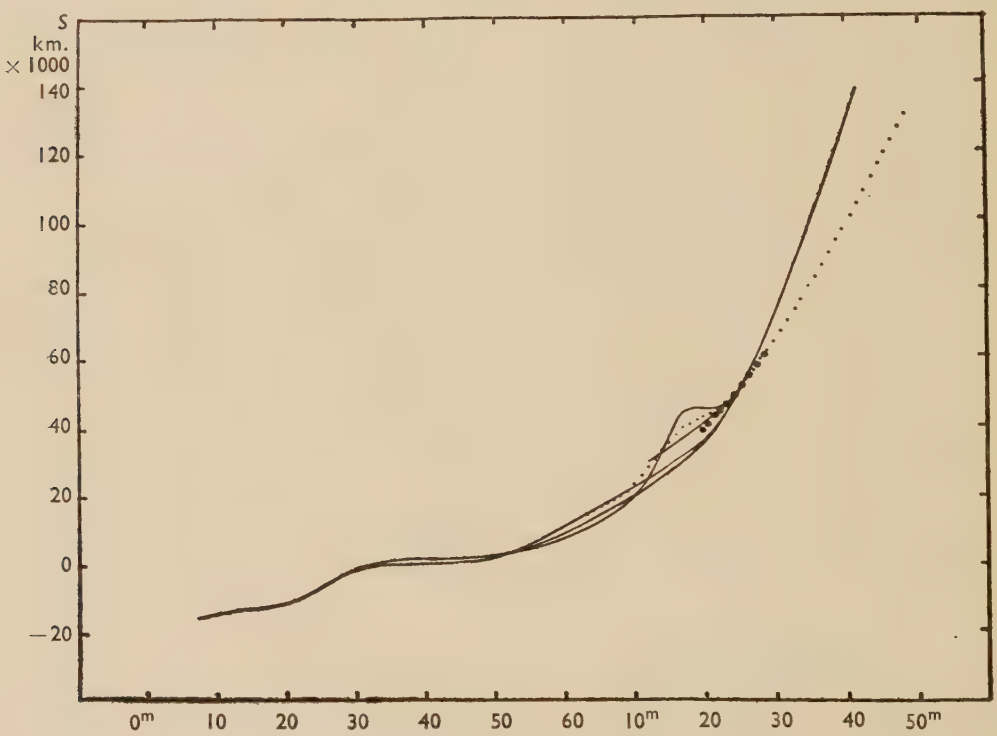

FIG. 11.—*Comparison of time-distance curves for fast- and slow-moving knots. The smaller dots represent knot 5b and the larger, knot 8b.*

This spot was an inconspicuous feature as it moved across the disk in the days preceding September 16, but its field strength, 2400 gauss, was relatively high. When it reappeared in October (Mount Wilson No. 8859) it was the largest spot group on the disk and had a field strength of 3000 gauss. During both transits it was a bipolar spot with the preceding member the principal component of the group.‡

During the three days of September 15, 16 and 17, material apparently entered the solar disk at a point in latitude 12° N.–13° N. (marked P in Plate 8).

* E. R. Hedeman and H. W. Dodson, *Astronomical Journal*, **53**, 111, 1948.
† Mount Wilson Observatory, *P.A.S.P.*, **59**, 338, 1947.
‡ *Ibid.*

On the last date, there was a brief period in which the material rose to a height of more than 200,000 km. before descending to the same point of attraction. Although the latitude of the point of entrance of the material is well determined, the longitude is less certain. It has been shown that on September 16, the trajectories were nearly across the line of sight and that the small radial velocities carried negative signs. The point of entrance was, therefore, probably only a few degrees east of the source-points, with longitude not less than 185°. In this region there is a bright *plage* in which small spots were observed on September 8, 9 and 11, but not later. The point of entrance for the nodules must have been just south of the well-defined filament marked "a" in Plate 8. The quiescent prominence, marked "a" in the prominence picture, is the projection of this filament against the sky. *The moving nodules actually passed over the filament from north to south and entered the disk in latitude* 12°. The "centre of attraction", as indicated by the acceleration vectors, was some 2° to 4° north of the point of entrance of the material. Again, there was no distinguishable feature on the disk in this position, other than the filament.

In conclusion, it can be said that for this one prominence, at least, it has been possible to find certain similarities in the motions of the knots and to trace the course of these moving objects with respect to other solar features. The relationships are far from clear, but it appears that the various nodules are moving, not as independent phenomena, but as a group or family. The similarity of their velocities over a large portion of their paths suggests that they are under the influence of the same force or forces. The accelerations become as large as one-third of solar gravity and have components both along and perpendicular to the apparent paths. The knots originate high above a sunspot group, move almost horizontally over the solar disk, and enter the chromosphere in a bright *plage*, which is apparently devoid of large sunspots. In the course of this motion, the knots pass over a low-lying, quiescent prominence or filament which is unaffected by the activity taking place above it. Sufficient primary data have been included to permit other investigators to use or interpret the observations in other ways, or as their needs may require.

The author wishes to express her sincere appreciation to Dr Robert R. McMath for his constant encouragement and guidance throughout the preparation of this paper. The motion pictures upon which the study is based were secured and prepared for analysis through the cooperative effort of the entire staff of the Observatory. The writer is especially indebted to Dr Orren C. Mohler and Mr John Brodie for their helpful suggestions and untiring assistance during the progress of this investigation, and to Miss Ruth Hedeman and Mr Jack Harned for their valued aid in the preparation of the plates and tables. Sincere thanks are tendered to McGregor Fund of Detroit for continuing grants-in-aid in support of the work of the McMath-Hulbert Observatory.

The McMath-Hulbert Observatory,
University of Michigan,
Lake Angelus, Michigan, U.S.A:
1948 *May* 11.

A PHOTOMETRIC LIGHT CURVE FOR μ^1 SCORPII

D. W. N. Stibbs

(Received 1948 March 16; received in revised form 1948 August 30)

Summary

The light variation of the eclipsing binary μ^1 Scorpii has been studied in the effective wave-length 3970 A. The 358 observations obtained have been assembled on the period $1^d{\cdot}44627$ and the reflected light curve has been analysed for the constants of ellipticity and reflection. The geometrical elements for uniform disks have been calculated from the rectified light curve by a method due to Kopal. These elements give a computed light variation which agrees closely with the observational normals, the probable error per normal being $0^m{\cdot}0020$. A comparison is made between the results of the photoelectric measurements of Rudnick and Elvey, the photovisual determinations of van Gent and the present work. Combining the photometric results with the spectroscopic elements of O. Struve the masses and dimensions of the components are derived.

1.—The star μ^1 Scorpii * was found to be a spectroscopic binary by Bailey in 1896, and was the third spectroscopic binary to be discovered. The elements of the relative orbit were calculated by Miss Maury †, who also found the star to be an eclipsing variable, and more recently O. Struve ‡ has published a two-spectra orbit. Two light curves have been obtained for μ^1 Scorpii, one by Rudnick and Elvey § using a potassium cell photoelectric photometer attached to the Yerkes twelve-inch refractor at the MacDonald Observatory, and another by H. van Gent || at the Union Observatory by means of photovisual observations in the effective wave-length 5604 A., using the ten-inch Franklin Adams telescope.

2. *The Observations.*—The photoelectric observations described in this paper were made with a gas-filled sodium cell attached to the Reynolds thirty-inch reflector at the Commonwealth Observatory. The spectral sensitivity of the apparatus has been calculated using the manufacturer's data for the cell, and the reflection and transmission coefficients given by Pettit.¶ The response of the cell to black-body radiation at 18,500 deg. K., allowance having been made for the atmospheric transmission and the reflection from three silvered surfaces, gives a maximum at 3700 A., and zero response at 3250 and 5700 A. The effective wave-length, taken to be the centre of gravity of the enclosed area, is 3970 A. The instrumental and electrical arrangement is the same as that used by Hogg **, and has already been described.

The comparison star used was μ^2 Scorpii.†† The observations were made on 42 nights between 1946 June 26 and October 8, a total of 358 observational

* Boss 4277, G.C. 22677, H.D. 151890 (α $16^h45^m{\cdot}1$, δ $-37°51'$, 1900).
† A. C. Maury, *Harvard Annals*, **84**, 169, 1920.
‡ O. Struve, *Festschrift für Elis Strömgren*, Copenhagen, p. 258, 1940.
§ P. Rudnick and C. T. Elvey, *Ap. J.*, **87**, 553, 1938.
|| H. van Gent, *B.A.N.*, **9**, 15, 1939.
¶ E. Pettit, *P.A.S.P.*, **46**, 28, 1934.
** A. R. Hogg, *M.N.*, **106**, 292, 1946.
†† Boss 4281, G.C. 22691, H.D. 151985.

points being finally adopted. An observation consists of five readings on the variable taken between two sets of five readings on the comparison star. On account of the proximity of the two stars the extinction corrections were usually small except for some larger hour angles met with later in the season. Corrections for sky background were applied when necessary. The observations were assembled on the period $1^d{\cdot}44627$. The observational points, reduced to heliocentric times by Prager's Tables*, are shown in Fig. 1, on which is also drawn the computed curve from the uniform solution of Section 6. The magnitude difference between μ^2 and the maximum light of μ^1 Scorpii was found to be $0^m{\cdot}574$.

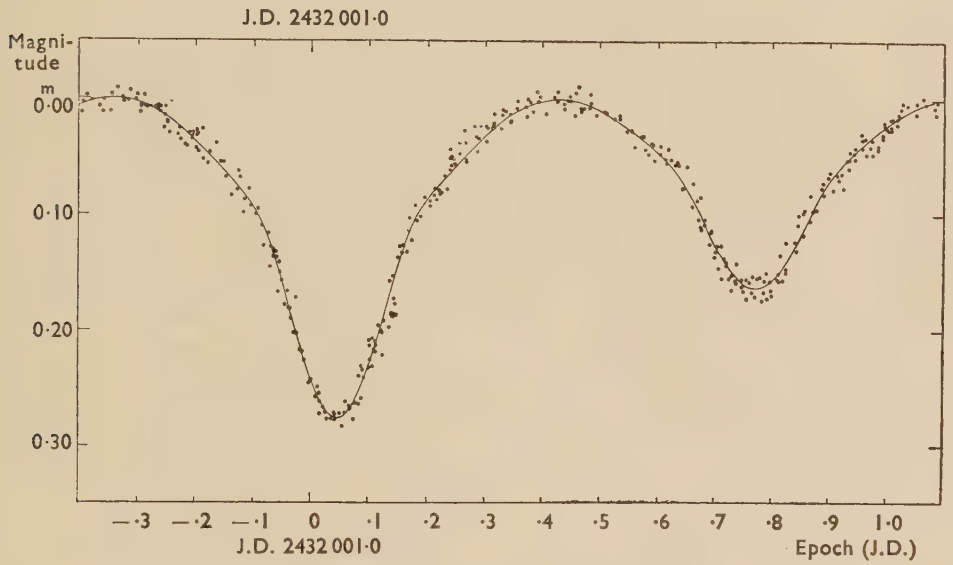

FIG. 1.—*Observational points and computed curve.*

3. *Epoch of Minimum.*—The epoch of minimum light has been determined by a method similar to that described by Hertzsprung† and used by van Gent.‡ The primary and secondary minima have been treated separately. The observational points within the minimum under consideration were grouped into normals containing ten observations, the normals being formed progressively by shifting along by one observation each time. From the curve resulting from the join of these normal points, magnitudes were read to $0^m{\cdot}001$ at intervals of $0^d{\cdot}005$. The method of determining the minimum is a numerical application of the method of least squares. The eclipse curve is folded about an epoch and the sum of the squares of the difference between the ordinates of pairs of points symmetrically placed with respect to the chosen epoch is formed. Taking three values of epoch a parabola may be used to determine the epoch of the least sum of squares. According to Pannekoek and van Dien§ the mean error in the value of an unknown determined in this way is simply the distance from the minimum to a point for which the ordinate is $n/(n-1)$ times the least sum of squares, where n is the number of "equations of condition" used. In both the primary and secondary

* Berlin-Babelsberg Observatory, *Kleinere Veröffentlichungen*, No. 12, 1932.
† E. Hertzsprung, *B.A.N.*, **4**, 178, 1928.
‡ *Loc. cit.*
§ A. Pannekoek and E. van Dien, *B.A.N.*, **8**, 141, 1937.

minimum we have taken $n=70$. The calculated epoch of minimum and the probable errors are as follows:—

$$\text{Primary: } t_1 = \text{J.D. } 2432\,001{\cdot}0451 \pm 0{\cdot}0002.$$

$$\text{Secondary: } t_2 = \text{J.D. } 2432\,001{\cdot}7712 \pm 0{\cdot}0003.$$

The probable errors in the determined values of epoch of minima are consequently of the same order as the uncertainty in the time at which an observation was made, namely about a quarter of a minute.

The component $e\cos\omega$ of the orbital eccentricity is connected with the separation of the two minima by the relation

$$P(1+\operatorname{cosec}^2 i)e\cos\omega = \pi(t_2 - t_1 - \tfrac{1}{2}P).$$

From the uniform solution of Section 6 we take $i=60°{\cdot}0$ and consequently $e\cos\omega = 0{\cdot}0027 \pm 0{\cdot}0003$ compared with the value 0·049 from the single-spectrum orbital elements of Miss Maury. A secular decrease in the value of $e\cos\omega$ is suggested by Luyten* from a study of the same material as used by Miss Maury. But the spectroscopic values of $e\cos\omega$ are liable to be uncertain because tidal distortion in close binary systems, coupled with gravity darkening, is known to invoke deformation of simple Keplerian velocity-curves which simulates orbital eccentricity.† However, in the determination of the elements of his two-spectra orbit Struve found the eccentricity to be so close to zero as to make the longitude of periastron practically indeterminate, and he derives circular elements. The present photometric work also calls for a nearly circular orbit.

The available determinations of epoch of principal minimum and their corresponding probable errors are as follows:—

a. Miss Maury ‡	J.D. 2415 591·6830 ± 0·0018
b. Rudnick and Elvey	2428 281·250 ± ?
c. van Gent	2428 414·2978 ± 0·0015
d. Present work	2432 001·0451 ± 0·0002

By assuming the appropriate number of intervening cycles a value of the period may be calculated for an epoch corresponding to mid-way between any two of these determinations.

Comparison	No. of Periods	Average Period
c–a	8866	$1^d{\cdot}4462\,6831 \pm 26 \times 10^{-8}$
d–c	2480	$1^d{\cdot}4462\,6907 \pm 61 \times 10^{-8}$

There does not appear to be any significant difference between the two periods.

4. *The Reflected Light Curve.*—The observational points for each minimum were "reflected" about the epoch of the minimum under consideration, and then combined into normals containing ten observations, the normals being formed progressively at intervals of five observations. This process gave 39 normals for the primary minimum portion of the composite curve and 33 for the secondary. The primary and secondary portions of the light curve have therefore been treated as symmetrical, the "reflecting" process having been carried out separately for each minimum in order to be quite free from the effect of the slightly uneven

* W. J. Luyten, *Pubs. Obs. Univ. Minnesota*, **2**, 38, 1935.

† T. E. Sterne, *Proc. Nat. Acad. Sci.*, **27**, 168, 1941. Z. Kopal, *P. Amer. Phil. Soc.*, **89**, 517, 1945. See also O. Struve, *Ap. J.*, **99**, 89, 1944; *P.A.S.P.*, **60**, 160, 1948.

‡ Epoch recalculated by van Gent (*loc. cit*).

spacing of the minima. The two portions of the resulting light curve were joined at a point corresponding to the phase $\theta\left(=\frac{2\pi}{P}t\right)=\frac{\pi}{2}$ outside eclipse. The normals in light intensity, and the magnitude difference measured from maximum light, together with the corresponding phase in days measured from the principal minimum are given in Table I.

TABLE I

Normal	Phase	Light	Mag.	O–C	Normal	Phase	Light	Mag.	O–C
	d		m	m		d		m	m
1	0·0000	0·7756	0·276	0·000	37	0·3329	0·9945	0·006	+0·001
2	·0100	·7769	·274	·000	38	·3416	·9972	·003	·000
3	·0197	·7805	·269	·000	39	·3531	·9991	·001	·000
4	·0284	·7834	·265	+·003	40	·3653	0·9991	·001	+·001
5	·0362	·7919	·254	·000	41	·3815	1·0000	·000	·000
6	·0449	·8017	·240	−·004	42	·3946	1·0000	·000	·000
7	·0536	·8091	·230	−·001	43	·4057	0·9963	·004	+·004
8	·0614	·8166	·220	+·001	44	·4170	·9963	·004	+·003
9	·0680	·8271	·206	−·002	45	·4313	·9982	·002	−·002
10	·0748	·8326	·199	+·002	46	·4484	·9941	·006	−·001
11	·0824	·8426	·186	+·002	47	·4667	·9900	·011	−·001
12	·0904	·8582	·166	−·004	48	·4820	·9863	·015	−·002
13	·0981	·8638	·159	+·002	49	·4923	·9809	·021	·000
14	·1050	·8770	·145	·000	50	·5018	·9745	·028	+·004
15	·1112	·8839	·134	−·001	51	·5139	·9665	·037	+·008
16	·1191	·8904	·126	+·003	52	·5271	·9638	·040	+·006
17	·1302	·9036	·110	+·002	53	·5372	·9656	·038	−·001
18	·1434	·9154	·096	+·002	54	·5464	·9620	·042	−·001
19	·1570	·9221	·088	+·003	55	·5573	·9568	·048	·000
20	·1669	·9281	·081	+·002	56	·5671	·9523	·053	+·001
21	·1780	·9342	·074	+·001	57	·5758	·9488	·057	+·001
22	·1900	·9428	·064	−·002	58	·5861	·9454	·061	−·001
23	·1987	·9515	·054	−·007	59	·5975	·9393	·068	−·002
24	·2091	·9585	·046	−·009	60	·6090	·9315	·077	−·003
25	·2210	·9603	·044	−·005	61	·6212	·9221	·088	−·004
26	·2327	·9638	·040	−·003	62	·6308	·9128	·099	−·003
27	·2418	·9692	·034	−·004	63	·6393	·9061	·107	−·003
28	·2479	·9701	·033	−·002	64	·6483	·9003	·114	−·005
29	·2555	·9709	·032	−·001	65	·6561	·8921	·124	−·002
30	·2647	·9745	·028	+·001	66	·6651	·8814	·137	+·003
31	·2753	·9809	·021	−·002	67	·6744	·8750	·145	+·003
32	·2858	·9835	·018	·000	68	·6823	·8702	·151	+·003
33	·2945	·9845	·017	+·002	69	·6903	·8646	·158	+·005
34	·3027	·9872	·014	+·002	70	·6986	·8622	·161	+·004
35	·3116	·9926	·008	−·002	71	·7070	·8598	·164	+·003
36	0·3227	0·9936	0·007	0·000	72	·7159	·8598	·164	+·001
					73	0·7261	(0·8598)	(0·164)	(0·000)

5. *Rectification of the Light Curve.*—To determine the phase corresponding to the beginning and end of eclipse, a preliminary plot was made of l^2 against $\cos^2\theta$. The phases were calculated from the formula $\theta=\frac{2\pi}{P}t$ for a circular orbit, the phase of the normals in the secondary portion of the curve being calculated from

$$\theta=\pi-\frac{2\pi}{P}(t_2-t_1-t).$$

The light variation outside eclipse was represented by the formula

$$l = a_0 + a_1 \cos\theta + a_2 \cos 2\theta.$$

The solution of the normal equations from 33 equations of condition gave the following values and probable errors for the constants:—

$$a_0 = +0{\cdot}9490 \pm 0{\cdot}0038,$$
$$a_1 = -0{\cdot}0179 \pm 0{\cdot}0029,$$
$$a_2 = -0{\cdot}0507 \pm 0{\cdot}0026.$$

Rectification for ellipticity was effected by dividing the observed intensities by $a_0 + a_2 \cos 2\theta$. From the resulting points l' the reflection constant was redetermined, the light variation outside eclipse being represented by the formula $l' = b_0 + b_1 \cos\theta$, the least squares solution for the constants giving the values

$$b_0 = \quad 1{\cdot}0000 \pm 0{\cdot}0063,$$
$$b_1 = -0{\cdot}0187 \pm 0{\cdot}0030.$$

Following Russell *, the effect of reflection was removed by addition of the quantity

$$\Delta l' = c_1 + c_2 + (c_1 - c_2)\cos\theta,$$

where the c's are defined by the equations

$$c_1/c_2 = J_1/J_2,$$
$$c_1 - c_2 = b_1.$$

An iterative process was used for determining the ratio of the surface brightnesses of the two stars, that value of the ratio being adopted which gave $(1-\lambda_1)/(1-\lambda_2) = J_1/J_2$, where $1-\lambda_1$, $1-\lambda_2$ are the depths of the rectified minima.

To summarize the method adopted for obtaining the rectified light curve, let l'' be the observed values of light intensity, l' the intensity after rectification for ellipticity, and l the light cleared of the effects of ellipticity and reflection; we then have

$$l' = \frac{l''}{a_0 + a_2 \cos 2\theta},$$
$$l = \frac{l' + \Delta l'}{1 + \delta_0},$$
$$\delta_0 = c_1 + c_2.$$

The values of l within eclipse are plotted in Fig. 2 together with the computed light curve of Section 6. The eclipse is calculated to end at phase $0^d{\cdot}1469$.

The geometrical ellipticity $z = \epsilon^2 \sin^2 i$ has been taken from Shapley † as $-4a_2 - \frac{8}{7} \cdot a_2^2$ for the uniform solution of Section 6. We find $z = 0{\cdot}200 \pm 0{\cdot}006$, the probable error in z being calculated only from the probable error in a_2.

6. *Determination of the Orbital Elements.*—Owing to the shallow nature of the eclipses it is not possible to solve for the orbital elements from the photometric material alone, and an appeal has to be made to the spectroscopic measures. The ratio of the radii of the two components can be calculated from the formula

$$k^2 = \frac{L_a}{L_b} \Big/ \frac{J_a}{J_b},$$

where L is the luminosity and J the mean surface brightness; the subscripts a and b refer to the smaller and larger star respectively. The ratio of the luminosities may be found from the relative intensities of the absorption lines from

* H. N. Russell, *Ap. J.*, **36**, 68, 1912.
† H. Shapley, *Princeton Contributions*, No. 3, p. 7.

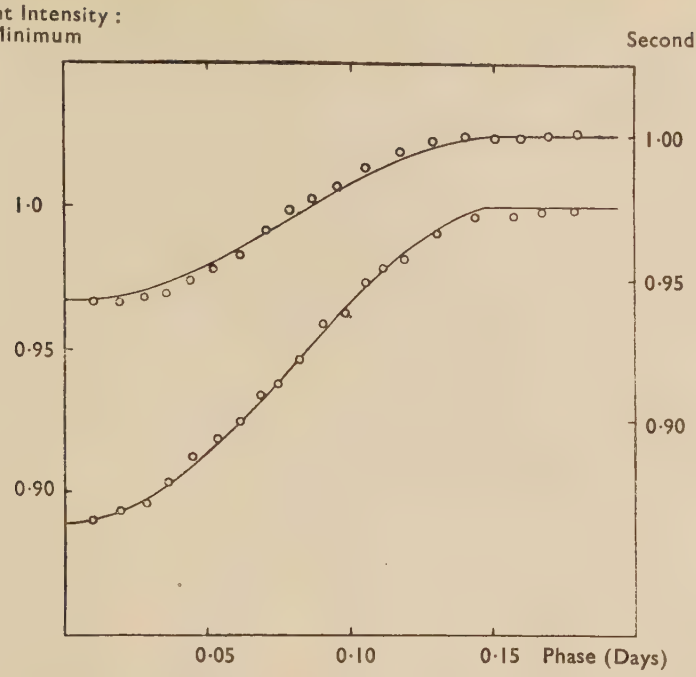

FIG. 2.—*Computed eclipse curve and "reflected" normals.*

the two components.* This has been investigated for μ^1 Scorpii by Struve and Elvey † who give for the ratio of the equivalent widths a mean value $0{\cdot}64 \pm 0{\cdot}04$. Accordingly we may take $L_b = 0{\cdot}65\, L_a$ ‡ and using $J_a = 1{\cdot}92\, J_b$ from Section 5 the value $k = 0{\cdot}90$ is adopted.

Following Kopal § we make the substitution $C = kr_b^2 \operatorname{cosec}^2 i$ in the fundamental equation

$$\sin^2\theta \sin^2 i + \cos^2 i = r_b^2(1 - z\cos^2\theta)(1 + kp)^2$$

and determine the geometrical elements of the eclipsing system by solving for C in the equation

$$\sin^2\theta(n) = C\{k[p^2(1 - z\cos^2\theta) - p_0^2(1 - z)] + 2[p(1 - z\cos^2\theta) - p_0(1 - z)] + z/k \,.\, \sin^2\theta(n)\}.$$

Each rectified eclipse normal gives an equation of condition, the unknown C being determined by taking a weighted mean. The orbital inclination and the semi-axes major of the two stars are then calculated from the formulae

$$\cot^2 i = \frac{C}{k}(1 - z)(1 + kp_0)^2,$$

$$r_a^2 = kC \sin^2 i,$$

$$r_b^2 = \frac{C}{k}\sin^2 i$$

The values of the function $p(k, \alpha)$ for uniform disks have been taken from Table VI of Zessewitsch. ‖ Considering the primary minimum alone and giving equal

* R. M. Petrie, *Pub. Amer. Astr. Soc.*, **9**, 162, 1933.
† O. Struve and C. T. Elvey, *P.A.S.P.*, **54**, 151, 1942.
‡ Rudnick and Elvey use $L_b = 0{\cdot}96 L_a$ so that their value $J_a = 1{\cdot}64 J_b$ will give $k = 0{\cdot}9$.
§ *Eclipsing Variables* (Harvard University Press, 1946), Ch. III, § 25, Ch. IX, § 77.
‖ W. Zessewitsch, *Astronomical Institute U.S.S.R. Bulletin*, No. 50, 1940 (Leningrad).

weight to the normals 2 to 17 inclusive we find

$$C = 0{\cdot}197 \pm 0{\cdot}003.$$

The calculated geometrical elements are as follows

$$i = 60°{\cdot}0, \qquad r_a = 0{\cdot}365, \qquad r_b = 0{\cdot}405,$$

the eclipse elements being

$$k = 0{\cdot}90, \qquad \alpha_0 = 0{\cdot}1830, \qquad p_0 = 0{\cdot}4223.$$

A light curve has been computed from the fundamental equation. These calculated values of rectified light have been converted into ordinary light intensity by means of the ellipticity and reflection constants of Section 5. The residuals, O–C, in magnitude difference are given in Table I. The probable residual per normal is calculated to be $0^m{\cdot}0020$.

7. *Comparisons.*—In the following table of elements a comparison is made between the photoelectric observations of Rudnick and Elvey, the photovisual determinations of van Gent, and the present work.

TABLE II

Element	Symbol	Present Work	Rudnick and Elvey	van Gent
Depth of Primary Minimum	...	$0^m{\cdot}276$	$0^m{\cdot}29$	$0^m{\cdot}30$
Depth of Secondary Minimum	...	$0^m{\cdot}164$	$0^m{\cdot}18$	$0^m{\cdot}19$
Ellipticity Constant	z	0·200	0·169	0·255
Reflection Constant	b	0·019	0·018	0·012
Rectified Light Loss at t_1	$1-\lambda_1$	0·111	0·135	0·094
Rectified Light Loss at t_2	$1-\lambda_2$	0·058	0·083	0·040
Ratio of Mean Surface Brightnesses	J_a/J_b	1·916	1·640	2·32
Light from smaller star	L_a	0·606	0·568	0·606
Light from larger star	L_b	0·394	0·432	0·394
Ratio of Radii	k	0·90	0·90	0·81
Maximum Obscuration	α_0	0·183	0·237	0·155
Inclination of Orbit	i	60°·0	62°·0	61°·1
Eccentricity of Meridional Section	ϵ	0·52	0·46	0·58
Semi-axis major smaller star	r_a	0·365	0·360	0·326
Semi-axis major larger star	r_b	0·405	0·400	0·402
Semi-axis minor smaller star	...	0·313	0·318	0·266
Semi-axis minor larger star	...	0·347	0·354	0·328

From the spectrographic observations of O. Struve we take the elements

$$m_1 \sin^3 i = 9{\cdot}1\odot,$$

$$m_2 \sin^3 i = 6{\cdot}0\odot,$$

$$(a_1 + a_2) \sin i = 9{\cdot}25 \times 10^6 \text{ km}.$$

Combining these results with the photometric solutions of Table II we make the following further comparisons.

Derived Element	Symbol	Present Work	Rudnick and Elvey	van Gent
Radius of relative orbit	a_1+a_2	$1{\cdot}068 \times 10^7$ km.	$1{\cdot}048 \times 10^7$ km.	$1{\cdot}056 \times 10^7$ km.
Mass of smaller star	m_1	14·01⊙	13·22⊙	13·56⊙
Mass of larger star	m_2	9·24	8·72	8·94
Semi-axis major smaller star	R_a	5·605⊙	5·424⊙	4·950⊙
Semi-axis major larger star	R_b	6·219	6·027	6·104
Semi-axis minor smaller star	...	4·800	4·800	4·043
Semi-axis minor larger star	...	5·326	5·334	4·986

Apparent and Absolute Magnitudes.—Taking μ^2 Scorpii to be $3^m{\cdot}680$ the magnitude of μ^1 at maximum brightness is $3^m{\cdot}106$. Since $L_a = 0{\cdot}606$, $L_b = 0{\cdot}394$ we find for the apparent brightness of the two components $3^m{\cdot}650$, $4^m{\cdot}117$. The parallax of μ^1 Scorpii may be obtained from the cluster parallax determinations of Kapteyn.* Using the recent value $0''{\cdot}0053 \pm 0{\cdot}0004$ given by Blaauw† we find for the absolute magnitudes of the components $-2^m{\cdot}7$, $-2^m{\cdot}3$.

8. *Conclusion.*—The observational work on this important eclipsing system is presented in the hope that it will prove to be of sufficient precision to warrant the application of refinements of solution in a detailed study of μ^1 Scorpii. It should be remarked that with such large distortion of figure which this system exhibits, the process of rectification should be carried out, taking into account the squares and cubes of the ellipticity. Furthermore the rather artificial assumption of uniformly bright disks deserves to be discarded, since it is in conflict with what we know about the darkening of other early type eclipsing systems for which an empirical determination of darkening has been made. The orbital solution from the observations given in this paper has been computed for the purpose of comparison with the existing uniform solutions.

The writer wishes to acknowledge the benefit of some correspondence with Dr Kopal.

Commonwealth Observatory,
Canberra, A.C.T. :
1948 *July.*

* J. C. Kapteyn, *Ap. J.*, **40**, 43, 1914.
† A. Blaauw, *Kapteyn Astronomical Laboratory Publications*, No. 52, 119, 1946.

ON THE CONSTITUTION OF THE TERRESTRIAL PLANETS

W. H. Ramsey

(Communicated by P. M. S. Blackett)

(Received 1948 November 9)

Summary

It is suggested that the density jump at the boundary of the Earth's core is due to a pressure transition from the molecular to a metallic phase, rather than to the appearance of a new material such as an alloy of iron and nickel. The pressure at the boundary of the core will then be characteristic of the chemical composition of the material, and so may be assumed to be the same for all the terrestrial planets. The mean densities of the terrestrial planets calculated on the basis of this assumption are in good, but not perfect, agreement with the empirical values. The calculated ellipticity of Mars is also satisfactory. If allowance is made for the tendency of the heavier elements to gravitate towards the centre of the Earth, the small discrepancies in the calculated mean densities can be removed.

Introduction.—It is known from seismology that the Earth possesses a central core which occupies about one-sixth of the total volume and contains about one-third of the total mass. The less dense material of the surrounding mantle is mainly olivine, a mixture of iron and magnesium silicates. It is generally assumed that the material of the core is an alloy of iron and nickel, though the only geophysical support for this hypothesis is the agreement of densities. The core is mainly responsible for the Earth's high mean density of 5·52 g./cm.^{3}, which is the highest in the Solar System. It is not surprising that the four great outer planets have low densities, as their masses have enabled them to retain hydrogen and other light volatile substances. On the other hand, the fact that the terrestrial planets have mean densities smaller than that of the Earth, even after allowance has been made for compression, presents a real difficulty. As all of these planets are smaller than the Earth, they cannot have retained a relatively higher percentage of the lighter constituents. It must therefore be admitted either that the planets were

TABLE I

Data for Terrestrial Planets *

	Relative Mass	Mean Diameter (km.)	Mean Density (g./cm^3.)
Earth	1	12,742	5·52
Venus	0·817 ±0·005	12,400±100	4·89±0·12
Mars	0·1078±0·0002	6,793± 16	3·93±0·03
Mercury	0·044 ±0·008	5,000±250	4·0 ±0·9
Moon	0·01230	3,476	3·34±0·01

* The values quoted and the estimated errors have been taken mainly from H. N. Russell, R. S. Dugan and J. Q. Stewart, *Astronomy*, Ginn & Company, 1945.

originally of different compositions or that the Earth's core and mantle are not chemically distinct. The former alternative cannot be reconciled with any current

theory of the origin of the Solar System; this point has been stressed by several authors, notably Jeffreys.* The second possibility will be examined in the present paper.

A breakdown of atomic structure is to be expected at very high pressures. By discarding the outer shell of electrons the atomic volume can be greatly reduced, but this process entails the loss of part of the molecular and crystal bindings. Nevertheless, if the pressure is sufficiently high (say, that at the centre of the Earth), the work done by the hydrostatic forces more than compensates for the loss of binding and, at equilibrium, the substance will be a metal of high density. It is therefore suggested that the core and mantle of the Earth are respectively metallic and molecular phases of the same chemical substance. It would be pointed out that the transition from a molecular to a metallic phase is essentially different from the ionization of gases by pressure, which has been studied in connection with stellar constitution. The former process occurs at a characteristic pressure; the degree of ionization in a gas increases continuously with pressure. Up to date the transition to a metallic phase has been examined only in the case of solid hydrogen; Kronig, de Boer and Korringa† have shown that the critical pressure is 7×10^{11} dynes/cm.^{2}, which corresponds to a depth of 1600 km. in the Earth. At the critical pressure metallic hydrogen is about twice as dense as the molecular form. The pressure at the boundary of the Earth's core is approximately $1{\cdot}4 \times 10^{12}$ dynes/cm.^{2}. The author has so far made only a rough estimate of the transition pressure for olivine. It is greater than that for solid hydrogen but probably less than the pressure at the centre of the Earth (4×10^{12} dynes/cm.^{2}). More refined calculations are at present in progress and will be presented in a later paper.

In the present paper it will be assumed that the hydrostatic pressure at the boundary of the Earth's core depends only on the chemical and crystallographic properties of the substance concerned; this is inevitably true if the proposed explanation of the core is correct. It will also be assumed that the chemical compositions of the terrestrial planets are similar to that of the Earth. The mean densities and moments of inertia of the terrestrial planets will then be calculated from seismological data.

Method of Calculation.—As a result of seismological observations the velocity of elastic waves in the interior of the Earth is known at all depths.‡ This knowledge by itself does not determine the internal density distribution. The density distribution is usually calculated on the assumption that, except at discontinuities such as the core boundary, the increase of density with depth is entirely due to adiabatic compression; that is,

$$d\rho/dr = \kappa\rho(dp/dr), \qquad (1)$$

where r is the distance from the centre of the Earth and where ρ, p and κ are respectively the density, pressure and adiabatic compressibility. The use of this relation has not led to any inconsistency and so it must be at least approximately correct. The discontinuities at which equation (1) breaks down are the base of the crustal layers (depth 33 km.), the "20° discontinuity" (depth 400 km.), the boundary of the core (depth 2900 km.) and the boundary of the inner core (depth

* Harold Jeffreys, *M.N.*, **94**, 823, 1934.

† R. Kronig, J. de Boer and J. Korringa, *Physica*, **12**, 245, 1946.

‡ For a survey of seismology see K. E. Bullen, *An Introduction to the Theory of Seismology*, Camb. Univ. Press, 1947, or Harold Jeffreys, *Rpts. on Progress in Physics*, **10**, 52, 1945.

5100 km.). The "20° discontinuity" has been explained by Bernal* as a transition to a crystal structure which is more stable at high pressures; it occurs, therefore, at a pressure characteristic of the substance concerned. In the present paper it is assumed that the density jump at the boundary of the core is also induced by hydrostatic pressure. Hence, in the approximation in which equation (1) is valid, the density in the region between the base of the crustal layers and the boundary of the inner core is a function of the pressure only. This pressure-density relationship will be used to calculate the mean densities and moments of inertia of the terrestrial planets. The nature of the inner core is of little importance in the present paper as the Earth is considerably larger than the other terrestrial planets; for simplicity it also will be assumed to be due to a transition under pressure.

Assuming the validity of equation (1), Bullen† has made an estimate of the density distribution in the interior of the Earth from the latest seismological data, and his figures will be adopted in this paper. The total mass and moment of inertia of the Earth are not sufficient to determine all of the jumps in density. The density jump at the boundary of the inner core must be chosen arbitrarily and Bullen's choice leads to a density of 17·2 g./cm.^{3} at the Earth's centre. As the inner core occupies only 1 per cent of the total volume, this ambiguity does not appreciably affect the densities outside the inner core and is consequently unimportant in the calculation of the mean densities of the terrestrial planets.

It will be assumed that the interiors of the planets are in hydrostatic equilibrium. The equations to be solved are

$$dp/dr = -\rho g, \tag{2}$$

$$g = 4\pi G r^{-2} \int_0^r \rho(x) x^2 \, dx, \tag{3}$$

where the density ρ is a known function of the pressure p, and where G is the constant of gravitation. These equations have been solved numerically by assuming an arbitrary pressure at the centre and by integrating outwards until the pressure vanishes. The mean density and the moment of inertia may then readily be computed. The layer of light surface rocks, which is approximately 33 km. thick in the Earth, has been assumed to constitute the same fraction of the total mass of all planets.

TABLE II

	Diameter (km.)	Diameter of Core	Mean Density (g./cm.^{3})	α
Earth	12,742	0·55D	5·52	
Venus	12,570	0·34D	4·70	2·7
Mars	7,020	...	3·56	1·18
Mercury	5,285	...	3·41	1·08
Moon	3,480	...	3·334	1·03

Calculated Mean Densities.—The mass of the planet M has been considered as given and the diameter D and the mean density ρ have been calculated. The results are shown in Table II and may be compared with the empirical values of Table I. The calculations have also been performed for several additional masses

* J. D. Bernal, *The Observatory*, **59**, 268, 1936.

† K. E. Bullen, *Bull. Seis. Soc. Amer.*, **30**, 235, 1940; **32**, 19, 1942.

in order to construct Fig. 1. This shows how the mean density decreases as the mass decreases. The discontinuity in the curve at $0{\cdot}793M_E$, M_E being the mass of the Earth, is a consequence of the assumption that the core boundary has a characteristic pressure. It is shown in the Appendix that with this assumption very small cores are unstable. Planets to the right of the discontinuity do not possess a core.

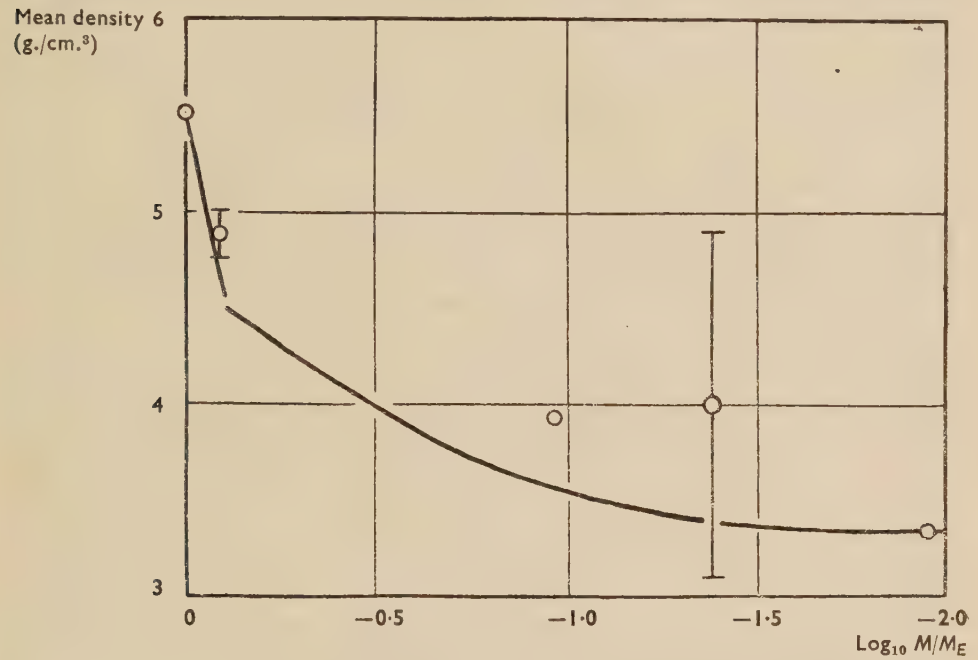

FIG. 1.—*The calculated variation of the mean density with the mass of the planet. The observed mean densities given in Table I are also shown.*

The calculated mean density of the Moon is in excellent agreement with the observed value. Jeffreys * has already shown that this is so and has used the agreement to support Bernal's explanation of the "20° discontinuity" as a change in crystal structure rather than the appearance of a new material. On the whole the calculated mean densities of the planets agree with the empirical values as well as could be expected on the simplifying assumptions which have been made, none of which can be strictly true. Mars alone has a mean density significantly different from that calculated, the discrepancy being about 10 per cent. The agreement for Venus is particularly satisfactory as the conditions in this planet approximate most closely to those in the Earth. It will be noted that the calculated mean density is low in all cases; the opposite is so if the planets are assumed to possess iron-nickel cores in proportion to their total masses.

Let $\rho(p)$ be increased by a small percentage to give agreement. Because of the greater compression the percentage increase required is less than the discrepancy in the mean density. Let α be the percentage increase in the mean density when $\rho(p)$ is increased by 1 per cent; the values of α for the different planets are given in Table II. The abnormally large value for Venus is due to an increase in the size of the core. For Venus $\rho(p)$ need be increased by only 1·5 per cent to get agreement; if allowance is made for the fact that the centrifugal acceleration in Venus

* Harold Jeffreys, *M.N., Geophys. Suppl.*, **4**, 50, 1937; **4**, 62, 1937.

is much smaller than in the Earth, the figure is 1·3 per cent. For Mars an increase of 9 per cent in $\rho(p)$ is required to remove the discrepancy.

Calculated Moments of Inertia.—The results of the calculations are shown in Table III in the form of a ratio I/MR^2, where I is the calculated moment of inertia and where R is the calculated radius. As is to be expected, the ratio for the smaller planets does not differ appreciably from 2/5, the value corresponding to uniform density.

TABLE III

Calculated Values of I/MR^2

Earth	Venus	Mars	Mercury	Moon
0·334	0·360	0·389	0·395	0·3977

The pole flattening of a planet due to its rotation depends on I/MR^2; this makes an indirect astronomical determination of the ratio possible. Let the parameter η be defined by the relation

$$\eta = 5m/2e - 2, \tag{4}$$

where m is the ratio of the centrifugal and gravitational forces at the planet's equator and where e is the ellipticity. The value of η is determined by the ratio I/MR^2 according to the well-known Radau-Darwin formula * :

$$I/MR^2 = \tfrac{2}{3}\{1 - \tfrac{2}{5}\sqrt{(1+\eta)}\}. \tag{5}$$

The ellipticity can be estimated from visual measurements or it can be calculated from the precession of the orbit of a satellite. As the periods of axial rotation of Venus and Mercury are very long, their ellipticities have not yet been resolved; neither planet possesses a satellite. Struve † estimates from the perturbations of Phobos that the ellipticity of Mars is 1/192; this is in good agreement with Lovell's visual determination of 1/190. The former figure is the more accurate and is probably correct to two or three per cent. On the equator of Mars gravity is approximately 219 times as great as the centrifugal force. The ellipticity calculated from the ratio I/MR^2 using equations (4) and (5) is 1/183; this is 5 per cent greater than the empirical value, a difference which is scarcely significant. The theoretical ellipticity is insensitive to a small percentage change in $\rho(p)$; an increase of 9 per cent which raises the calculated mean density to the correct value, reduces the ellipticity by only 1 per cent to 1/184.

Validity of Assumptions.—The assumptions that the density is a function of the pressure alone and that the planets are in hydrostatic equilibrium have led to fairly good, but not perfect, agreement with the observed mean densities. As neither of these assumptions is exactly true, better agreement could not have been expected.

Deviations from hydrostatic equilibrium are known to exist in both the Earth and the Moon. The Radau-Darwin formula (5), which assumes hydrostatic equilibrium, cannot account for even the order of magnitude of the ellipticity of the Moon. An example of a departure from hydrostatic conditions in the Earth is the ellipticity of the Equator, the difference between the principal diameters being approximately 1·4 km. However, these effects are small in magnitude and are probably due to the great mechanical strength of the material at pressures below

* *Cf.* H. Jeffreys, *The Earth*, Camb. Univ. Press, 1929.

† H. Struve, *Ast. Nach.*, **138**, 216, 1895. See also H. N. Russell, R. S. Dugan and J. Q. Stewart, *loc. cit.*

4×10^{10} dynes/cm.^{2} (that is, the first 1000 km. of the Earth). In contrast to these examples, Bullard * has shown recently that the assumption of hydrostatic equilibrium leads to a value for the ellipticity of the Earth which is in error by not more than 0·5 per cent. The assumption therefore appears to be a good one and is unlikely to introduce serious errors in the calculated mean densities; a discrepancy of a few per cent in the ellipticity of Mars would not, however, be surprising.

No allowance has been made in the calculations for difference in temperature. As the Earth has the greatest mass in comparison with its surface area, the temperature at a given pressure will probably be higher than in the other planets; consequently $\rho(p)$ as found from the Earth will be too low. At low pressures the relevant coefficient of thermal expansion is about 10^{-5} per degree Centigrade, and temperature differences in the neighbourhood of 100 deg. C. may be expected; the correction to $\rho(p)$ will therefore be only of the order of 0·1 per cent. The differences in the temperatures of the interiors of the planets may be much greater. On the other hand, it is known from Bridgman's † work that the coefficient of thermal expansion will be much smaller. The thermal expansion coefficient and the compressibility ‡ decrease with pressure roughly hand-in-hand, and so the former probably does not exceed 10^{-6} per degree Centigrade in the core; the effect of temperature therefore remains negligible. The variation of temperature within the Earth will modify the estimated density distribution; this has been discussed by Bullen § and does not appear to be of great importance.

No allowance has been made for the tendency of the heavier elements to condense towards the centre of the Earth. For example, the proportion of iron silicate to magnesium silicate in olivine will increase with depth. Thus the procedure of this paper does not give a representative proportion of the heavier elements to the smaller planets, and consequently the calculated mean densities are too small; this appears to be the chief source of the discrepancy. The extent of the central condensation will depend on the early history of the Earth, and an *a priori* estimation will not be attempted here. In making his estimate of the density distribution within the Earth, Bullen ‖ made use of equation (1) which assumes constant chemical composition; his figures must therefore be modified. The effects of central condensation can be allowed for, at least approximately, by adding to Bullen's density distribution a small percentage correction linear in r :

$$\left.\begin{aligned} \Delta\rho/\rho &= \gamma(1-r/R), && R>r>R_b, \\ &= \delta_1+\gamma(1-r/R), && R_b>r>R_c, \\ &= \delta_2+\gamma(1-r/R), && R_c>r, \end{aligned}\right\} \qquad (6)$$

where R_b, R_c are the radii of the "20° discontinuity" and the core respectively, and where γ, δ_1, δ_2 are constants to be determined. The "20° discontinuity" is not sharp and the mean value $0{\cdot}91R$ will be used for R_b. The variation (6) must not alter the total mass or moment of inertia of the Earth : this disposes of two of the three arbitrary parameters :

$$\delta_1 = -0{\cdot}23\gamma, \qquad \delta_2 = -0{\cdot}68\gamma.$$

* E. C. Bullard, *M.N., Geophys. Suppl.*, **5**, 186, 1948.

† *Cf.* P. W. Bridgman, *The Physics of High Pressures*, G. Bell & Sons, 1930.

‡ For the variation of compressibility with pressure, see K. E. Bullen, *An Introduction to the Theory of Seismology*, Camb. Univ. Press, 1947.

§ K. E. Bullen, *Bull. Seis. Soc. Amer.*, **30**, 235, 1940; **32**, 19, 1942.

‖ *Loc. cit.*

Let the mean atomic weight of the upper layers of the Earth be $\bar{A}$. Up to date the variation of density with depth has been ascribed entirely to pressure, and so the mean atomic weight of the whole Earth has been assumed to be $\bar{A}$. If equation (6) is interpreted in terms of a condensation of heavy atoms towards the centre, the mean atomic weight of the Earth will exceed $\bar{A}$ by

$$\Delta\bar{A} = 0{\cdot}33\gamma\bar{A}. \qquad (7)$$

The previous calculations for the planets must be modified to include correction (6); also $\rho(p)$ must be increased by the percentage required to raise the mean atomic weight of the planet to $\bar{A}+\Delta\bar{A}$. The resultant increase in the mean density of a very small planet is

$$\Delta\bar{\rho} = 0{\cdot}33\gamma\alpha\bar{\rho}, \qquad (8)$$

where α is the factor given in Table II. In order to lead to the correct mean density of Mars γ must be chosen as 0·24; this value also gives good agreement for Venus. This choice of γ is probably too large, as a greater fraction of the lighter material will have escaped from the smaller planets. The correction (6) to Bullen's densities exceeds 6 per cent only in the inner core, and over the greater part of the Earth it is less than 2 per cent. A satisfactory feature of the modification is that the density jump at the "20° discontinuity" is reduced and is now in very good agreement with that expected by Bernal* from the suggested change in crystal structure. Conversely, Bernal's estimate of the jump in density can be used to determine the constant γ of equations (6) and the theory will then predict the correct mean densities of the planets from terrestrial data. The jump in density at the boundary of the core is reduced by nearly 1 g./cm.^{3}. The gravitation of the heavier elements towards the centre of the Earth can therefore account for the discrepancies in the calculated mean densities of the planets without leading to a contradiction with geophysical data. It will be noted that no allowance for the condensation of heavy elements need be made in the case of the Moon (*cf.* Fig. 1). The condensation had therefore taken place before its formation.

Conclusion.—The theory presented can account for the mean densities of the planets in a manner which is satisfactory from the point of view of cosmogony. It cannot, however, be regarded as completely established until the pressure characteristic of the boundary of the core has been calculated from atomic theory. Only a rough estimate of this pressure has yet been made by the author, and it is consistent with that observed. The possibility that the inner core of the Earth is a second stage in the atomic breakdown should also be examined.

Further observations of Pluto may afford an additional check on the hypothesis put forward in this paper. The mass of this planet is $0{\cdot}93 \pm 0{\cdot}09 M_E$†, and so a mean density of $5{\cdot}2 \pm 0{\cdot}4$ g./cm.^{3} is expected. The mean density of Pluto is not known, as its radius has not yet been resolved. If the condensation of the heavy elements is allowed for according to equation (8), the calculated mean density of Mercury is 3·7 g./cm.^{3}. The empirical value is very uncertain, and a more accurate determination would provide an important check on the expected monotonic decrease in the mean density which is illustrated in Fig. 1.

Acknowledgments.—The author would like to express his appreciation to Professor L. Rosenfeld and to Professor Harold Jeffreys for the advice which they have given so willingly.

* J. D. Bernal, *The Observatory*, **59**, 268, 1936.

† *Cf.* H. N. Russell, R. S. Dugan and J. Q. Stewart, *loc. cit.*

APPENDIX

The Instability of Small Cores.—To illustrate this effect, consider planets composed of a material which has a constant density ρ_0 at pressures below a critical pressure p_c, and a constant density $\lambda\rho_0$, which is greater than ρ_0, at higher pressures. The radius of the core R_c and the total radius R must satisfy the relation

$$R(R_0^2+R_c^2-R^2)=2(\lambda-1)R_c^2(R-R_c),$$

where R_0 is the radius of the planet whose central pressure is p_c. This relation can be used to express R, and hence the total mass M, in terms of R_c. If R_c is small compared with R_0 the mass is given by the following power series in R_c/R_0 :

$$M/M_0=1-3(\lambda-\tfrac{3}{2})(R_c/R_0)^2+4(\lambda-1)(R_c/R_0)^3+\ldots., \qquad (9)$$

where M_0 is the mass of the planet with central pressure p_c. If $\lambda<\frac{3}{2}$ the total mass increases monotonically with R_c and so the radius of the core is always uniquely determined if the mass is specified. This is no longer so if $\lambda>\frac{3}{2}$ as the function (9) then possesses a minimum with respect to R_c; let the values of R_c and M at the minimum be R_c' and M', where M' is clearly less than M_0. Planets whose mass lies between M' and M_0 have three possible configurations, two with cores and one without a core. It may easily be verified that the configuration with the larger core has the smallest energy and is therefore the only one which will occur in nature. Thus a planet will never have a core of radius less than R_c' as it can exist in a more stable configuration. It is this effect which leads to the discontinuity in Fig. 1; the density jump at the boundary of the Earth's core corresponds to $\lambda=\frac{5}{3}$.

Using the pressure density relationship given by seismology it is found that a planet whose mass lies between $0{\cdot}793M_E$ and $0{\cdot}795M_E$ can exist in three configurations. If the mass is $0{\cdot}793M_E$ the radius of the core is approximately 1000 km., and this is the smallest core possible in a stable configuration.

The Physical Laboratories,
The University,
Manchester:
1948 *November* 8.

RADIAL OSCILLATIONS OF A PARTICULAR STELLAR MODEL

Chandrika Prasad

(Communicated by E. A. Milne, F.R.S.)

(Received 1948 October 21)

Summary

The radial oscillations of a stellar model having a point mass at the centre and constant density throughout the rest, have been considered. It is shown that an algebraic solution is possible when the point mass is one-third of the total mass of the star.

---

1. The light variation in cepheid stars is well known to be caused by radial oscillations of the star. The theory of adiabatic radial oscillation was developed by Eddington * who applied it to find the period of oscillation of polytropic models. Sterne † applied this theory to three particular models with specified density distributions and he was able to obtain algebraic expressions for the amplitude of oscillation.

It is instructive to study the oscillations of stellar models with as many different density distributions as possible. But besides Sterne's three models, the author is unaware of any other model for which algebraic solutions have been found as yet. In this paper a model has been found which gives an algebraic solution, and expressions for the amplitude and period of oscillation have been obtained. This model has a point mass at the centre and the density is constant throughout the rest of it.

2. The differential equation for small radial oscillation, as given by Eddington, is

$$\frac{d^2\xi_1}{d\xi_0^2}+\frac{4-\mu}{\xi_0}\frac{d\xi_1}{d\xi_0}+\left(\frac{n^2\rho_0}{\gamma P_0}-\frac{\alpha\mu}{\xi_0^2}\right)\xi_1=0, \tag{1}$$

where ξ_1 is the amplitude of the displacement $\delta\xi_0/\xi_0$; ρ_0, P_0, g_0 are the mean values of density, pressure and gravity at distance ξ_0 from the centre; $\mu=g_0\rho_0\xi_0/P_0$; $\alpha=3-4/\gamma$, γ being the ratio of specific heats and $n=2\pi\nu$, where ν is the frequency of oscillation. The boundary conditions require the solution to be non-singular both at $\xi_0=0$ and $\xi_0=R$, the surface of the star.

Suppose that the model has a point mass M_0 at the centre and has constant density ρ_0 throughout the rest. Then the mass within any distance ξ_0 is

$$M(\xi_0)=M_0+\tfrac{4}{3}\pi\xi_0^3\rho_0,$$

$$g_0=GM_0/\xi_0^2+\tfrac{4}{3}\pi G\rho_0\xi_0$$

and

$$P_0=GM_0\rho_0\left(\frac{1}{\xi_0}-\frac{1}{R}\right)+\tfrac{2}{3}\pi G\rho_0^2(R^2-\xi_0^2).$$

Substituting these values in equation (1) we get a differential equation not solvable in finite terms, in general. But if we choose the point mass such that

$$M_0=\tfrac{2}{3}\pi\rho_0R^3,$$

---

* A. S. Eddington, *The Internal Constitution of Stars*, pp. 186 *et seq.*, 1926.

† T. E. Sterne, *M.N.*, **97**, 583, 1937.

then the expression for the pressure P_0 reduces to

$$\tfrac{2}{3}\pi G\rho_0^2 R^2\left(\frac{R}{\xi_0}-\frac{\xi_0^2}{R^2}\right).$$

In this case the point mass is one-third of the total mass of the star; and if $\bar{\rho}$ be the mean density of the star, $\bar{\rho}=\frac{3}{2}\rho_0$.

With these values we have on putting ξ_0 equal to Rx,

$$\mu=\frac{1+2x^3}{1-x^3} \qquad \text{and} \qquad \frac{n^2\rho_0}{\gamma P_0}=\frac{9n^2}{4\pi G\gamma\bar{\rho}R^2}\cdot\frac{x}{1-x^3}.$$

Substitution in (1) gives

$$(1-x^3)\frac{d^2\xi_1}{dx^2}+\frac{3-6x^3}{x}\frac{d\xi_1}{dx}+(\mathcal{J}x^3-\alpha)\frac{\xi_1}{x^2}=0, \tag{2}$$

where

$$\mathcal{J}=\frac{9n^2}{4\pi G\gamma\bar{\rho}}-2\alpha. \tag{3}$$

3. Assuming a solution in series

$$\xi_1=x^q\sum_0^\infty a_k x^k, \tag{4}$$

the indicial equation gives $q=-1\pm\sqrt{1+\alpha}$. To avoid singularity at the centre we take

$$q=\sqrt{1+\alpha}-1. \tag{5}$$

The coefficients for which k is of the form $3j+1$ or $3j+2$ vanish. The rest are given by the recurrence formula

$$a_{k+3}=a_k\frac{(q+k)(q+k+5)-\mathcal{J}}{(q+k+3)(q+k+5)-\alpha}. \tag{6}$$

The infinite series (4) converges for $x<1$, but diverges for $x=1$. So to avoid singularity at $x=1$, the series must be a terminating series. This is possible only if

$$\mathcal{J}=(q+3j)(q+3j+5), \tag{7}$$

where j is zero or a positive integer. This gives a set of values of $\mathcal{J}$ for which oscillations are possible. By giving to j different values we get different modes of oscillation. The period T of the j'th mode is $2\pi/n$, where

$$n^2=\tfrac{4}{9}\pi G\gamma\bar{\rho}(\mathcal{J}+2\alpha),$$

in which $\mathcal{J}$ is given by (7).

4. It is seen from above that when $\alpha<0$, all the modes are unstable, for then q is negative and therefore the origin is a point of singularity for all values of $\mathcal{J}$. For $\alpha=0$, the period is infinite when $j=0$, showing that the model is in neutral equilibrium with respect to zero'th mode; but the higher modes are stable. For $\alpha>0$ all the modes are stable.

The values of the amplitude ξ_1 for the particular case $\alpha=0{\cdot}4$ are given below:

$$\xi_1=a_0x^q, \qquad (j=0)$$
$$\xi_1=a_0x^q(1-1{\cdot}56x^3), \qquad (j=1)$$
$$\xi_1=a_0x^q(1-4{\cdot}24x^3+3{\cdot}64x^6), \qquad (j=2)$$

ere $q=0{\cdot}183$.

The values of $T\sqrt{(G\bar{\rho}/6\pi)}$ for the first few modes are given in the following table :

α \ j	0	1	2
0·2	1·088	0·203	0·124
0·4	0·746	0·191	0·118
0·6	0·589	0·179	0·112

It is instructive to compare these with Sterne's results. The period of zero'th mode lies between those of Sterne's models 1 and 2, as should be expected from the density condensation. But the periods of the higher modes are much less.

Taking the values of α and $\bar{\rho}$ from Eddington these values give the period of δ Cephei as $9\frac{1}{3}$ days, whereas the actual period is 5·37 days. Similarly the periods of X Cygni and RR Lyrae come out as 22 days and 1 day, whereas the actual periods are 16·4 and 0·57 days. This shows that the above method gives the right order of periods for cepheid as well as cluster-type variables.

I am grateful to Professor E. A. Milne for his kind encouragement and suggestions for improvement.

Queen's College, Oxford :
1948 *October* 19.

SOME ASPECTS OF STELLAR EVOLUTION—IV

The Mean Random Velocity of the Stars

K. E. Edgeworth

(Received 1948 October 1)

Summary

It was suggested in a previous paper that the mean random velocity of the stars was originally much lower than it is now. The present paper explains the subsequent increase of random velocity as being due to " viscous friction ". The magnitude of the effect can be calculated, and leads to an estimate of the age of the Galaxy of about 9×10^9 years, in good agreement with other similar estimates.

In a previous paper * the suggestion was made that the thickness of the galactic disk at the time the stars were formed was only about one hundredth part of what it is to-day and the mean random velocity was also correspondingly less. In the course of the discussion on the paper the question was asked : if the mean random velocity of the stars at the beginning was so much smaller than it is now, how have the stars acquired the comparatively high random velocities they possess to-day ? The present paper is an attempt to answer this question.

Collisions between the stars are too rare to be of serious importance, but close encounters take place and have the same effect as elastic collisions. The dynamical theory of gases is therefore applicable to a cloud of stars, in which case the stars become " molecules " and their random velocities become " molecular velocities ".

There are several points of similarity between a rotating cloud of gas and a rotating cloud of stars, but there are also important differences.

In the case of a rotating disk of gas, heat may be generated by contraction or by viscous friction, and any heat generated in this way may be converted into radiation and may escape into space. On the other hand, there is no similar mechanism for the dissipation of " molecular energy " (i. e. the reduction of random velocities) in the case of a cloud of stars ; if, for any reason, " molecular energy " is increased, the increase is permanent.

It was pointed out in a previous paper † that the thickness of a rotating disk of gas is proportional to the temperature, that is to say, to the molecular energy ; and so long as the material consisted of gas, the galactic disk lost heat and grew thinner. During the formation of the stars it may be assumed that the thickness of the disk remained unchanged and that the " molecular velocities " of the stars (i. e. their random velocities) were of the same order as the molecular velocities in the original gas. After the formation of the stars the " molecular velocity " increased and the disk grew thicker again.

An estimate of the rate of increase is not without interest.

A rotating cloud such as the Galaxy, whether composed of stars or gas, usually exhibits a certain measure of condensation in the central regions, and the angular velocity decreases as we move outwards from the centre. In consequence of this

* *M.N.*, **106**, 472 and 475, 1946.

† *Loc. cit.*, p. 472, eqn. (10).

difference in angular velocity viscous friction is set up between the different rings, so that the random velocity of the molecules increases with lapse of time.

Consider two parallel planes moving with velocities v_1, v_2.

Let x = the distance between the planes.

η = the coefficient of viscosity.

$\omega = (v_1 - v_2)/x$.

ρ = the density of the fluid.

The force acting across an area A of either plane is $\eta A(v_1 - v_2)/x = \eta A\omega$. The energy lost by plane 1 in time dt is $\eta A\omega v_1\, dt$. The energy gained by plane 2 in time dt is $\eta A\omega v_2\, dt$. The energy lost by conversion into molecular energy is $\eta A\omega(v_1 - v_2)\, dt = \eta Ax\omega^2\, dt$. The energy lost per unit volume is $\eta\omega^2\, dt$. And the energy lost per unit mass is $\eta\omega^2\, dt/\rho$. The value of η in the dynamical theory of gases is $0{\cdot}44\rho c\lambda$, where c is the molecular velocity and λ is the mean free path.

It is evident that an essential factor in determining the value of η is the depth to which a molecule from one layer is able to penetrate into adjacent layers. This depends on the length of the free path, which is represented in the formula by the symbol λ.

The formula itself is worked out on the assumption that the free path between collisions is a straight line and that it is traversed at uniform velocity. In the case of a rotating cloud of stars this assumption is not valid; the random velocity of a star must be represented by an oscillation about its mean position, and it is the amplitude of the oscillation that must be identified with the symbol λ in the formula.

The amplitude of the stellar oscillations is related to the thickness of the disk, and, for the purpose of numerical calculation, it may be assumed that λ is one-quarter of this thickness.

In the paper already referred to, it was shown that the thickness of the disk is proportional to c^2, where c is the molecular velocity. We may therefore write

$$\lambda = kc^2.$$

Reverting to the main argument, the formula for the loss of energy per unit mass, which must now be identified with the increase in molecular energy, becomes

$$0{\cdot}44kc^3\omega^2\, dt.$$

Let E = the molecular energy per unit mass. Then

$$E = \tfrac{1}{2}c^2,$$
$$dE = c\, dc,$$
$$dc/dt = 0{\cdot}44kc^2\omega^2,$$
$$t = -2{\cdot}3k^{-1}\omega^{-2}c^{-1} + C,$$
$$t_2 - t_1 = 2{\cdot}3k^{-1}\omega^{-2}(c_1^{-1} - c_2^{-1})$$
$$= 2{\cdot}3(c\lambda^{-\frac{1}{2}})\omega^{-2}(\lambda_1^{-\frac{1}{2}} - \lambda_2^{-\frac{1}{2}}).$$

At the present time we may write $c_2 = 4 \times 10^6$ cm./sec. and $\lambda_2 = 1{\cdot}2 \times 10^{21}$ cm., so that

$$c\lambda^{-\frac{1}{2}} = 1{\cdot}2 \times 10^{-4}.$$

The angular velocity of the Sun in its orbit about the centre of the Galaxy is 10^{-15}, and ω may be taken to be about one-half of this.

Finally, λ_1 may be taken as about one hundredth part of λ_2, so that

$$\lambda_1^{-\frac{1}{2}} - \lambda_2^{-\frac{1}{2}} = 2{\cdot}6 \times 10^{-10}.$$

This gives $t_2 - t_1 = 2{\cdot}8 \times 10^{17}$ secs.

$$= 9 \times 10^9 \text{ years.}$$

This estimate of the age of the Galaxy is of the same order as other estimates based on considerations of quite a different character, but it is perhaps desirable to point out that there are certain factors not taken into account in the derivation of the formula.

It was assumed that the random velocity of the stars at the time t_1 was the same as the molecular velocity of the gas out of which the stars were formed. Actually it might be considerably less than this, and the age of the Galaxy would be correspondingly increased. On the other hand, it is necessary to take into account the viscous friction due to local condensations, and this would reduce the estimate.

Nevertheless, making all due allowance for factors of this sort, the agreement between this and other estimates of the age of the Galaxy is remarkably good, and affords striking confirmation of the conclusion reached in the previous paper that the Galaxy was at one time very much thinner than it is now.

Cherbury,
Booterstown,
Co. Dublin :
1948 *September* 29.

MEAN AREAS AND HELIOGRAPHIC LATITUDES OF SUNSPOTS IN THE YEAR 1941

Royal Observatory, Greenwich

(Communicated by the Astronomer Royal)

(Received 1948 September 9)

The following results are in continuation of those given in *M.N.*, **108**, 177, 1948, and are derived from the measurement at Greenwich of photographs taken at the Royal Observatories of Greenwich and the Cape and at the Kodaikanal Observatory, India. Photographs for six days unrepresented in the series, were kindly supplied by the Superintendent, U.S. Naval Observatory, Washington.

Table I gives the mean daily areas of umbrae, whole spots and faculae for each synodic rotation of the Sun included in the year 1941; the means for the year as a whole are included in Table II, which summarizes the yearly values from 1933–41.

Table III gives for each rotation in the year 1941 the mean daily area of the whole spots (corrected for foreshortening) and the mean heliographic latitude of the spotted areas for both northern and southern hemispheres.

The mean heliographic latitude of the entire spotted area and the mean distance from the equator of all spots are also tabulated. The mean values for the year 1941 are included in Table IV.

Tables II and IV are in continuation of similar tables given in *Monthly Notices*: for the years 1874 to 1888—**49**, 381–382; 1889 to 1902—**63**, 465–466; 1901 to 1914—**76**, 402–403; 1913 to 1924—**85**, 1007–1008; 1923 to 1933—**94**, 870–871.

The rotations in Tables I and III are numbered in continuation of Carrington's series.

The chief features of this record for the year 1941 are as follows:—

(1) The continued decline towards solar minimum shown by the yearly values of the mean daily areas of sunspots and of faculae given in Table II. However, with a mean daily area of 658 for sunspots and 1282 millionths for faculae, the Sun has evidently not yet entered into the minimum phase of the 11-year cycle.

Mean areas for the separate rotations in 1941 (Table I) show a subsidiary double peak in Nos. 1175–77. In the latter rotation occurred the biggest spot of the year with an average area during disk passage of 1862 millionths of the Sun's hemisphere.

The run of mean daily areas of faculae from rotation to rotation is comparatively smooth with peak values about rotation 1175.

(2) On eight days in the year no sunspots were seen, viz. August 16, November 7–11 inclusive and December 20–21. These are the first spotless days since the year 1935. On no days were faculae absent.

TABLE I

No. of Rotation	Rotation Commenced U.T. 1941	Days Photographed	Mean Daily Areas: Projected Umbrae	Projected Whole Spots	Projected Faculae	Corrected for Foreshortening Umbrae	Corrected for Foreshortening Whole Spots	Corrected for Foreshortening Faculae
1168	Jan. 3·18	27	96	571	913	72	439	1138
1169	Jan. 30·52	28	114	718	917	82	492	1123
1170	Feb. 26·86	27	157	894	908	110	631	1127
1171	Mar. 26·18	28	60	289	858	45	218	1065
1172	Apr. 22·45	27	102	495	1149	73	358	1366
1173	May 19·68	27	167	812	1127	108	532	1348
1174	June 15·89	27	211	1004	1220	157	754	1533
1175	July 13·09	27	327	1823	1238	231	1279	1540
1176	Aug. 9·30	27	160	818	1159	125	642	1464
1177	Sept. 5·55	28	326	1975	1117	235	1417	1357
1178	Oct. 2·82	27	215	1155	1020	151	820	1279
1179	Oct. 30·11	28	138	769	852	108	613	1076
1180	Nov. 26·42	27	124	721	1079	83	482	1307

Projected areas are expressed in millionths of the Sun's disk, and areas corrected for foreshortening in millionths of the Sun's hemisphere.

(3) The northern hemisphere had a greater spotted area than the southern in the ratio of nearly 2 : 1.

(4) The number of spot groups lasting for two days or longer was 209; 117 were in the northern hemisphere and 92 in the southern. In addition, there were 49 mostly very small groups seen on one day only; 23 were in the northern hemisphere and 26 in the southern.

There were seven spot groups (all in the latter half of the year) with average area greater than 500 millionths of the Sun's hemisphere. Two of these exceeded 1000 millionths, the larger having a mean area of 1862 and a peak area greater than 3000 millionths on September 21. For other notes, see *Monthly Notices*, **102**, 198, 1942.

TABLE II

Year	No. of Days: Photographed	No. of Days: Without Spots	Mean Daily Areas: Projected Umbrae	Projected Whole Spots	Projected Faculae	Corrected for Foreshortening Umbrae	Corrected for Foreshortening Whole Spots	Corrected for Foreshortening Faculae
1933	365	234	24	120	225	18	88	267
1934	365	145	27	142	297	22	119	354
1935	365	21	152	810	910	117	624	1100
1936	366	0	288	1529	2106	217	1141	2545
1937	365	0	509	2795	2856	375	2074	3505
1938	365	0	501	2706	2578	371	2019	3205
1939	365	0	404	2163	1907	295	1579	2349
1940	366	0	279	1434	1224	200	1039	1522
1941	365	8	167	915	1041	120	658	1282

Projected areas are expressed in millionths of the Sun's disk, and areas corrected for foreshortening in millionths of the Sun's hemisphere.

TABLE III

No. of Rotation	Rotation commenced U.T.	Spots North of the Equator: Mean Daily Area	Spots North of the Equator: Mean Heliographic Latitude	Spots South of the Equator: Mean Daily Area	Spots South of the Equator: Mean Heliographic Latitude	Mean Latitude of Entire Spotted Area	Mean Distance from Equator of all Spots
	1941		°		°	°	°
1168	Jan. 3·18	289	11·11	150	8·26	+4·49	10·13
1169	Jan. 30·52	263	11·99	230	9·68	+1·89	10·92
1170	Feb. 26·86	499	11·19	132	12·55	+6·23	11·48
1171	Mar. 26·18	47	8·62	171	7·23	−3·79	7·53
1172	Apr. 22·45	121	17·01	236	4·16	+3·03	8·52
1173	May 19·68	296	10·84	236	12·89	+0·30	11·75
1174	June 15·89	538	11·77	216	6·39	+6·57	10·23
1175	July 13·09	660	11·49	618	6·46	+2·81	9·06
1176	Aug. 9·30	391	10·78	251	6·46	+4·05	9·09
1177	Sept. 5·55	1196	11·38	221	8·12	+8·33	10·87
1178	Oct. 2·82	733	11·09	87	10·89	+8·75	11·07
1179	Oct. 30·11	435	10·23	178	14·54	+3·03	11·48
1180	Nov. 26·42	150	9·11	331	11·42	−5·01	10·70

TABLE IV

Year	Days Photographed		Spots North of the Equator: Mean Daily Area	Spots North of the Equator: Mean Heliographic Latitude	Spots South of the Equator: Mean Daily Area	Spots South of the Equator: Mean Heliographic Latitude	Mean Latitude of Entire Spotted Area	Mean Distance from Equator of all Spots
				°		°	°	°
1933	365		86	10·60	2	8·35	+10·23	10·56
1934	365		44	16·45	74	28·09	−11·49	23·75
1934	365	Old Cycle	19	4·10	1	4·37	+ 3·79	4·11
		New Cycle	26	25·44	74	28·31	−14·46	27·57
1935	365		205	22·42	419	23·72	− 8·57	23·30
1936	366		463	19·36	678	21·02	− 4·63	20·35
1937	365		1317	17·63	757	15·96	+ 5·36	17·02
1938	365		899	15·55	1120	14·17	− 0·94	14·79
1939	365		649	14·64	931	12·57	− 1·39	13·42
1940	366		499	11·65	540	10·72	+ 0·03	11·17
1941	365		427	11·13	232	8·67	+ 4·28	10·38

(5) The weighted mean latitude of all sunspots was 10°·38, less than 1° lower than the value for the previous year. Latitudes of individual spots ranged from the equator to 26°. Southern spots were on the average $2\frac{1}{2}$° nearer the Sun's equator.

Royal Observatory,
Greenwich :
1948 *August* 25.

ERRATUM

M.N., **108**, No. 4, C. M. Bondi's paper:

P. 332, line 20, in the expression for L as a function of $\overline{M}_s$ for $\frac{1}{\phi(1+X)}$ read $\frac{\mu^4}{\phi(1+X)}$.

OBSERVATIONAL ASPECTS OF THE SUNSPOT-GEOMAGNETIC STORM RELATIONSHIPS *

H. W. Newton

(Communicated by the Astronomer Royal)

(Received 1948 September 15)

Summary

With the use of international magnetic character figures, the statistical rise of geomagnetic activity is investigated for the solar disk passage of four area groupings of sunspots, 1914–1944. This is the reverse process of earlier Greenwich work in which the comparison was made from geomagnetic storms to sunspots.

For sunspots exceeding 1500 millionths of the Sun's hemisphere there is a very definite increase of geomagnetic activity centred at about two days after the date of central meridian passages of the sunspots. But this relationship rapidly degenerates, and from the area criterion alone ceases to be significant below the area group 1000–750 millionths. Other sunspot groupings based on solar flare incidence greatly improve the correlation, and for the minor naked-eye sunspots, around 500 millionths, a peak of geomagnetic actively now appears.

Twenty-seven-day recurrence tendencies of the geomagnetic activity associated with the various sunspot groupings are examined, and the pseudo-character of what is found is contrasted with the strong and more precise twenty-seven-day recurrence tendency of the smaller storms, especially those without SC onset and not apparently dependent upon sunspot or solar flare incidence.

The statistical non-recurrence of great magnetic storms is confirmed from 1907–1944 data.

* The full text of this paper will be published in *M.N., Geophys. Suppl.*, **5**, No. 8, 1949.